Université du Québec

Institut national de la recherche scientifique

Centre Énergie Matériaux Télécommunications

STUDY AND DESIGN OF RECONFIGURABLE METASURFACE-BASED ANTENNAS AT MM-WAVE FREQUENCY BANDS

Par

Peyman PourMohammadi

Thèse présentée pour l'obtention du grade de
Philosophiae Doctor, Ph.D.
en Télécommunications

Jury d'évaluation

Président du jury et examinateur interne	Prof. Shervin Vakili Institut National de la Recherche Scientifique
Examinateur externe	Prof. Elham Baladi Polytechnique Montréal
Examinateur externe	Prof. Niamat Hussain University of Glasgow
Directeur de recherche	Prof. Tayeb A. Denidni Institut National de la Recherche Scientifique

DÉDICACE

À ma chère famille :

mes parents, Hamid et Mahrokh

ma sœur, Sara

et mon frère, Saeed.

DEDICATION

To my beloved family :

my parents, Hamid and Mahrokh

my sister, Sara

and my brother, Saeed.

REMERCIEMENTS

Bien que cette page soit l'une des premières de ma thèse, c'est en fait la dernière que j'ai écrite. Elle sert d'espace sincère pour remercier tous ceux qui ont cru en moi, m'ont soutenu, et ont contribué à rendre ce parcours de doctorat possible.

Avant tout, louanges et remerciements à Dieu, le Miséricordieux et Compatissant, pour m'avoir guidé depuis le tout début de mon parcours académique jusqu'à la réussite de ce doctorat. Cette réussite n'aurait pas été possible sans le soutien immense et les encouragements que j'ai reçus de nombreuses personnes en chemin.

Je suis profondément reconnaissant au Prof. Tayeb Denidni pour ses conseils inestimables et son soutien tout au long de mes études doctorales. J'ai beaucoup appris de lui, tant sur le plan académique que personnel. Sa patience, ses conseils, et ses encouragements ont été essentiels dans la réalisation de cette recherche et dans mon développement en tant que chercheur. Terminer ce parcours n'aurait pas été possible sans sa confiance et son encouragement.

Je remercie également le Dr. Amjad Iqbal, de qui j'ai beaucoup appris — et dont l'amitié, la confiance, et le soutien me tiennent particulièrement à cœur. Je suis reconnaissant envers les merveilleux collègues et amis de l'Institut National de la Recherche Scientifique (INRS). Votre soutien, collaboration, et amitié ont rendu ce parcours non seulement productif, mais aussi inoubliable.

Ce fut un honneur d'avoir les membres du jury — le Prof. Shervin Vakili, la Prof. Elham Baladi, et le Prof. Niamat Hussain. Je leur adresse mes sincères remerciements pour leur temps, leur examen attentif de ma thèse, et leurs commentaires précieux qui ont contribué à renforcer ce travail.

Je tiens également à remercier l'INRS ainsi que le Fonds de Recherche du Québec – Nature et Technologies (FRQNT) pour le financement de mes études de doctorat. Leur générosité m'a permis de me consacrer pleinement à ma recherche.

À tous mes amis au Canada et à travers le monde — merci. Votre compagnie, vos encouragements, et vos paroles motivantes, même à distance par des appels téléphoniques, ont joué un rôle vital pour me garder ancré et inspiré tout au long de ce parcours.

Enfin, ma plus profonde reconnaissance va à ma famille — mes parents, Hamid et Mahrokh; ma sœur, Sara; et mon frère, Saeed. Je ne saurais exprimer à quel point je leur suis reconnaissant pour leur amour inconditionnel, leur soutien sans fin, et leur foi inébranlable en moi. Leur force, leurs encouragements, et leurs sacrifices ont été le véritable fondement de cette réussite.

ACKNOWLEDGMENT

Although this is one of the first pages in my thesis, it is, in fact, the last one I wrote. It serves as a heartfelt space to thank all those who believed in me, supported me, and helped make this PhD journey possible.

First and foremost, all praises and thanks to God, the Merciful and Compassionate, for guiding me from the very beginning of my academic journey to the successful completion of this PhD. This achievement would not have been possible without the immense support and encouragement I received from many individuals along the way.

I am deeply grateful to Prof. Tayeb Denidni for his invaluable guidance and support throughout my doctoral studies. I have learned a lot from him, both academically and personally. His patience, advice, and encouragement were instrumental in shaping this research and in my development as a researcher. Completing this journey would not have been possible without his trust and encouragement.

I am also thankful to Dr. Amjad Iqbal, from whom I learned a great deal—and whose friendship, trust, and support I truly appreciate. I am grateful to the wonderful colleagues and friends at the Institut National de la Recherche Scientifique (INRS). Your support, collaboration, and friendship made this journey not only productive but truly memorable.

It was an honor to have the jury members—Prof. Shervin Vakili, Prof. Elham Baladi, and Prof. Niamat Hussain. My sincere thanks to them for their time, careful review of my thesis, and valuable comments that helped strengthen this work.

I must also acknowledge the INRS and the Fonds de Recherche du Québec – Nature et Technologies (FRQNT) for funding my PhD studies. Their generosity allowed me to focus fully on my research.

To all my friends in Canada and around the world—thank you. Your companionship, encouragement, and motivating words, even from afar through long-distance phone calls, played a vital role in keeping me grounded and inspired throughout this journey.

Finally, my deepest appreciation goes to my family—my parents, Hamid and Mahrokh; my sister, Sara; and my brother, Saeed. I cannot adequately express how grateful I am for their unconditional love, endless support, and unwavering belief in me. Their strength, encouragement, and sacrifices have been the true foundation of this achievement.

RÉSUMÉ

Les systèmes de communication mobile évoluent rapidement, ce qui engendre une demande croissante de débits de données plus élevés et de latence réduite, notamment pour les services multimédias. Les fréquences millimétriques représentent une solution prometteuse, car elles offrent une large bande passante disponible et permettent la conception de composants RF compacts et économiques. Malgré ces avantages, les signaux haute fréquence présentent des limitations en termes de portée de propagation et de capacité de pénétration. Ces limitations peuvent être surmontées grâce aux antennes à formation de faisceau (beamforming). L'intégration des capacités de commutation de faisceau avec d'autres fonctions dans une structure d'antenne reconfigurable améliore les performances du système tout en réduisant l'encombrement et les interférences. L'un des objectifs clés de la recherche pour les systèmes 5G futurs est de développer des antennes de formation de faisceau à faibles pertes, compactes et économiques grâce à l'intégration de métasurfaces. Dans ce contexte, cette thèse présente une conception et une analyse complètes d'antennes transmitarray reconfigurables fonctionnant aux fréquences millimétriques.

Les systèmes d'antennes à balayage de faisceau se composent généralement de deux composants principaux : une antenne d'alimentation et un panneau de métasurface. Une antenne à fentes à guide d'ondes intégré au substrat (SIW) est d'abord proposée comme source rayonnante en raison de son gain élevé, de ses faibles pertes et de sa grande capacité d'intégration. En parallèle, une antenne cornet imprimée en 3D est également conçue et évaluée comme une solution alternative bien connue et facilement simulable. Ces deux options d'alimentation offrent une flexibilité de conception : l'antenne SIW est adaptée à une mise en œuvre finale, tandis que l'antenne cornet est privilégiée pour les simulations et les prototypes de première étape en raison de sa géométrie simplifiée et de ses temps de simulation plus courts. Les deux antennes sont destinées à fonctionner avec des panneaux de métasurface composés de cellules unitaires à phase reconfigurable.

Le panneau de métasurface, deuxième composant principal, est réalisé à l'aide de cellules unitaires basées sur deux concepts fondamentaux : l'utilisation du couplage mutuel de manière constructive avec la technique d'inversion de courant, et le principe de Huygens. Pour chaque méthodologie de conception, le processus débute par une cellule unitaire passive. Après validation réussie, une version active est développée afin de permettre une modulation de phase dynamique et une reconfiguration du faisceau en temps réel.

Pour chaque type de cellule unitaire, une antenne transmitarray complète, constituée d'un réseau des cellules proposées, est simulée pour démontrer les performances de formation de faisceau. La distribution de phase simulée et les diagrammes de rayonnement en champ lointain confirment la formation de faisceaux directionnels aux angles souhaités, avec un gain élevé et un niveau de lobes secondaires acceptable. Une analyse comparative met en évidence l'efficacité des structures proposées à fournir des performances élevées avec une complexité relativement faible.

En résumé, les résultats valident les antennes transmitarray reconfigurables proposées comme une solution viable pour les applications aux fréquences millimétriques, offrant une plateforme à faible coût, compacte et à haute efficacité, adaptée aux réseaux de communication sans fil 5G et au-delà.

ABSTRACT

Mobile communication systems are advancing quickly which creates demand for faster data speeds and reduced latency especially for multimedia services. Millimeter-wave frequencies represent a promising solution because they provide large available bandwidth and allow the creation of compact and cost-effective RF components. Despite their advantages high-frequency signals struggle with short propagation distances and weak penetration abilities which beamforming antennas help to overcome. Combining beam-switching capabilities with other functions in one reconfigurable antenna structure boosts system performance and saves space while reducing interference. A key research objective for future 5G systems is to develop low-loss, compact, and cost-effective beamforming antennas through the integration of metasurfaces. In this context, this thesis presents comprehensive design and analysis of reconfigurable transmitarray antennas operating at mm-wave frequencies.

Beam-steering antenna systems generally consist of two primary components : a feeding antenna and a metasurface panel. A Substrate Integrated Waveguide (SIW) slot antenna is first proposed as the radiating source due to its high gain, low loss, and high integration capability. In parallel, a 3D-printed horn antenna is also designed and evaluated as a well-understood and easily simulated alternative. These two feed options offer design flexibility : the SIW antenna is suited for final implementation, while the horn antenna is employed in simulations and early-stage prototyping due to its simpler geometry and faster simulation times. Both feeds are intended to operate in conjunction with metasurface panels composed of phase-reconfigurable unit cells.

The metasurface panel, the second main component, is realized using unit cells based on two core concepts : using mutual coupling in a constructive way with current reversal technique and Huygens' principle. For each design methodology, the process begins with a passive unit cell. Following successful validation, an active version is developed to enable dynamic phase modulation and real-time beam reconfiguration.

For each unit cell type, a complete transmitarray antenna comprising an array of the proposed unit cells is simulated to demonstrate beamforming performance. The simulated phase distribution and far-field radiation patterns confirm directional beam steering at desired angles, accompanied by high gain and acceptable side lobe levels. Comparative analysis highlights the effectiveness of the proposed structures in delivering high performance with relatively low complexity.

In summary, the results validate the proposed reconfigurable transmitarray antennas as the viable solution for mm-wave applications, offering a low-cost, compact, and high-efficiency platform suitable for future 5G and beyond wireless communication networks.

Keywords : Reconfigurable Antennas, Transmitarray Antennas, Beamforming Antennas, Millimeter-wave Frequencies, Substrate Integrated Waveguide, Metasurface.

SOMMAIRE RECAPITULATIF

A.1 Titre de la Thèse en Français

ÉTUDE ET CONCEPTION D'ANTENNES RECONFIGURABLES BASÉES SUR DES MÉTA-SURFACES AUX BANDES DE FRÉQUENCES MILLIMÉTRIQUES

A.2 Introduction

Les technologies de communication mobile sont devenues de plus en plus omniprésentes dans la société, grâce à l'utilisation répandue des smartphones et autres appareils mobiles. Par conséquent, les réseaux mobiles doivent répondre aux exigences croissantes des consommateurs en termes de débits plus élevés, tout en faisant face à l'augmentation prévisible du volume de trafic, qui croît à un rythme exponentiel. Dans ce but, les fournisseurs de services cellulaires s'efforcent d'offrir des applications multimédias et vidéos de haute qualité avec une faible latence pour les dispositifs sans fil. Plusieurs avancées technologiques émergent indépendamment afin d'améliorer de manière significative les performances des systèmes de communication sans fil. L'une de ces avancées concerne l'utilisation des bandes de fréquences millimétriques (mm-wave), qui offrent plus de spectres disponibles car elles sont en grande partie inexploitées. De plus, l'utilisation de fréquences plus élevées permet d'obtenir des antennes et des circuits plus petits, rendant ainsi les émetteurs-récepteurs RF plus abordables [1–3].

Même si les hautes fréquences ont le potentiel de transmettre davantage de données, elles sont limitées par leur incapacité à pénétrer et à couvrir de grandes zones. Ainsi, l'une des façons d'étendre la couverture à longue portée consiste à augmenter la puissance d'émission sans accroître le coût du système de communication. Cela peut être accompli en utilisant un grand nombre d'antennes, capables de gérer plusieurs utilisateurs simultanément. Ces antennes peuvent être pilotées par des systèmes intelligents intégrant des techniques de formation de faisceaux (beamforming) et de MIMO (entrées multiples, sorties multiples). Il est donc nécessaire de concevoir une antenne capable d'assurer plusieurs fonctions en les intégrant dans un même élément. Pour résoudre les problèmes d'interférence de rayonnement, cet élément doit pouvoir orienter le faisceau dans une direction précise tout en évitant les faisceaux indésirables dans d'autres directions. Ainsi, les antennes à commutation de faisceau, couramment utilisées dans les antennes à diagramme reconfigurable, ont suscité beaucoup d'intérêt dans les systèmes de communication sans fil. Ces antennes permettent de réduire significativement les signaux d'interférence et d'améliorer la capacité du système. En les utilisant, des fonctionnalités supplémentaires et des propriétés plus flexibles peuvent être obtenues, tout en occupant le même espace physique, voire moins, que les réseaux d'antennes intelligentes traditionnels [4–9].

Par ailleurs, pour répondre aux besoins futurs des consommateurs et de la technologie, les sous-systèmes et composants de formation de faisceaux doivent respecter certains critères, tels qu'une faible perte, une compacité et une facilité de fabrication. Ils doivent également relever les défis liés à la rentabilité de la conception et à l'utilisation de fréquences élevées. Par conséquent,

l'objectif principal de cette thèse est l'étude et la conception d'antennes reconfigurables avec fonctionnalité de beamforming dans les bandes de fréquences mm-wave.

A.3 Motivation

La demande en communication à haute vitesse entre de nombreux utilisateurs et appareils de l'Internet des objets (IoT) est appelée à croître dans un avenir proche en raison de la montée en puissance d'applications telles que les voitures autonomes, les vidéos en réalité virtuelle et la chirurgie à distance. En réponse à ce besoin, une recherche approfondie sera menée sur les antennes reconfigurables à capacité de dépointage de faisceau. Plus précisément, notre objectif est de concevoir et de développer des antennes transmitarray innovantes à fréquences millimétriques, en exploitant les propriétés uniques des métasurfaces.

A.4 Problème

Une antenne reconfigurable est une antenne capable de modifier ses propriétés de rayonnement afin d'améliorer les systèmes de communication sans fil en offrant des fonctionnalités supplémentaires. Cette classification dépend du paramètre d'antenne pouvant être ajusté dynamiquement, incluant généralement la fréquence de fonctionnement, le diagramme de rayonnement ou la polarisation. Pour modifier le diagramme, les courants électriques ou magétiques de la structure rayonnante peuvent être changés en contrôlant les propriétés des matériaux ou en incorporant des éléments parasites autour de l'antenne principale [10].

De plus, plusieurs méthodes existent pour contrôler la direction du faisceau du diagramme de rayonnement, notamment les antennes à lentilles intégrées (ILA) [11–13], les antennes à onde progressive [14, 15], les réseaux adaptatifs [16], les réseaux phasés [17], et les structures actives à bande interdite photonique métallique (AMPBG) [18]. Toutefois, chacune de ces technologies présente des avantages et des inconvénients. Par exemple, les antennes à onde progressive sont généralement encombrantes lorsqu'elles sont utilisées pour le dépointage de faisceau. Les réseaux phasés requièrent un contrôle précis de l'amplitude et de la phase de chaque élément pour orienter le faisceau, ce qui complique leur structure et augmente leur coût de fabrication. De plus, les structures AMPBG sont volumineuses avec des lobes secondaires élevés et une forte polarisation croissée.

Pour surmonter les complexités, la grande taille et le coût élevé des techniques précédentes, les chercheurs se sont récemment tournés vers les métasurfaces pour le dépointage de faisceau [19–22]. Dans [23], une antenne à dépointage électrique est créée en connectant une métasurface à des diodes varactors. En manipulant la tension de polarisation, une couverture de 360° du diagramme de rayonnement peut être réalisée pour les modes à faisceau unique et à double faisceau. Bien que les diodes PIN présentent un comportement non linéaire, elles sont couramment utilisées pour reconfigurer la réponse électromagnétique (EM). En contrôlant les caractéristiques de transmission et de réflexion des diodes PIN, il est possible de diriger les ondes EM incidentes [24–28]. Par exemple, dans [29], 48 diodes PIN ont été utilisées pour réaliser le dépointage, mais ce grand nombre d'éléments actifs a augmenté la complexité de la conception et le coût de fabrication. Un autre chercheur a proposé une antenne à dépointage avec moins d'éléments actifs insérés dans une géométrie cylindrique [30].

A.5 Objectif de la recherche

L'objectif principal de cette thèse est le développement d'une nouvelle classe d'antennes transmitarray reconfigurables avec capacité de formation de faisceaux pour les futurs systèmes de communication sans fil à fréquences millimétriques. Cette recherche est menée dans le cadre d'un projet financé par l'industrie, dans lequel l'entreprise partenaire a spécifié des objectifs de performance clés, incluant une configuration d'antenne beamforming centrée à 28 GHz (fonctionnant dans la plage 27–29 GHz), un gain réalisé supérieur à 16 dBi, et des lobes secondaires inférieurs à –10 dB. Pour atteindre ces objectifs, étant donné qu'une antenne transmitarray reconfigurable pour le dépointage de faisceau comprend généralement deux composants principaux - une antenne d'alimentation et un panneau de métasurface - cette thèse se concentre sur la conception et l'intégration de ces deux éléments. Ces composants sont intégrés pour former un système transmitarray complet capable de dépointage dynamique du faisceau à des fréquences mm-wave. Ainsi, les objectifs spécifiques de la thèse sont :

- Concevoir et évaluer deux types d'antennes d'alimentation :

  (1) Une antenne à fente intégrée sur guide d'onde (SIW) pour l'implémentation finale.

  (2) Une antenne à cornet pour la simulation simplifiée et le prototypage.

- Concevoir et analyser des panneaux de métasurface composés de cellules unitaires à phase reconfigurable selon deux principes, en configuration passive et active :

  (1) Couplage mutuel avec technique d'inversion de courant.

  (2) Principe de Huygens.

A.6 Méthodologie

Sur la base des objectifs de recherche, cette thèse sera généralement réalisée en deux principaux volets de travail.

A.6.1 Volet de Travail 1 (Antennes d'alimentation)

La technologie SIW (Substrate Integrated Waveguide) est une méthode efficace pour alimenter des antennes planaires et des réseaux dans la bande des ondes millimétriques. Ces réseaux d'alimentation seront utilisés pour alimenter des réseaux d'antennes mm-wave à l'aide de fentes et de patches, comme illustré à la Figure 1.1.a. La conception de réseaux d'antennes basés sur la technologie SIW promet un gain plus élevé, un fonctionnement à large bande, une faible perte et une grande efficacité. De plus, l'antenne à cornet constitue une alternative simplifiée et bien connue. Ces deux options d'alimentation offrent une grande flexibilité : l'antenne SIW est destinée à l'implémentation finale, tandis que l'antenne à cornet, grâce à sa géométrie plus simple et à la réduction de la complexité de simulation, est préférée pour les premières simulations et le prototypage. Les deux structures d'alimentation sont conçues pour fonctionner avec des panneaux de métasurface.

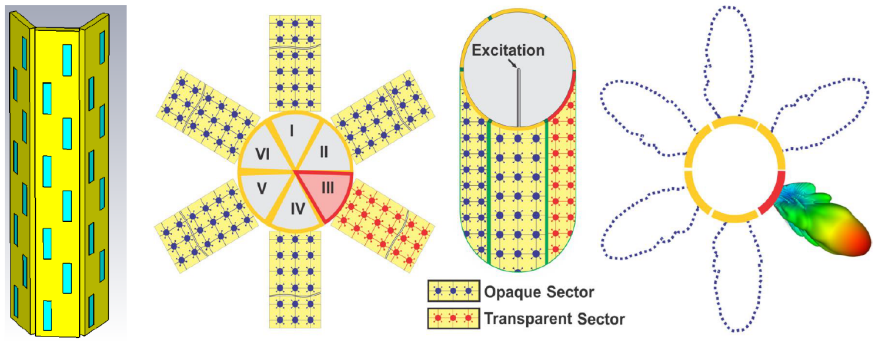

(a) (b) (c) (d)

FIGURE A.1 : (a) Conception d'un réseau d'antennes utilisant la technologie SIW servant de source pour les antennes reconfigurables, concept proposé pour les antennes reconfigurables utilisant des structures de métasurfaces, (b) Vue éclatée, (c) Vue en perspective, (d) Concept de fonctionnement.

A.6.2 Volet de Travail 2 (Métasurfaces)

Dans la deuxième partie, la recherche proposée se concentrera sur l'étude et l'investigation de structures périodiques électromagnétiques accordables, notamment les métasurfaces, ainsi que sur l'exploration de leurs propriétés pour améliorer les caractéristiques de rayonnement et le gain des antennes reconfigurables mm-wave à diagrammes de rayonnement dynamiques, comme illustré aux Figures 1.1.b-d.

Récemment, les métasurfaces ont suscité un grand intérêt dans le domaine des antennes en raison de leur capacité à contrôler la propagation des ondes électromagnétiques. Ces structures sont des réseaux planaires diélectriques ou métalliques périodiques qui peuvent effectuer un filtrage spectral, spatial ou angulaire des ondes électromagnétiques incidentes. Elles peuvent être configurées comme des surfaces transparentes ou opaques aux ondes électromagnétiques dans une certaine bande de fréquence, ce qui permet de contrôler la propagation des ondes. Cette technologie fascinante peut fournir des solutions innovantes et très efficaces à des problèmes critiques de conception d'antennes. Plus particulièrement, pour les antennes reconfigurables avec fonctionnalité de formation de faisceaux, l'utilisation de structures de métasurfaces devient particulièrement attrayante [19–22]. En contrôlant la propagation des ondes grâce à ces structures, nous pouvons concevoir de nouvelles antennes reconfigurables avec des capacités de beamforming.

A.7 Contributions

Les principales contributions de cette thèse peuvent être résumées comme suit :

Stratégie d'alimentation double : Deux antennes d'alimentation différentes, une antenne compacte à fente SIW et une antenne à cornet, ont été conçues et utilisées. Cette approche double offre une flexibilité pour l'implémentation pratique et l'évaluation par simulation.

Conception de nouvelles cellules unitaires : Deux méthodologies distinctes de conception de cellules unitaires pour les transmitarrays millimétriques ont été développées, l'une basée sur le couplage mutuel et la technique d'inversion de courant, et l'autre sur le principe de Huygens.

Configurations passives et actives : Des versions passives et actives (1-bit) de chaque cellule unitaire ont été réalisées. Les conceptions actives intègrent des diodes PIN pour permettre une reconfigurabilité de phase et un dépointage dynamique du faisceau à 28 GHz.

Implémentation de transmitarrays : Les cellules unitaires proposées ont été intégrées dans des panneaux transmitarray complets. Les capacités de beamforming ont été démontrées par des simulations électromagnétiques complètes, confirmant le contrôle directionnel et la manipulation de phase.

Évaluation complète des performances : Les systèmes d'antennes proposés ont été analysés en termes de gain, de niveau des lobes secondaires, de performance de formation de faisceau et de compromis de conception. Les résultats confirment la viabilité des structures proposées pour les futures applications sans fil haute fréquence, y compris la 5G et au-delà.

Ces contributions font progresser le développement d'antennes millimétriques reconfigurables, offrant des solutions compactes, à faibles pertes et rentables pour les systèmes de formation de faisceau de nouvelle génération.

A.8 Structure de la Thèse

La structure de la thèse comprend six chapitres principaux, détaillés ci-dessous :

Chapitre 1 (Introduction) : Ce chapitre présente la motivation de la recherche, la problématique, les objectifs ainsi que la méthodologie. Il donne également un aperçu de la structure de la thèse avec une liste des publications associées et des distinctions reçues.

Chapitre 2 (Revue de la littérature) : Ce chapitre couvre les avancées récentes et les résultats de recherche sur les antennes transmitarray basées sur les métasurfaces. Les concepts clés tels que les techniques de formation de faisceau, les métasurfaces reconfigurables et les compromis de conception y sont discutés afin de justifier le travail proposé.

Chapitre 3 (Conception des alimentations) : Ce chapitre présente la conception et le développement de deux antennes d'alimentation différentes, y compris une antenne SIW et une antenne à cornet, utilisées pour illuminer les structures transmitarray proposées.

Chapitre 4 (Cellule unitaire basée sur le couplage mutuel et l'inversion de courant) : Ce chapitre introduit une nouvelle cellule unitaire passive 1-bit et une version active basée sur le couplage mutuel et la technique d'inversion de courant pour améliorer le contrôle du faisceau. Leur performance en configuration transmitarray est évaluée.

Chapitre 5 (Cellule unitaire basée sur le principe de Huygens) : Ce chapitre présente la conception et l'implémentation d'une cellule unitaire fondée sur le principe de Huygens. Deux versions de cette cellule ainsi que leurs configurations transmitarray respectives sont analysées et comparées.

Chapitre 6 (Conclusion et perspectives) : Ce chapitre résume les principaux résultats de la thèse et discute des perspectives futures dans le domaine des antennes reconfigurables et des technologies de formation de faisceaux à haute efficacité.

A.9 Publications

Revues Scientifiques :

1. **P. PourMohammadi**, H. Naseri, N. Melouki, F. Ahmed, Q. Zheng, A. Iqbal, and T. A. Denidni, “A Wideband Beam Steering Transmitarray Antenna for Ka-Band Applications,” AEU-International Journal of Electronics and Communications, 2025.
2. **P. PourMohammadi**, H. Naseri, N. Melouki, F. Ahmed, Q. Zheng, A. Iqbal, G. A. Vandenbosch and T. A. Denidni, “Highly isolated compact self-diplexing antenna,” AEU-International Journal of Electronics and Communications, vol. 173, p. 155025, 2024.
3. **P. PourMohammadi**, H. Naseri, N. Melouki, F. Ahmed, M.S. Bizan, A. Iqbal, and T. A.Denidni, “A Fabry–Perot antenna using a frequency selective surface layer with wideband and Low RCS for Mm-wave applications,” AEU-International Journal of Electronics and Communications, vol. 169, p. 154736, 2023.
4. **P. PourMohammadi**, H. Naseri, N. Melouki, F. Ahmed, A. Iqbal, G. A. Vandenbosch and T. A. Denidni, “Compact SIW-based self-quadruplexing antenna for microwave and mm-wave communications,” IEEE Transactions on Circuits and Systems II : Express Briefs, vol. 70, no. 9, pp. 3368–3372, 2023.
5. **P. PourMohammadi**, P. Fei, H. Naseri, Q. Zheng, O. J. Babarinde, V. Volski, G. A. Vandenbosch, and T. A. Denidni, “A Single-Layer Compact Wideband Circularly Polarized Patch Array for 5G Communications,” IEEE Antennas and Wireless Propagation Letters, vol. 22, no. 4, pp. 754–758, 2022.
6. **P. PourMohammadi**, H. Naseri, N. Melouki, F. Ahmed, and A. Iqbal, and T. A. Denidni, “Substrate integrated waveguide-based full-duplex antenna with improved out-of-band suppression,” IEEE Transactions on Circuits and Systems II : Express Briefs, vol. 70, no. 4, pp. 1430–1434, 2022.
7. N. Melouki, F. Ahmed, **P. PourMohammadi**, H. Naseri, and T. A. Denidni, “Wideband transmitarray with independent phase/amplitude control for millimeter-wave vehicular sensing and communication,” AEU-International Journal of Electronics and Communications, 2025.
8. M. S. Bizan, **P. PourMohammadi**, A. Iqbal, and T. A. Denidni, “High-gain dual-band antenna with independent frequency operation for Sub-6 GHz and millimeter-wave applications,” AEU-International Journal of Electronics and Communications, 2025.
9. N. Melouki, F. Ahmed, **P. PourMohammadi**, H. Naseri, and T. A. Denidni, “Wideband Transmitarray with Independent Phase/Amplitude Control for MillimeterWave Vehicular Sensing and Communication,” AEU-International Journal of Electronics and Communications, 2025.
10. Z. Mousavirazi, M. M. Ali, **P. PourMohammadi**, P. Fei, T. A. Denidni, “High-Performance CP Magneto-Electric Dipole Antenna Fed by Printed Ridge Gap Waveguide at Millimeter-Wave,” Sensors, vol. 24, no. 24, 2024.
11. F. Ahmed, F. Faisal, N. Melouki, A. Ahmed, H. Naseri, **P. PourMohammadi**, and Tayeb A. Denidni, “A Multi-Functional Reflective Polarization Transforming Surface with In-Band and Out-Band Transmission Characteristics,” IEEE Antennas and Wireless Propagation Letters, pp. 1–5, 2024.
12. F. Ahmed, A. Ahmed, N. Melouki, **P. PourMohammadi**, H. Naseri Gheisanab, N. Shoaib, T. A Denidni “A wideband bianisotropic FSS absorber with angular stable and polarization-insensitive properties,” Waves in Random and Complex Media, pp. 1–16, 2024.

13. N. Melouki, F. Ahmed, **P. PourMohammadi**, H. Naseri, M. S. Bizan, A. Iqbal, and T. A. Denidni, "3D-Printed Conformal Meta-Lens with Multiple Beam-Shaping Functionalities for Mm-Wave Sensing Applications," Sensors, vol. 24, no. 9, p. 2826, 2024.
14. H. Naseri, **P. PourMohammadi**, N. Melouki, F. Ahmed, A. Iqbal, and T. Denidni, "Frequency-adjustable OAM antenna with co-divergent beams for IoT applications," AEU-International Journal of Electronics and Communications, vol. 177, p. 155188, 2024.
15. H. Naseri, **P. PourMohammadi**, N. Melouki, F. Ahmed, A. Iqbal, and T. A. Denidni, "Reconfigurable OAM Antenna with Flexibility on Mode Numbers, Polarization and Frequency," IEEE Antennas and Wireless Propagation Letters, 2024.
16. N. Melouki, **P. PourMohammadi**, H. Naseri, F. Ahmed, A. Iqbal, and T. A. Denidni, "Ultra-compact Quarter-Mode SIW Self-Hexaplexing Antenna for C-band and X-band Applications," IEEE Antennas and Wireless Propagation Letters, 2023.
17. F. Ahmed, T. Hassan, N. Melouki, H. Naseri, **P. PourMohammadi**, A. Iqbal, and T. A. Denidni, "A multi-bit and frequency-reconfigurable reflecting surface for RIS applications," IEEE Antennas and Wireless Propagation Letters, 2023.
18. H. Naseri, **P. PourMohammadi**, P. Fei, N. Melouki, A. Iqbal, and T. Denidni, "Butler matrix-based beamforming with polarization reconfigurability for reducing electromagnetic interference," AEU-International Journal of Electronics and Communications, vol. 170, p. 154833, 2023.
19. M. S. Bizan, H. Naseri, **P. PourMohammadi**, N. Melouki, A. Iqbal, and T. A. Denidni, "Dual-band dielectric resonator antenna with filtering features for microwave and mm-wave applications," Micromachines, vol. 14, no. 6, p. 1236, 2023.
20. H. Naseri, **P. PourMohammadi**, N. Melouki, F. Ahmed, A. Iqbal, and T. A. Denidni, "Substrate integrated waveguide-based dual-polarized self-diplexing antenna array," IEEE Transactions on Circuits and Systems II : Express Briefs, vol. 70, no. 8, pp. 2839–2843, 2023.
21. H. Naseri, **P. PourMohammadi**, N. Melouki, F. Ahmed, A. Iqbal, and T. A. Denidni, "Generation of mixed-OAM-carrying waves using huygens' metasurface for mm-wave applications," Sensors, vol. 23, no. 5, p. 2590, 2023.
22. H. Naseri, **P. PourMohammadi**, Z. Mousavirazi, A. Iqbal, G. A. Vandenbosch, and T. A. Denidni, "A Low-Profile Dual-Band Hybrid Coupler with Flexible Frequency Band Ratio," Progress in Electromagnetics Research Letters. Nov 1;107, 2022.
23. H. Naseri, **P. PourMohammadi**, N. Melouki, A. Iqbal, and T. A. Denidni, "A low-profile antenna system for generating reconfigurable OAM-carrying beams," IEEE Antennas and Wireless Propagation Letters, vol. 22, no. 2, pp. 402–406, 2022.
24. N. Melouki, A. Hocini, F. Z. Fegriche, **P. PourMohammadi**, H. Naseri, A. Iqbal, and T. A. Denidni, "High-gain wideband circularly polarised Fabry–Perot resonator array antenna using a single-layered pixelated PRS for millimetre-wave applications," Micromachines, vol. 13, no. 10, p. 1658, 2022.
25. H. Naseri, **P. PourMohammadi**, A. Iqbal, A. A. Kishk, and T. A. Denidni, "SIW-based self-quadruplexing antenna for microwave and mm-wave frequencies," IEEE Antennas and Wireless Propagation Letters, vol. 21, no. 7, pp. 1482–1486, 2022.

Conférences :

1. **P. PourMohammadi**, H. Naseri, N. Melouki and T. Denidni, "Single-Layer Electronically Beam Steering Transmitarray Antenna for the Ka-band Applications," in 2025 IEEE International

Symposium on Antennas and Propagation and USNC-URSI Radio Science Meeting (USNC-URSI), 2025 (Accepted).

2. **P. PourMohammadi**, H. Naseri, N. Melouki and T. Denidni, "A 1-Bit Wideband Electronically Beam Steering Transmitarray For 5G Communication Systems," in 2024 IEEE International Symposium on Antennas and Propagation and USNC-URSI Radio Science Meeting (USNC-URSI), 2024.
3. **P. PourMohammadi**, H. Naseri, F. Ahamed and T. Denidni, "A Wideband Transmit Array based on Huygens' Metasurface for Millimeter-Wave Applications," in 2024 IEEE International Symposium on Antennas and Propagation and USNC-URSI Radio Science Meeting (USNC-URSI), 2024.
4. **P. PourMohammadi**, H. Naseri, N. Melouki, F. Ahmed, A. Iqbal, G. A. Vandenbosch and T. A. Denidni, "A low-profile self-duplexing antenna for millimeter-wave and microwave frequency bands," in 2023 IEEE international symposium on antennas and propagation and USNC-URSI radio science meeting (USNC-URSI), 2023, pp. 605–606.
5. **P. PourMohammadi**, H. Naseri, N. Melouki, F. Ahmed, M. Bizan, A. Iqbal and T. A.Denidni, "A Wideband Fabry-Perot Antenna with a Bianisotropic FSS Layer," in 2023 IEEE International Symposium on Antennas and Propagation and USNC-URSI Radio Science Meeting (USNC-URSI), 2023 Jul 23, pp. 649-650.
6. **P. PourMohammadi**, H. Naseri, N. Melouki, F. Ahmed, M. Bizan, A. Iqbal and T. A. Denidni, "A Wideband Anisotropic Metasurface for Cross-Polarization Applications," 2023 URSI International Symposium on Electromagnetic Theory, 2023.
7. **P. PourMohammadi**, H. Naseri, R. Alwahishi, G. A. Vandenbosch, and T. A. Denidni, "A 2×3 high-gain coupled patch array for body area network applications," in 2022 IEEE international symposium on antennas and propagation and USNC-URSI radio science meeting (AP-S/URSI), 2022, pp. 2068–2069.
8. H. Naseri, **P. PourMohammadi**, M. Bizan and T. A. Denidni, "Dual-Polarized Reconfigurable Beam-Steering Using the New Feeding Network Topology," in 2025 IEEE International Symposium on Antennas and Propagation and USNC-URSI Radio Science Meeting (USNC-URSI), 2025 (Accepted).
9. N. Melouki, F. Ahmed, **P. PourMohammadi** and T. A. Denidni, "Hybrid 3D-Printed Lens with 360° Beam-Steering for UAV Search and Rescue and Advanced 5G Communication," in 2025 IEEE International Symposium on Antennas and Propagation and USNC-URSI Radio Science Meeting (USNC-URSI), 2025 (Accepted).
10. H. Wu, H. Naseri, **P. PourMohammadi**, F. Abderrazak and T. A. Denidni, "Reconfigurable Dual-band OAM Antenna for Microwave and Millimeter-Wave Applications," in 2025 IEEE International Symposium on Antennas and Propagation and USNC-URSI Radio Science Meeting (USNC-URSI), 2025 (Accepted).
11. F. Ahmed, N. Melouki, **P. PourMohammadi** and T. Denidni, "A Reconfigurable Dual-Band Transmit Array Antenna for K-Band and Millimeter-Wave Applications," in 2025 IEEE International Symposium on Antennas and Propagation and USNC-URSI Radio Science Meeting (USNC-URSI), 2025 (Accepted).
12. H. Naseri, **P. PourMohammadi**, N. Melouki, F. Ahmed, A. Iqbal, and T. A. Denidni, "Dual-Polarized OAM Antenna with Frequency and Mode Agility for Intelligent OAM Communications," in 2024 18th European Conference on Antennas and Propagation (EuCAP), 2024, pp. 1–4.
13. N. Melouki, F. Ahmed, H. Nasseri, **P. PourMohammadi**, A. Iqbal, and T. A. Denidni, "Multi-Bit Wideband Transmitarray Aperture with Independent Phase and Amplitude Control for

High Gain with Low Sidelobe Mm-Wave Applications," in 2024 18th European Conference on Antennas and Propagation (EuCAP), 2024, pp. 01–04.

14. F. Abderrazak, **P. PourMohammadi**, L. Talbi, E. Antonino-Daviu, T. Denidni and M. Ferrando-Bataller, "Selective Excitation Technique for Wireless Power Transfer in Wearable Devices Using CMA," in 7th Conference on Cloud and Internet of Things (IEEE/IFIP 2024 CIoT), 2024.
15. N. Melouki, F. Ahmed, **P. PourMohammadi** and T. A. Denidni, "3D-Printed Conformal Meta-Lens with Multi-mode Orbital Angular Momentum (OAM) Generation and Beam-steering Capabilities," in 2024 IEEE International Symposium on Antennas and Propagation and USNC-URSI Radio Science Meeting (USNC-URSI), 2024.
16. H. Naseri, **P. PourMohammadi**, M. Bizan and T. A. Denidni, "Butler Matrix-based Beam Switching with Frequency-tunable MIMO Array," in 2024 IEEE International Symposium on Antennas and Propagation and USNC-URSI Radio Science Meeting (USNC-URSI), 2024.
17. F. Ahmed, N. Melouki, **P. PourMohammadi** and T. Denidni, "A Multifunctional Bianisotropic Frequency Selective Surface for Microwave Applications," in 2024 IEEE International Symposium on Antennas and Propagation and USNC-URSI Radio Science Meeting (USNC-URSI), 2024.
18. M. Bizan, H. Naseri, **P. PourMohammadi** and T. A. Denidni, "Ultra-Wideband Dielectric Resonator Antenna Fed by Printed Ridge Gap Waveguide Technology," in 2024 IEEE International Symposium on Antennas and Propagation and USNC-URSI Radio Science Meeting (USNC-URSI), 2024.
19. M. S. Bizan, H. Naseri, **P. PourMohammadi**, and T. A. Denidni, "Integrate Fabry–Perot Resonator into Dielectric Resonator Antenna for Microwave and Mm-wave Operations," in 2023 IEEE International Symposium on Antennas and Propagation and USNC-URSI Radio Science Meeting (USNC-URSI), 2023, pp. 1161–1162.
20. F. Ahmed, N. Melouki, **P. PourMohammadi**, H. Naseri and T. A. Denidni, "A 2-Bit Reconfigurable Reflecting Metasurface for Mm-Wave Applications," in 2023 IEEE International Symposium on Antennas and Propagation and USNC-URSI Radio Science Meeting (USNC-URSI), 2023 Jul 23, pp. 1425–1426.
21. H. Naseri, **P. PourMohammadi**, M. Bizan, N. Melouki, F. Ahmed, A. Iqbal and T. A. Denidni, "Reconfigurable Dielectric Resonator OAM Antenna with Augmented Modes," in 2023 IEEE International Symposium on Antennas and Propagation and USNC-URSI Radio Science Meeting (USNC-URSI) 2023 Jul 23 (pp. 703-704). IEEE.
22. N. Melouki, F. Ahmed, **P. PourMohammadi**, H. Naseri and T. A. Denidni, "3D-Printed Conformal Metamaterial Lens with Multiple Beam Steering Functionalities," in 2023 IEEE International Symposium on Antennas and Propagation and USNC-URSI Radio Science Meeting (USNC-URSI) 2023 Jul 23 (pp. 791-792). IEEE.
23. H. N. Gheisanab, **P. PourMohammadi**, N. Melouki, A. Iqbal, and T. A. Denidni, "Self-diplexing Antenna Operating at Sub-6 GHz and Millimeter-wave Frequency Bands," in 2023 17th European Conference on Antennas and Propagation (EuCAP), 2023, pp. 1–3.
24. H. Naseri, **P. PourMohammadi**, M. Bizan, N. Melouki, F. Ahmed, A. Iqbal, and T. A. Denidni, "Triple-Mode OAM Generating Dielectric Resonator Antenna," 2023 URSI International Symposium on Electromagnetic Theory, 2023.
25. M. Bizan, H. Naseri, **P. PourMohammadi**, A. Iqbal and T. A. Denidni, "Ultra-Wideband Dielectric Resonator Antenna with Integrated Fabry-Perot Cavity," 2023 URSI International Symposium on Electromagnetic Theory, 2023.

26. F. Ahmed, N. Melouki, **P. PourMohammadi**, H. Naseri and T. A. Denidni, “4-Bit Reconfigurable Reflecting Metasurface for Sub-6 GHz Band,” 2023 URSI International Symposium on Electromagnetic Theory, 2023.
27. N. Melouki, F. Ahmed, **P. PourMohammadi**, H. Naseri and T. A. Denidni, “Low-Loss 2-Bit Reflective Intelligent Surface for mm-Wave Applications,” 2023 URSI International Symposium on Electromagnetic Theory, 2023.
28. H. Naseri, **P. PourMohammadi**, Z. Mousavirazi, A. Iqbal, and T. A. Denidni, “Full azimuth beam steering by means of radiation pattern with the narrow beamwidth,” in 2022 IEEE International Symposium on Antennas and Propagation and USNC-URSI Radio Science Meeting (AP-S/URSI), 2022, pp. 1630–1631.
29. R. Alwahishi, **P. PourMohammadi**, M. M. M. Ali, and T. A. Denidni, “A dual-band intelligent frequency selective surface unit cell for future communication systems,” in 2022 IEEE International Symposium on Antennas and Propagation and USNC-URSI Radio Science Meeting (AP-S/URSI), 2022, pp. 986–987.

A.10 Réalisations

1. Classé 1er – Récipiendaire de la bourse de recherche postdoctorale du FRQNT, Fonds de recherche du Québec, Canada, 2025.
2. Récipiendaire de la subvention de participation à une conférence, INRS, Université du Québec, Canada, 2025.
3. Reconnaissance de la contribution en tant que mentor, INRS, Université du Québec, Canada, 2025.
4. Classé 2^{e} – Récipiendaire de la bourse de recherche doctorale du FRQNT, Fonds de recherche du Québec, Canada, 2024.
5. Reconnaissance de la contribution en tant que mentor, INRS, Université du Québec, Canada, 2024.
6. Sélectionné par l’INRS, Université du Québec, pour le concours du programme PBEEE, Canada, 2023.
7. Sélectionné comme l’un des 48 récipiendaires à l’échelle mondiale du prix AP-S Fellowship, Antenna Propagation Society (AP-S), 2023.
8. Classé 2^{e} – Meilleur prix d’affiche étudiante, STARaCom, Université McGill, Canada, 2023.

A.11 Honneurs

1. Rédacteur en chef invité principal du numéro spécial de *Electronics* (Q1), 2025.
2. Coprésident de session « Transmitarrays et métasurfaces transmissives » à l’IEEE AP-S/URSI, Ottawa, Canada, 2025.
3. Coprésident de session « Antennes multibandes » à l’IEEE AP-S/URSI, Ottawa, Canada, 2025.
4. Coprésident général du Colloque scientifique de l’INRS-EMT, avril 2023 – avril 2024.

TABLE DES MATIÈRES

REMERCIEMENTS ..... **vii**
ACKNOWLEDGMENT ..... **ix**
RÉSUMÉ ..... **xi**
ABSTRACT ..... **xiii**
SOMMAIRE RECAPITULATIF ..... **xv**
A.1 Titre de la Thèse en Français xv
A.2 Introduction xv
A.3 Motivation xvi
A.4 Problème xvi
A.5 Objectif de la recherche xvii
A.6 Méthodologie xvii
A.6.1 Volet de Travail 1 (Antennes d'alimentation) xvii
A.6.2 Volet de Travail 2 (Métasurfaces) xviii
A.7 Contributions xviii
A.8 Structure de la Thèse xix
A.9 Publications xx
A.10 Réalisations xxiv
A.11 Honneurs xxiv
TABLE DES MATIÈRES ..... **xxv**
LISTE DES FIGURES ..... **xxvii**
LISTE DES TABLEAUX ..... **xxxiii**
LISTE DES ABREVIATIONS ..... **xxxv**
1 INTRODUCTION **1**
1.1 Motivation 2
1.2 Problem 2
1.3 Research Objective 3
1.4 Methodology 3
1.4.1 Work Package 1 (Feed Antennas) 3
1.4.2 Work Package 2 (Metasurfaces) 4
1.5 Contributions 4

1.6 PUBLICATIONS 5
1.7 ACHIEVEMENTS 10
1.8 HONORS 11
1.9 OUTLINE OF THE THESIS 11
2 LITERATURE REVIEW 13
2.1 INTRODUCTION 13
2.2 FUNDAMENTALS OF METASURFACE-BASED TRANSMITARRAY ANTENNAS 13
2.3 TRANSMITARRAY ANTENNAS AND BEAM STEERING TECHNIQUES 14
2.3.1 Concepts and approaches 14
2.3.2 Conventional Beam Steering Techniques and Limitations 16
2.4 EMERGENCE AND ADVANCES OF RECONFIGURABLE METASURFACES 18
2.5 KEY RESEARCH TRENDS AND DEVELOPMENTS 19
2.5.1 Fixed vs. Reconfigurable Transmitarrays 19
2.5.2 Analog vs. Digital Beam Control 19
2.5.3 1-Bit vs. Multi-Bit Phase Designs 20
2.5.4 Material Innovations in Transmitarrays 20
2.5.5 Application-Specific Transmitarray Designs 21
2.6 CONCLUSION 23
3 FEED ANTENNA 26
3.1 INTRODUCTION 26
3.2 PROPOSED SIW ANTENNA 26
3.3 PROPOSED HORN ANTENNA CONFIGURATION 31
3.4 SUMMARY 35
4 UNIT CELL DESIGN BASED ON USING MUTUAL COUPLING IN A CONSTRUCTIVE WAY AND CURRENT REVERSAL TECHNIQUE 37
4.1 1-BIT PASSIVE UNIT CELL CONFIGURATION 37
4.1.1 Introduction 37
4.1.2 Proposed Passive Unit Cell 40
4.1.3 Transmitarray Configuration 43
4.1.4 Results and Discussions 46
4.1.5 Conclusion 50
4.2 ACTIVE UNIT CELL DESIGN AND IMPLEMENTATION 51
4.2.1 PIN Diode Characterization 51

4.3 Proposed Active Unit Cell 52
4.4 Summary 58
5 DESIGN OF HUYGENS-BASED METASURFACE UNIT CELLS 65
5.1 Passive Unit Cell Design and Implementation 65
5.1.1 Introduction 65
5.1.2 Proposed Passive Unit Cell 66
5.1.3 Transmitarray Configuration 68
5.1.4 Conclusion 71
5.2 Active Unit Cell Design and Implementation 71
5.2.1 Introduction 72
5.2.2 Proposed Active Unit Cell 73
5.2.3 Transmitarray Configuration 75
5.2.4 Conclusion 78
5.3 Summary 78
6 CONCLUSION AND FUTURE WORK 80
6.1 Conclusions 80
6.2 Future Work 81
BIBLIOGRAPHIE 85

LISTE DES FIGURES

FIGURE A.1 (A) CONCEPTION D'UN RÉSEAU D'ANTENNES UTILISANT LA TECHNOLOGIE SIW SERVANT DE SOURCE POUR LES ANTENNES RECONFIGURABLES, CONCEPT PROPOSÉ POUR LES ANTENNES RECONFIGURABLES UTILISANT DES STRUCTURES DE MÉTASURFACES, (B) VUE ÉCLATÉE, (C) VUE EN PERSPECTIVE, (D) CONCEPT DE FONCTIONNEMENT xviii

FIGURE 1.1 (A) ANTENNA ARRAY DESIGN USING SIW TECHNOLOGY THAT WILL BE USED AS A SOURCE FOR RECONFIGURABLE ANTENNAS, THE PROPOSED CONCEPT FOR RECONFIGURABLE ANTENNAS USING METASURFACE STRUCTURES, (B) EXPLODED VIEW, (C) PERSPECTIVE VIEW, (D) OPERATING CONCEPT 4

FIGURE 2.1 (A) SKETCH OF THE PROPOSED ULTRATHIN HMTS-BASED FLAT-LENS ANTENNA, (B) PHASE COMPENSATION OF HMTS-BASED FLAT-LENS ANTENNA 14

FIGURE 2.2 OPERATION PRINCIPLE OF A TRANSMITARRAY BASED ON RT CONFIGURATION 15

FIGURE 2.3 EXPERIMENTAL SETUP FOR THE 2D LUNEBURG LENS BASED ON COMPLEMENTARY I-SHAPED METAMATERIALS 15

FIGURE 2.4 ARRANGEMENT ON MULTILAYER TRANSMITARRAY 16

FIGURE 2.5 MANUFACTURED THREE LENS ANTENNAS FOR MECHANICALLY BEAMSTEERING .. 16

FIGURE 2.6 (A) ANALOG (B) DIGITAL BEAMFORMING 17

FIGURE 2.7 SWITCHED-BEAM LENS ANTENNA 17

FIGURE 2.8 PHOTOGRAPHS OF FABRICATED RECONFIGURABLE HMTS-BASED FLAT LENS PROTOTYPE 18

FIGURE 2.9 PHOTOGRAPHS OF FABRICATED RECONFIGURABLE TRANSMITARRAY PROTOTYPE 18

FIGURE 2.10 FABRICATED METASURFACE CYLINDRICAL LENS ANTENNA 19

FIGURE 2.11 ELECTRONICALLY RECONFIGURABLE TRANSMITARRAY 19

FIGURE 2.12 DEPICTION OF TRANSMITARRAY LENS MOUNTED ON SATELLITE 22

FIGURE 2.13 TRANSMITARRAY ANTENNA IN VEHICULAR SENSING AND COMMUNICATION 22

FIGURE 2.14 CONCEPTUAL ILLUSTRATION OF A TRANSMIT ARRAY ANTENNA IN BASE STATIONS 23

FIGURE 2.15 SCHEMATICS OF A CONFORMAL TRANSMITARRAY INTEGRATED WITH AN UAV ... 23

FIGURE 3.1 (A) BASIC STRUCTURE OF SIW SLOT ANTENNA, (B) STEP 1, (C) STEP 2, (D) STEP 3, AND (E) STEP 4 OF THE PROPOSED SIW SLOT ANTENNA 28

FIGURE 3.2 RADIATION PATTERNS OF THE PROPOSED SIW ANTENNA FOR DIFFERENT EXCITATION PORTS 28

Figure 3.3 Proposed SIW slot antenna (a) configuration (b) prototype (c) the reflection coefficient 29

Figure 3.4 Proposed SIW slot antenna : (a) transmission coefficients (b) gain ... 29

Figure 3.5 Radiation pattern of the proposed SIW slot antenna 30

Figure 3.6 Configuration of the beamforming structure using proposed SIW slot antenna..... 30

Figure 3.7 Proposed 3D-printed horn antenna (D = 26.2, Wa = 8.6, La = 4.3, Wb = 24.5, Lb = 20, all in mm)..... 32

Figure 3.8 Fabricated prototype of the proposed 3D-printed antenna..... 32

Figure 3.9 (a) Reflection coefficient, and (b) measurement setup of the proposed 3D-printed horn antenna..... 33

Figure 3.10 The radiation pattern of the proposed 3D-printed horn antenna for different frequencies..... 33

Figure 3.11 (a) Proposed configuration of the transmitarray antenna, (b) etched layout for connections and wiring, (c) proposed antenna enclosed with radome, (d) standalone radome structure..... 34

Figure 4.1 Configuration of the proposed 1-bit unit cell 40

Figure 4.2 Vector plot of the current distribution on the proposed unit cell (a) top layer, (b) bottom layer at 28 GHz, and (c) the equivalent circuit model of the proposed unit cell 41

Figure 4.3 Electric field on the proposed structure..... 41

Figure 4.4 Simulated transmission results 42

Figure 4.5 The schematic of a linear transmitarray antenna 43

Figure 4.6 (a) Linear Metasurface Lens using single feed antenna (b) electric field at 28 GHz and (c) steering the beam to Theta = 25 degree, in COMSOL..... 45

Figure 4.7 (a) Linear metasurface lens using the proposed horn antenna as a feed antenna, (b) steering the beam to Theta = 0 degree, (c) steering the beam to Theta = 15 degree, (d) steering the beam to Theta = -30 degree..... 45

Figure 4.8 (a) Linear metasurface lens using the proposed SIW slot antenna as a feed antenna, (b) steering the beam to Theta = 0 degree, (c) steering the beam to Theta = 30 degree..... 46

Figure 4.9 Initial phase distributions at (a) 0°,(b) 30°, and (c) 50° 46

Figure 4.10 Illustration of (a) illumination loss, (b) spillover loss..... 47

Figure 4.11 (a) Fabricated prototype with mounting block, (b) the measurement setup in the anechoic chamber..... 48

Figure 4.12 Simulated and measured normalized radiation patterns of the proposed TA at 28 GHz (a) E-planes, and (b) H-planes for beam-steered at 0°, 30°, and 50° 48

Figure 4.13 Simulated and measured peak gains and the corresponding aperture efficiencies 49
Figure 4.14 (a) microstrip line with gap, (b) micro stripline with diode installed 52
Figure 4.15 The proposed active unit cell : (a) top view, (b) bottom view, (c) 3D view 53
Figure 4.16 The stack-up of the proposed active unit cell 53
Figure 4.17 Prototype of the proposed active unit cell (a) front side, (b) back side, (c) measurement setup to measure the unit cell in the WR34 waveguide 54
Figure 4.18 Transmission magnitude of the proposed active unit cell 55
Figure 4.19 Transmission phase of the proposed active unit cell 55
Figure 4.20 The biasing lines in the proposed unit cell 56
Figure 4.21 The front side view of the proposed beamfroming structure 56
Figure 4.22 The back side view of the proposed beamfroming structure 57
Figure 4.23 Phase distributions at 0° and 30° beam directions and corresponding radiation patterns 57
Figure 4.24 The placement of the biasing lines in the proposed active unit cell in layer 1-top 59
Figure 4.25 The placement of inductors in the proposed active unit cell in layer 1-top 60
Figure 4.26 The socket ports and ground line in the layer 1-top 61
Figure 4.27 The layer 1-bottom in the proposed active unit cell 62
Figure 4.28 The layer 2-top in the proposed active unit cell 63

Figure 5.1 The proposed unit cell (a) top view, (b) bottom view, (c) 3D view (d) transmit array based on the proposed unit cell 67
Figure 5.2 Simulated transmission results 68
Figure 5.3 Schematic of a generalized transmitarray antenna 69
Figure 5.4 Phase distributions at (a) 0°, (b) 10°, (c) 20°, (d) 30° 69
Figure 5.5 Beamsteering performance at three different angles at 28 GHz 70
Figure 5.6 The proposed unit cell (a) top view, (b) bottom view, (c) 3D view, and (d) transmitarray antenna based on the proposed unit cell 73
Figure 5.7 Simulated transmission results of the proposed unit cell with both PIN diodes in the ON state and both PIN diodes in the OFF state 74
Figure 5.8 Current distributions on the proposed unit cell (a) $t = 0$, (b) $t = T/4$, (c) $t = T/2$ and (d) $t = 3T/4$ 75
Figure 5.9 Phase distributions at (a) 0°, (b) 10°, (c) 20°, (d) 30°. 76

FIGURE 5.10 RADIATION PATTERNS OF THE PROPOSED TRANSMITARRAY ANTENNA IN THE H-PLANE AND E-PLANE..... 77

LISTE DES TABLEAUX

TABLEAU 3.1 REALIZED GAIN OF THE PROPOSED 3D-PRINTED HORN ANTENNA 32

TABLEAU 4.1 PERFORMANCE COMPARISON BETWEEN THE PROPOSED TRANSMIT ARRAY ANTENNA AND STATE-OF-THE-ART TRANSMIT ARRAY ANTENNAS (λ_L = FREE SPACE WAVELENGTH AT THE LOWEST FREQUENCY) 50

TABLEAU 4.2 PERFORMANCE METRICS FOR INTENDED VS. ACHIEVED ANGLES 58

TABLEAU 5.1 UNIT CELLS WITH TRANSMISSION PERFORMANCE 68

TABLEAU 5.2 BEAMSTEERING PERFORMANCE AT FOUR DIFFERENT ANGLES OF 0°, 10°, 20°, 30° AT THE CENTER FREQUENCY OF 28 GHZ 77

LISTE DES ABREVIATIONS

5G 5th Generation Mobile Network

6G 6th Generation Mobile Network

AMPBG Active Metallic Photonic Bandgap

BW Bandwidth

EM Electromagnetic

FSS Frequency Selective Surface

ILA Integrated Lens Antenna

IoT Internet of Things

IRS Intelligent Reconfigurable Surface

M-FSS Multilayer Frequency Selective Surface

MIMO Multiple-Input Multiple-Output

Mm-wave Frequency Millimeter wave Frequency

RAs Reflect-array Antennas

RF Radio Frequency

RT Configuration Receiver-Transmitter Configuration

RTA Reconfigurable Transmitarray Antenna

TA Transmitarray Antenna

UAV Unmanned Aerial Vehicle

1 INTRODUCTION

Mobile communication technologies have become increasingly ubiquitous in society, with the widespread use of smartphones and other mobile devices. Hence, mobile networks have to meet the increasing demands of consumers for higher data rates, and they will also have to deal with the predicted surge in traffic volumes, which is growing at an exponential rate. To this end, cellular providers are striving to offer superior-quality, low-latency video and multimedia applications for wireless devices. Several technological advancements are emerging independently to attain a significant enhancement in wireless communication system performance. One of these advancements involves utilizing the Millimeter Wave (mm-wave) frequency bands, which offer more available spectrums since they are predominantly unused. In addition, the utilization of higher frequencies results in the availability of smaller antennas and circuits, thus enabling RF transceivers to become more affordable [1–3].

Even though high frequencies have the potential to convey more data, they are constrained by their inability to penetrate and cover larger areas. Therefore, one way to extend coverage at longer ranges is by enhancing transmitting power without raising the cost of the communication system. One way to accomplish this is by using a large number of antennas, which can handle multiple users simultaneously. These antennas can be operated by smart systems that incorporate beamforming and Multiple-Input Multiple-Output (MIMO) systems techniques. Thus, it is necessary to design an antenna that can perform multiple functions by integrating them into a single element. To tackle the issue of radiation interference, this element should be capable of directing the beam toward a specific direction while preventing unwanted beams in other directions. Hence, beam-switching antennas, which are commonly used in pattern reconfigurable antennas, have garnered a lot of attention in wireless communication systems. These antennas can significantly reduce interfering signals and improve the system's capacity. By employing these antennas, additional functionalities and more flexible properties can be achieved, and they occupy the same or even less physical space than traditional smart antenna arrays [4–9].

Furthermore, to meet the future needs of consumers and technology, the beamforming subsystems and components must fulfill certain criteria, such as being low-loss, compact, and easy to manufacture. Additionally, they must address the challenges associated with designing cost-effectiveness and working with high frequencies. Therefore, the primary goal of this thesis is, study and design of reconfigurable antennas with beamforming functionality at mm-wave frequency bands.

1.1 Motivation

The demand for high-speed communication between numerous users and Internet of Things (IoT) devices is set to increase in the near future due to the rise of applications like self-driving cars, virtual reality videos, and remote surgery. As a response to this need, a comprehensive research will be conducted on reconfigurable antennas with beam steering capabilities. Specifically, our aim is to design and development novel and innovative transmitarray antennas at mm-wave frequencies, leveraging the unique properties of metasurfaces.

1.2 Problem

A reconfigurable antenna is an antenna that can modify its radiation properties to enhance wireless communication systems by providing additional features. The classification of this antenna depends on the antenna parameter that can be dynamically adjusted, usually including operation frequency, radiation pattern, or polarization. To change the pattern, the electric or magnetic currents of the radiating structure can be modified by controlling material properties or incorporating parasitic elements around the primary antenna [10].

Moreover, there are several methods available to control the direction of the radiation pattern beam, including integrated lens antennas (ILAs) [11–13], traveling-wave antennas [14, 15], adaptive arrays [16], phased arrays [17], and active metallic photonic bandgap (AMPBG) [18]. However, each of these technologies has its own advantages and disadvantages. For instance, traveling wave antennas are generally large when used for beam steering. Phased antenna arrays require the precise control of the amplitude and phase of each element to steer the beam, which complicates their structure and increases their manufacturing cost. Furthermore, the AMPBG is a bulky structure with higher side-lobe levels and cross-polarization.

In order to address the complexities, large size, and high cost of the previously mentioned techniques, researchers have recently started using metasurfaces for beam steering [19–22]. In [23], an electrical beam-steerable antenna is created by connecting a metasurface structure with varactor diodes. By manipulating the bias voltage, a 360° radiation pattern sweep can be achieved for both single-beam and dual-beam modes. Although pin diodes exhibit nonlinear behavior, they are commonly used to reconfigure the electromagnetic (EM) response. By controlling the transmission and reflection characteristics of the pin diodes, it can direct the incident EM waves [24–28]. For example, in [29], 48 pin-diodes were utilized to achieve beam steering, but this large number of active elements increased the complexity of the design and the cost of fabrication. Another researcher proposed a beam-steering antenna with fewer active elements inserted in a cylindrical geometry [30].

1.3 Research Objective

The central focus of this thesis is development of novel class of reconfigurable transmitarray antennas with beamforming capabilities for future mm-wave wireless communication systems. This research is conducted within the framework of an industrially funded project, where the collaborating company specified key performance targets, including a beamforming antenna configuration centered at 28 GHz (operating over the 27–29 GHz range), a realized gain exceeding 16 dBi, and sidelobe levels better than –10 dB. To acquire this, since a reconfigurable transmitarray antenna for beam steering typically consists of two main components - a feeding antenna and a metasurface panel - this thesis focuses on the design and integration of both elements. These components are integrated to form a complete transmitarray system capable of dynamic beam steering at mm-wave frequencies. Accordingly, the specific objectives of the thesis are :

- To design and evaluate two types of feed antennas :

  (1) A Substrate Integrated Waveguide (SIW) slot antenna for final implementation.

  (2) A 3D-printed horn antenna for simplified simulation and prototyping.

- To design and analyze metasurface panels composed of phase-reconfigurable unit cells based on two principles in both passive and active configurations :

  (1) Using mutual coupling in a constructive way with current reversal technique.

  (2) Huygens' principle.

- To integrate the feed antenna and metasurface panel, and to measure the performance of the fabricated structures.

1.4 Methodology

Based on the research objectives, this thesis will generally be completed in two main work packages.

1.4.1 Work Package 1 (Feed Antennas)

SIW technology is an impressive method to feed planar antennas and arrays in the mm-wave band. These feeding networks will be used to feed mm-wave antenna arrays using slots and patches, as illustrated in Figure 1.1.a. SIW-based antenna array design promises a higher gain, broadband operations, low loss, and high efficiency. In addition, horn antennas is a simplified, well-understood alternative. These two feeding options offer flexibility : the SIW antenna is intended for final deployment, while the horn antenna, due to its simpler geometry and reduced simulation

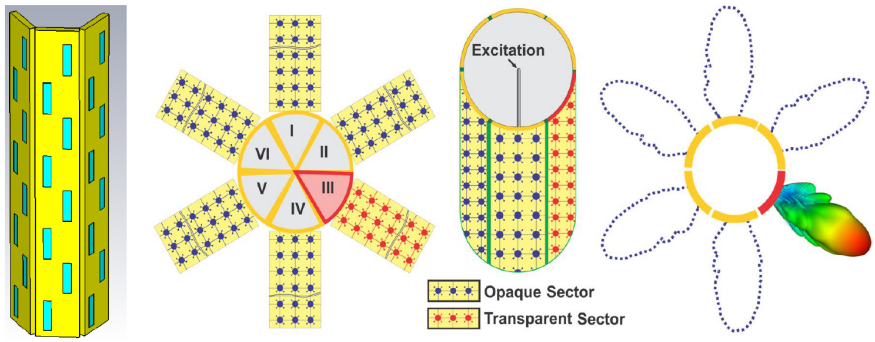

(a) (b) (c) (d)

FIGURE 1.1 : (a) Antenna array design using SIW technology that will be used as a source for reconfigurable antennas, the proposed concept for reconfigurable antennas using metasurface structures, (b) Exploded view, (c) Perspective view, (d) Operating concept.

complexity, is preferred for initial simulations and prototyping. Both feeding structures are designed to work with metasurface panels.

1.4.2 Work Package 2 (Metasurfaces)

In the second part, the proposed research will focus on the study and investigation of tunable electromagnetic periodic structures, including metasurfaces, and exploring their properties to improve the radiation characteristics and gain of mm-wave reconfigurable antennas with dynamic radiation patterns, as shown in Figure 1.1.b-d.

Recently, metasurfaces have attracted a lot of interest in the antenna domain because of their ability to control the propagation of electromagnetic waves. These structures are periodic dielectric or metallic planar structures that can perform spectral, spatial, or angular filtering of the incident electromagnetic waves. They can be configured as transparent or opaque surfaces to electromagnetic waves at a specific frequency bandwidth, leading to control of the wave propagation. This fascinating technology can provide innovative and highly efficient solutions for critical problems in antenna design. More specifically, for reconfigurable antennas with beamforming functionality, it would be more attractive to use metasurface structures [19–22]. By controlling wave propagation using these structures, we can design new reconfigurable antennas with beamforming capability.

1.5 Contributions

The primary contributions of this thesis can be summarized as follows :

1. Dual-Feed Strategy : Two different feed antennas, a compact SIW-based slot antenna and a 3D-printed horn antenna, were designed and studied. This dual approach offers flexibility for both practical implementation and simulation-based evaluation

2. Novel Unit Cell Designs : Two distinct unit cell design methodologies were developed for millimeter-wave transmitarrays, one based on using constructively mutual coupling and current reversal techniques, and the other leveraging Huygens' principle.

3. Passive and Active Configurations : Both passive and 1-bit active versions of each unit cell were realized. The active designs incorporate PIN diodes to enable phase reconfigurability and dynamic beam steering at 28 GHz.

4. Transmitarray Implementation : The proposed unit cells were integrated into complete transmitarray panels. Beamforming capabilities were demonstrated through full-wave electromagnetic simulations, confirming directional control and phase manipulation.

5. Comprehensive Performance Evaluation : The proposed antenna systems were analyzed in terms of gain, sidelobe level, beam-steering performance, and design trade-offs. The results confirm the viability of the proposed structures for future high-frequency wireless applications, including 5G and beyond.

These contributions push forward the development of reconfigurable millimeter-wave transmitarray antennas, offering compact, low-loss, and cost-effective solutions for next-generation beamforming systems.

1.6 Publications

Journals :

1. **P. PourMohammadi**, H. Naseri, N. Melouki, F. Ahmed, Q. Zheng, A. Iqbal, and T. A. Denidni, "A Wideband Beam Steering Transmitarray Antenna for Ka-Band Applications," AEU-International Journal of Electronics and Communications, 2025.
2. **P. PourMohammadi**, H. Naseri, N. Melouki, F. Ahmed, Q. Zheng, A. Iqbal, G. A. Vandenbosch and T. A. Denidni, "Highly isolated compact self-diplexing antenna," AEU-International Journal of Electronics and Communications, vol. 173, p. 155025, 2024.
3. **P. PourMohammadi**, H. Naseri, N. Melouki, F. Ahmed, M.S. Bizan, A. Iqbal, and T. A.Denidni, "A Fabry–Perot antenna using a frequency selective surface layer with wideband and Low RCS for Mm-wave applications," AEU-International Journal of Electronics and Communications, vol. 169, p. 154736, 2023.
4. **P. PourMohammadi**, H. Naseri, N. Melouki, F. Ahmed, A. Iqbal, G. A. Vandenbosch and T. A. Denidni, "Compact SIW-based self-quadruplexing antenna for microwave and mm-wave communications," IEEE Transactions on Circuits and Systems, vol. 70, no. 9, pp. 3368–3372, 2023.
5. **P. PourMohammadi**, P. Fei, H. Naseri, Q. Zheng, O. J. Babarinde, V. Volski, G. A. Vandenbosch, and T. A. Denidni, "A Single-Layer Compact Wideband Circularly Polarized Patch

Array for 5G Communications," IEEE Antennas and Wireless Propagation Letters, vol. 22, no. 4, pp. 754–758, 2022.

6. **P. PourMohammadi**, H. Naseri, N. Melouki, F. Ahmed, and A. Iqbal, and T. A. Denidni, "Substrate integrated waveguide-based full-duplex antenna with improved out-of-band suppression," IEEE Transactions on Circuits and Systems, vol. 70, no. 4, pp. 1430–1434, 2022.
7. N. Melouki, F. Ahmed, **P. PourMohammadi**, H. Naseri, and T. A. Denidni, "Wideband transmitarray with independent phase/amplitude control for millimeter-wave vehicular sensing and communication," AEU-International Journal of Electronics and Communications, 2025.
8. M. S. Bizan, **P. PourMohammadi**, A. Iqbal, and T. A. Denidni, "High-gain dual-band antenna with independent frequency operation for Sub-6 GHz and millimeter-wave applications," AEU-International Journal of Electronics and Communications, 2025.
9. N. Melouki, F. Ahmed, **P. PourMohammadi**, H. Naseri, and T. A. Denidni, "Wideband Transmitarray with Independent Phase/Amplitude Control for MillimeterWave Vehicular Sensing and Communication," AEU-International Journal of Electronics and Communications, 2025.
10. Z. Mousavirazi, M. M. Ali, **P. PourMohammadi**, P. Fei, T. A. Denidni, "High-Performance CP Magneto-Electric Dipole Antenna Fed by Printed Ridge Gap Waveguide at Millimeter-Wave," Sensors, vol. 24, no. 24, 2024.
11. F. Ahmed, F. Faisal, N. Melouki, A. Ahmed, H. Naseri, **P. PourMohammadi**, and Tayeb A. Denidni, "A Multi-Functional Reflective Polarization Transforming Surface with In-Band and Out-Band Transmission Characteristics," IEEE Antennas and Wireless Propagation Letters, pp. 1–5, 2024.
12. F. Ahmed, A. Ahmed, N. Melouki, **P. PourMohammadi**, H. Naseri Gheisanab, N. Shoaib, T. A Denidni "A wideband bianisotropic FSS absorber with angular stable and polarization-insensitive properties," Waves in Random and Complex Media, pp. 1–16, 2024.
13. N. Melouki, F. Ahmed, **P. PourMohammadi**, H. Naseri, M. S. Bizan, A. Iqbal, and T. A. Denidni, "3D-Printed Conformal Meta-Lens with Multiple Beam-Shaping Functionalities for Mm-Wave Sensing Applications," Sensors, vol. 24, no. 9, p. 2826, 2024.
14. H. Naseri, **P. PourMohammadi**, N. Melouki, F. Ahmed, A. Iqbal, and T. Denidni, "Frequency-adjustable OAM antenna with co-divergent beams for IoT applications," AEU-International Journal of Electronics and Communications, vol. 177, p. 155188, 2024.
15. H. Naseri, **P. PourMohammadi**, N. Melouki, F. Ahmed, A. Iqbal, and T. A. Denidni, "Reconfigurable OAM Antenna with Flexibility on Mode Numbers, Polarization and Frequency," IEEE Antennas and Wireless Propagation Letters, 2024.
16. N. Melouki, **P. PourMohammadi**, H. Naseri, F. Ahmed, A. Iqbal, and T. A. Denidni, "Ultra-compact Quarter-Mode SIW Self-Hexaplexing Antenna for C-band and X-band Applications," IEEE Antennas and Wireless Propagation Letters, 2023.
17. F. Ahmed, T. Hassan, N. Melouki, H. Naseri, **P. PourMohammadi**, A. Iqbal, and T. A. Denidni, "A multi-bit and frequency-reconfigurable reflecting surface for RIS applications," IEEE Antennas and Wireless Propagation Letters, 2023.

18. H. Naseri, **P. PourMohammadi**, P. Fei, N. Melouki, A. Iqbal, and T. Denidni, "Butler matrix-based beamforming with polarization reconfigurability for reducing electromagnetic interference," AEU-International Journal of Electronics and Communications, vol. 170, p. 154833, 2023.
19. M. S. Bizan, H. Naseri, **P. PourMohammadi**, N. Melouki, A. Iqbal, and T. A. Denidni, "Dual-band dielectric resonator antenna with filtering features for microwave and mm-wave applications," Micromachines, vol. 14, no. 6, p. 1236, 2023.
20. H. Naseri, **P. PourMohammadi**, N. Melouki, F. Ahmed, A. Iqbal, and T. A. Denidni, "Substrate integrated waveguide-based dual-polarized self-diplexing antenna array," IEEE Transactions on Circuits and Systems II : Express Briefs, vol. 70, no. 8, pp. 2839–2843, 2023.
21. H. Naseri, **P. PourMohammadi**, N. Melouki, F. Ahmed, A. Iqbal, and T. A. Denidni, "Generation of mixed-OAM-carrying waves using huygens' metasurface for mm-wave applications," Sensors, vol. 23, no. 5, p. 2590, 2023.
22. H. Naseri, **P. PourMohammadi**, Z. Mousavirazi, A. Iqbal, G. A. Vandenbosch, and T. A. Denidni, "A Low-Profile Dual-Band Hybrid Coupler with Flexible Frequency Band Ratio," Progress in Electromagnetics Research Letters. Nov 1;107, 2022.
23. H. Naseri, **P. PourMohammadi**, N. Melouki, A. Iqbal, and T. A. Denidni, "A low-profile antenna system for generating reconfigurable OAM-carrying beams," IEEE Antennas and Wireless Propagation Letters, vol. 22, no. 2, pp. 402–406, 2022.
24. N. Melouki, A. Hocini, F. Z. Fegriche, **P. PourMohammadi**, H. Naseri, A. Iqbal, and T. A. Denidni, "High-gain wideband circularly polarised Fabry–Perot resonator array antenna using a single-layered pixelated PRS for millimetre-wave applications," Micromachines, vol. 13, no. 10, p. 1658, 2022.
25. H. Naseri, **P. PourMohammadi**, A. Iqbal, A. A. Kishk, and T. A. Denidni, "SIW-based self-quadruplexing antenna for microwave and mm-wave frequencies," IEEE Antennas and Wireless Propagation Letters, vol. 21, no. 7, pp. 1482–1486, 2022.

Conferences :

1. **P. PourMohammadi**, H. Naseri, N. Melouki and T. Denidni, "Single-Layer Electronically Beam Steering Transmitarray Antenna for the Ka-band Applications," in 2025 IEEE International Symposium on Antennas and Propagation and USNC-URSI Radio Science Meeting (USNC-URSI), 2025 (Accepted).
2. **P. PourMohammadi**, H. Naseri, N. Melouki and T. Denidni, "A 1-Bit Wideband Electronically Beam Steering Transmitarray For 5G Communication Systems," in 2024 IEEE International Symposium on Antennas and Propagation and USNC-URSI Radio Science Meeting (USNC-URSI), 2024.
3. **P. PourMohammadi**, H. Naseri, F. Ahamed and T. Denidni, "A Wideband Transmit Array based on Huygens' Metasurface for Millimeter-Wave Applications," in 2024 IEEE International

Symposium on Antennas and Propagation and USNC-URSI Radio Science Meeting (USNC-URSI), 2024.

4. **P. PourMohammadi**, H. Naseri, N. Melouki, F. Ahmed, A. Iqbal, G. A. Vandenbosch and T. A. Denidni, "A low-profile self-duplexing antenna for millimeter-wave and microwave frequency bands," in 2023 IEEE international symposium on antennas and propagation and USNC-URSI radio science meeting (USNC-URSI), 2023, pp. 605–606.
5. **P. PourMohammadi**, H. Naseri, N. Melouki, F. Ahmed, M. Bizan, A. Iqbal and T. A.Denidni, "A Wideband Fabry-Perot Antenna with a Bianisotropic FSS Layer," in 2023 IEEE International Symposium on Antennas and Propagation and USNC-URSI Radio Science Meeting (USNC-URSI), 2023 Jul 23, pp. 649-650.
6. **P. PourMohammadi**, H. Naseri, N. Melouki, F. Ahmed, M. Bizan, A. Iqbal and T. A. Denidni, "A Wideband Anisotropic Metasurface for Cross-Polarization Applications," 2023 URSI International Symposium on Electromagnetic Theory, 2023.
7. **P. PourMohammadi**, H. Naseri, R. Alwahishi, G. A. Vandenbosch, and T. A. Denidni, "A 2×3 high-gain coupled patch array for body area network applications," in 2022 IEEE international symposium on antennas and propagation and USNC-URSI radio science meeting (AP-S/URSI), 2022, pp. 2068–2069.
8. H. Naseri, **P. PourMohammadi**, M. Bizan and T. A. Denidni, "Dual-Polarized Reconfigurable Beam-Steering Using the New Feeding Network Topology," in 2025 IEEE International Symposium on Antennas and Propagation and USNC-URSI Radio Science Meeting (USNC-URSI), 2025 (Accepted).
9. N. Melouki, F. Ahmed, **P. PourMohammadi** and T. A. Denidni, "Hybrid 3D-Printed Lens with 360° Beam-Steering for UAV Search and Rescue and Advanced 5G Communication," in 2025 IEEE International Symposium on Antennas and Propagation and USNC-URSI Radio Science Meeting (USNC-URSI), 2025 (Accepted).
10. H. Wu, H. Naseri, **P. PourMohammadi**, F. Abderrazak and T. A. Denidni, "Reconfigurable Dual-band OAM Antenna for Microwave and Millimeter-Wave Applications," in 2025 IEEE International Symposium on Antennas and Propagation and USNC-URSI Radio Science Meeting (USNC-URSI), 2025 (Accepted).
11. F. Ahmed, N. Melouki, **P. PourMohammadi** and T. Denidni, "A Reconfigurable Dual-Band Transmit Array Antenna for K-Band and Millimeter-Wave Applications," in 2025 IEEE International Symposium on Antennas and Propagation and USNC-URSI Radio Science Meeting (USNC-URSI), 2025 (Accepted).
12. H. Naseri, **P. PourMohammadi**, N. Melouki, F. Ahmed, A. Iqbal, and T. A. Denidni, "Dual-Polarized OAM Antenna with Frequency and Mode Agility for Intelligent OAM Communications," in 2024 18th European Conference on Antennas and Propagation (EuCAP), 2024, pp. 1–4.
13. N. Melouki, F. Ahmed, H. Nasseri, **P. PourMohammadi**, A. Iqbal, and T. A. Denidni, "Multi-Bit Wideband Transmitarray Aperture with Independent Phase and Amplitude Control for

High Gain with Low Sidelobe Mm-Wave Applications," in 2024 18th European Conference on Antennas and Propagation (EuCAP), 2024, pp. 01–04.

14. F. Abderrazak, **P. PourMohammadi**, L. Talbi, E. Antonino-Daviu, T. Denidni and M. Ferrando-Bataller, "Selective Excitation Technique for Wireless Power Transfer in Wearable Devices Using CMA," in 7th Conference on Cloud and Internet of Things (IEEE/IFIP 2024 CIoT), 2024.

15. N. Melouki, F. Ahmed, **P. PourMohammadi** and T. A. Denidni, "3D-Printed Conformal Meta-Lens with Multi-mode Orbital Angular Momentum (OAM) Generation and Beam-steering Capabilities," in 2024 IEEE International Symposium on Antennas and Propagation and USNC-URSI Radio Science Meeting (USNC-URSI), 2024.

16. H. Naseri, **P. PourMohammadi**, M. Bizan and T. A. Denidni, "Butler Matrix-based Beam Switching with Frequency-tunable MIMO Array," in 2024 IEEE International Symposium on Antennas and Propagation and USNC-URSI Radio Science Meeting (USNC-URSI), 2024.

17. F. Ahmed, N. Melouki, **P. PourMohammadi** and T. Denidni, "A Multifunctional Bianisotropic Frequency Selective Surface for Microwave Applications," in 2024 IEEE International Symposium on Antennas and Propagation and USNC-URSI Radio Science Meeting (USNC-URSI), 2024.

18. M. Bizan, H. Naseri, **P. PourMohammadi** and T. A. Denidni, "Ultra-Wideband Dielectric Resonator Antenna Fed by Printed Ridge Gap Waveguide Technology," in 2024 IEEE International Symposium on Antennas and Propagation and USNC-URSI Radio Science Meeting (USNC-URSI), 2024.

19. M. S. Bizan, H. Naseri, **P. PourMohammadi**, and T. A. Denidni, "Integrate Fabry–Perot Resonator into Dielectric Resonator Antenna for Microwave and Mm-wave Operations," in 2023 IEEE International Symposium on Antennas and Propagation and USNC-URSI Radio Science Meeting (USNC-URSI), 2023, pp. 1161–1162.

20. F. Ahmed, N. Melouki, **P. PourMohammadi**, H. Naseri and T. A. Denidni, "A 2-Bit Reconfigurable Reflecting Metasurface for Mm-Wave Applications," in 2023 IEEE International Symposium on Antennas and Propagation and USNC-URSI Radio Science Meeting (USNC-URSI), 2023 Jul 23, pp. 1425–1426.

21. H. Naseri, **P. PourMohammadi**, M. Bizan, N. Melouki, F. Ahmed, A. Iqbal and T. A. Denidni, "Reconfigurable Dielectric Resonator OAM Antenna with Augmented Modes," in 2023 IEEE International Symposium on Antennas and Propagation and USNC-URSI Radio Science Meeting (USNC-URSI) 2023 Jul 23 (pp. 703-704). IEEE.

22. N. Melouki, F. Ahmed, **P. PourMohammadi**, H. Naseri and T. A. Denidni, "3D-Printed Conformal Metamaterial Lens with Multiple Beam Steering Functionalities," in 2023 IEEE International Symposium on Antennas and Propagation and USNC-URSI Radio Science Meeting (USNC-URSI) 2023 Jul 23 (pp. 791-792). IEEE.

23. H. N. Gheisanab, **P. PourMohammadi**, N. Melouki, A. Iqbal, and T. A. Denidni, “Self-diplexing Antenna Operating at Sub-6 GHz and Millimeter-wave Frequency Bands,” in 2023 17th European Conference on Antennas and Propagation (EuCAP), 2023, pp. 1–3.
24. H. Naseri, **P. PourMohammadi**, M. Bizan, N. Melouki, F. Ahmed, A. Iqbal, and T. A. Denidni, “Triple-Mode OAM Generating Dielectric Resonator Antenna,” 2023 URSI International Symposium on Electromagnetic Theory, 2023.
25. M. Bizan, H. Naseri, **P. PourMohammadi**, A. Iqbal and T. A. Denidni, “Ultra-Wideband Dielectric Resonator Antenna with Integrated Fabry-Perot Cavity,” 2023 URSI International Symposium on Electromagnetic Theory, 2023.
26. F. Ahmed, N. Melouki, **P. PourMohammadi**, H. Naseri and T. A. Denidni, “4-Bit Reconfigurable Reflecting Metasurface for Sub-6 GHz Band,” 2023 URSI International Symposium on Electromagnetic Theory, 2023.
27. N. Melouki, F. Ahmed, **P. PourMohammadi**, H. Naseri and T. A. Denidni, “Low-Loss 2-Bit Reflective Intelligent Surface for mm-Wave Applications,” 2023 URSI International Symposium on Electromagnetic Theory, 2023.
28. H. Naseri, **P. PourMohammadi**, Z. Mousavirazi, A. Iqbal, and T. A. Denidni, “Full azimuth beam steering by means of radiation pattern with the narrow beamwidth,” in 2022 IEEE International Symposium on Antennas and Propagation and USNC-URSI Radio Science Meeting (AP-S/URSI), 2022, pp. 1630–1631.
29. R. Alwahishi, **P. PourMohammadi**, M. M. M. Ali, and T. A. Denidni, “A dual-band intelligent frequency selective surface unit cell for future communication systems,” in 2022 IEEE International Symposium on Antennas and Propagation and USNC-URSI Radio Science Meeting (AP-S/URSI), 2022, pp. 986–987.

1.7 Achievements

1. Ranked 1st – FRQNT Postdoctoral Research Scholarship Recipient, Fonds de recherche du Québec, Canada, 2025.
2. Conference Participation Grant Recipient, INRS, Université du Québec, Canada, 2025.
3. Recognition for Contribution as a Mentor, INRS, Université du Québec, Canada, 2025.
4. Ranked 2nd – FRQNT Doctoral Research Scholarship Recipient, Fonds de recherche du Québec, Canada, 2024.
5. Recognition for Contribution as a Mentor, INRS, Université du Québec, Canada, 2024.
6. Selected by INRS, Université du Québec for PBEEE Program Competition, Canada, 2023.
7. Selected as One of 48 Recipients Worldwide for the AP-S Fellowship Award, Antenna Propagation Society (AP-S), 2023.
8. Ranked 2nd – Best Student Poster Award, STARaCom, McGill University, Canada, 2023.

1.8 Honors

1. Lead Guest Editor of Special Issue in Electronics (Q1), 2025.
2. Session Chair for “Transmitarrays and Transmissive Metasurfaces” at IEEE AP-S/URSI Ottawa, Canada, 2025.
3. Session Chair for “Multi-band Antennas” at IEEE AP-S/URSI ,Ottawa, Canada, 2025.
4. General Chair of the INRS-EMT Scientific Colloquium, April 2023 – April 2024.

1.9 Outline of the Thesis

The thesis structure consists of six main chapters, detailed below :

Chapter 1 (Introduction) : The first chapter provides research motivation, establishes the problem statement, and presents both objectives and methodology. This chapter presents a summary of the thesis structure along with a list of related publications and notable honors and awards.

Chapter 2 (Literature Review) : The review covers the latest advancements and research findings in metasurface-based transmitarray antennas. Key concepts such as beam steering techniques, reconfigurable metasurfaces, and design trade-offs are discussed to highlight research gaps and justify the proposed work.

Chapter 3 (Feed Design) : This chapter covers the design and development of two different feed antennas, including a SIW antenna and a 3D-printed horn antenna configuration, which are employed to illuminate the proposed transmitarray structures.

Chapter 4 (Unit Cell Design Based on Using Mutual Coupling in a Constructive Way and Current Reversal Technique) : This chapter introduces a novel 1-bit passive unit cell and an active unit cell design that leverages mutual coupling and current reversal techniques to enhance beam control. Their performance in transmitarray configurations is evaluated.

Chapter 5 (Unit Cell Design Based on Huygens’ Principle) : The design and implementation of unit cells based on Huygens’ principle are presented. Two versions of the Huygens-based unit cell and their corresponding transmitarray configurations are analyzed and compared.

Chapter 6 (Conclusion and Future Work) : The chapter presents a summary of the thesis’s main results and discusses future research possibilities in reconfigurable and high-efficiency beamforming antenna technology.

2 LITERATURE REVIEW

This chapter provides a comprehensive review of metasurface-based reconfigurable transmitarray antennas, with a focus on their beamforming capabilities at millimeter-wave frequencies. Beginning with an overview of conventional beam steering methods, the discussion highlights the limitations of traditional mechanical, analog, and digital approaches. The chapter then explores foundational concepts of transmitarrays. Emphasis is placed on the evolution toward reconfigurable metasurfaces, enabled by tunable elements such as PIN diodes and varactors. Recent trends in analog/digital beam control, phase resolution, material innovations, and hybrid techniques are studied. Finally, application-specific developments are analyzed across domains such as satellite communication, vehicular sensing, base stations, and Unmanned Aerial Vehicles (UAV) platforms.

2.1 Introduction

Transmitarray Antennas (TAs) represent an innovative approach to achieve high-gain directional beamforming in contemporary wireless communication networks. Transmitarray antennas direct beams electronically by controlling the phase of waves passing through their planar unit cell arrays without requiring mechanical movement.

There are several methods available to control the direction of the radiation pattern beam, including Integrated Lens Antennas (ILAs), traveling-wave antennas, adaptive arrays, phased arrays, and Active Metallic Photonic Bandgap (AMPBG). However, each of these technologies has its own advantages and disadvantages. For instance, traveling wave antennas are generally large when used for beam steering. Phased antenna arrays require the precise control of the amplitude and phase of each element to steer the beam, which complicates their structure and increases their manufacturing cost. Furthermore, the AMPBG is a bulky structure with higher side lobe levels and cross-polarization. However, transmitarray antennas integrate the benefits of phased arrays and lens antennas but eliminate the bulkiness and complexity found in conventional designs. The importance of these antennas stands out in mmwave applications because traditional methods struggle with financial cost and physical dimensions, as well as operational efficiency [31, 32].

2.2 Fundamentals of Metasurface-Based Transmitarray Antennas

A transmitarray transforms a spherical wavefront from a feed source into a planar wavefront using a transmission surface which consists of multiple unit cells. The transmission surface consists of unit cells that deliver specific phase shifts which enable the creation of focused or steerable beams. Metasurfaces function as two-dimensional metamaterial versions which enable detailed

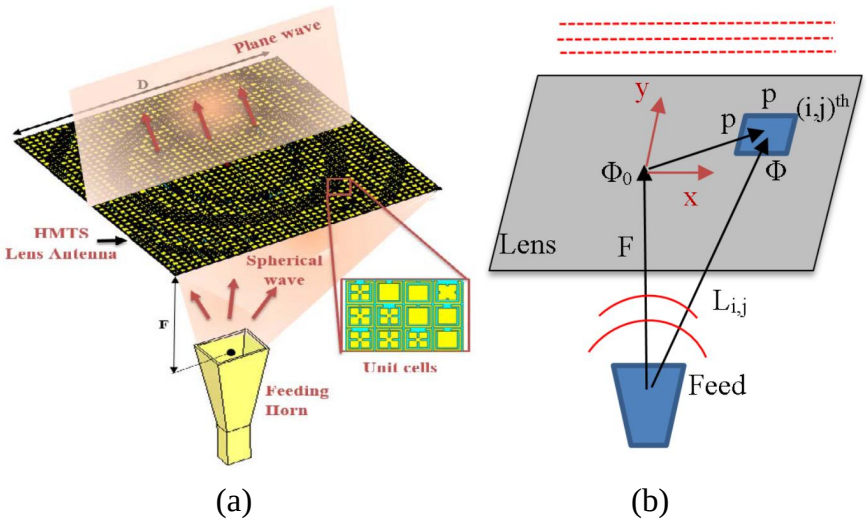

FIGURE 2.1 : (a) Sketch of the proposed ultrathin HMTS-based flat-lens antenna, (b) Phase compensation of HMTS-based flat-lens antenna [35].

electromagnetic manipulation on subwavelength scales and thus prove ideal for high-performance transmitarrays with reduced profiles [33, 34].

2.3 Transmitarray Antennas and Beam Steering Techniques

2.3.1 Concepts and approaches

Transmitarray antennas, also called flat lens antennas or planar lenses, consist of an illuminating feed and a transmissive surface populated with subwavelength unit cells. These elements convert the feed's spherical wavefront into a planar wavefront, creating high-gain, focused radiation [35], as shown in Fig. 2.1. There are primarily three methods to design a transmitarray antenna :

1) **Receiver-Transmitter (RT) Configuration** : Utilizes back-to-back receiver and transmitter layers composed of unit cells, suitable for broadband and circular polarization, see Fig. 2.2.

In [36], several transmitarray antennas operating at 60 GHz were designed and evaluated for both linear and circular polarization, using a new three-layer unit-cell structure based on standard PCB technology. Experimental results demonstrated gains of 22–23 dBi, a 1-dB bandwidth of 7%, and a power efficiency of 50%, making these antennas promising candidates for low-cost, high-data-rate applications in the V- and E-bands.

2) **Metamaterial Transformation Lenses** : Employ gradient index profiles inspired by transformation optics, offering broadband performance and wide-angle scanning.

As shown in Fig. 2.3, a two-dimensional broadband low-loss Luneburg lens was designed using complementary I-shaped metamaterial units, providing nearly constant effective parameters at low

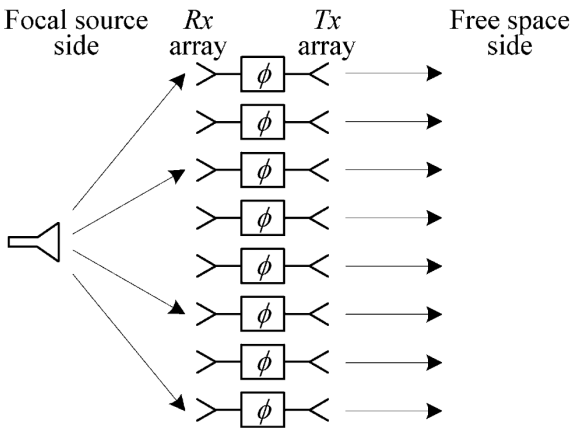

FIGURE 2.2 : Operation principle of a transmitarray based on RT configuration [36].

frequencies. Numerical simulations established the link between unit geometry and refractive index, and experimental validation showed good agreement with simulations, confirming strong focusing performance [37].

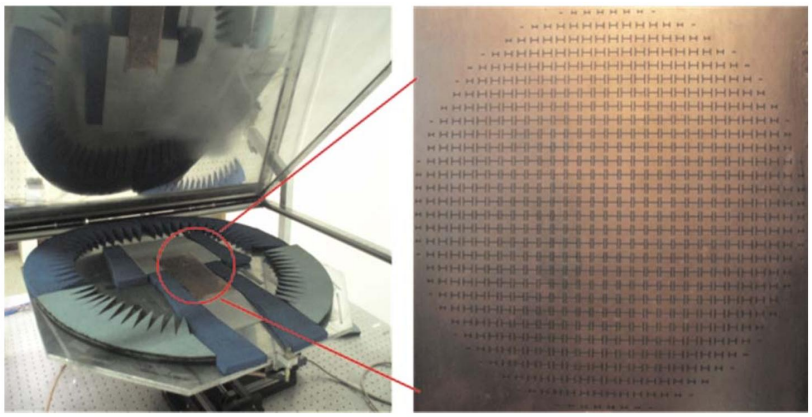

FIGURE 2.3 : Experimental setup for the 2D Luneburg lens based on complementary I-shaped metamaterials, and the fabricated sample of the Luneburg lens. [37].

3) **Multilayer Frequency Selective Surfaces (M-FSS)** : Stacked resonator layers providing broadband and wide-angle beam steering, typically requiring three or more layers , as shown in Fig. 2.4.

In [38], a four-layer transmitarray operating at 30 GHz was designed using dual-resonant double square ring unit cells, with a detailed procedure for both single-layer and cascaded four-layer configurations. The final design achieved a 7.5% -1 dB gain bandwidth and 47% radiation efficiency, demonstrating a 50% improvement in bandwidth compared to previous transmitarrays.

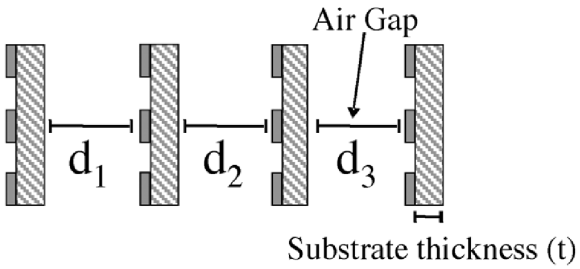

FIGURE 2.4 : Arrangement on multilayer transmitarray. [38].

2.3.2 Conventional Beam Steering Techniques and Limitations

Effective beam steering is crucial for mm-wave systems, where high path loss and blockage sensitivity occur [31, 32]. Traditional techniques face several limitations :

1) Mechanical steering : Slow response time and mechanical wear [39–41], see Figure 2.5.

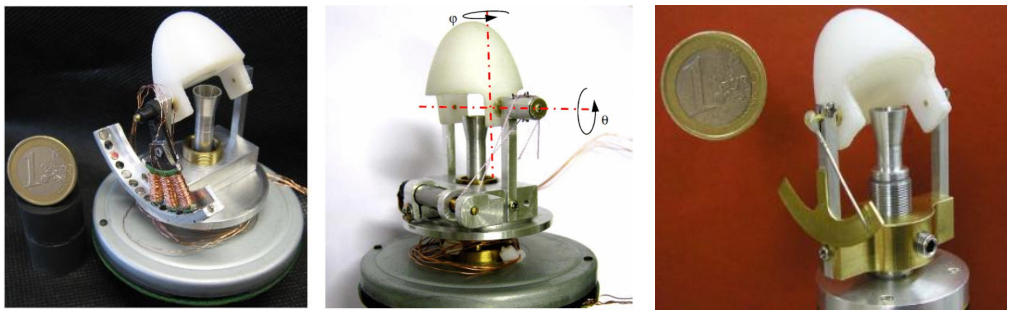

(a) (b) (c)

FIGURE 2.5 : Manufactured three lens antennas for mechanically beamsteering (a) [39], (b) [40] and (c) [41].

A millimeter-wave indoor wireless system to support multi-Gbps data rates as a replacement for short-range technologies like Bluetooth and PANs was investigated in [39]. To address the mobility limitations of high-gain (20 dBi) directional antennas, a new antenna concept with automatic beam tracking was developed. The system integrated the antenna with a simplified RF front-end and tracking control algorithms, enabling low-cost and fully operational video transmission. In [40], a steerable beam antenna was proposed based on a mechanically pivoting dielectric lens placed in front of a stationary moderate-gain feed. The lens enabled beam steering in both elevation and full azimuth while enhancing the gain up to 21 dBi over a wide bandwidth from 57 to 66 GHz. A fabricated prototype demonstrated beam tilt from -45° to +45° in all azimuth directions, with scan loss below 1.1 dB and radiation efficiency above 95%. The design was compact, low-cost, and did not require rotary joints, with a total volume of approximately 3×3×3 cm^3 and lens weight under 10 grams.

2) Analog beamforming : High insertion losses and phase inaccuracies at higher frequencies [42, 43], see Figure 2.6. a.

3) Digital beamforming : High complexity, power consumption, and cost, particularly at mmwave frequencies [42, 44], see Figure 2.6. b.

The analog beamforming technique uses one signal input per antenna through phase shifters to direct the beam direction just like phased arrays do. Digital beamforming operates by sending distinct digital signals to each antenna which enables precise control of power levels, phase settings, and frequency adjustments.

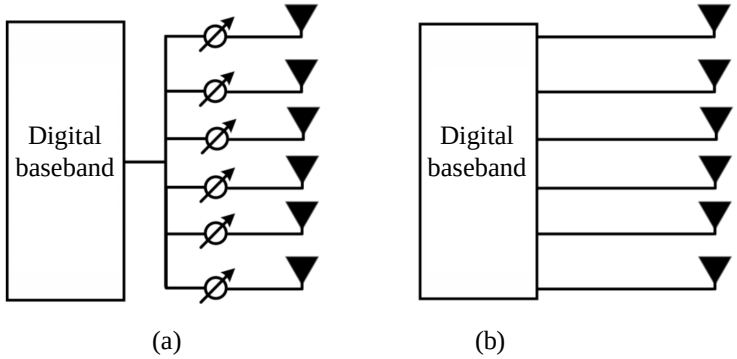

FIGURE 2.6 : (a) analog (b) digital beamforming.

4) Switched-beam and integrated lens antennas : Limited resolution and redundant hardware [45].

In [46], a 16-switched-beam lens-based antenna was designed for smart repeaters in 5G wireless systems operating from 24.25 to 27.5 GHz. The antenna achieved a coverage of ±30° horizontally and from 0° to -20° vertically. Implemented with advanced materials and components, the antenna demonstrated an overall loss of approximately 8 dB and maintained a realized gain exceeding 11 dB across 80% of its coverage area; see Figure 2.7.

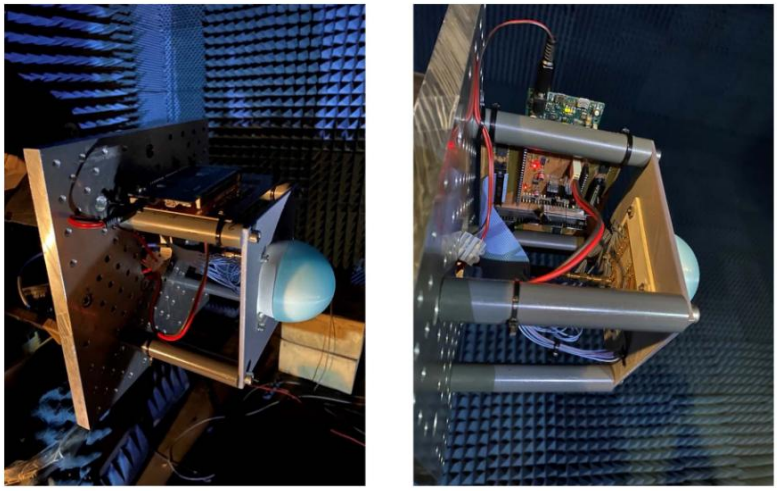

FIGURE 2.7 : Switched-beam lens antenna [46].

2.4 Emergence and Advances of Reconfigurable Metasurfaces

Metasurfaces consist of engineered subwavelength resonators capable of imparting abrupt phase discontinuities. Huygens' metasurfaces exploit electric and magnetic resonances, offering complete phase control with negligible reflection, ideal for transmitarrays [33, 47, 48]. Recent advancements demonstrate that these metasurfaces can be dynamically reconfigured by integrating tunable elements such as PIN diodes and varactors, enabling programmable beamsteering, as shown in Figure 2.8 and 2.9 [49–51].

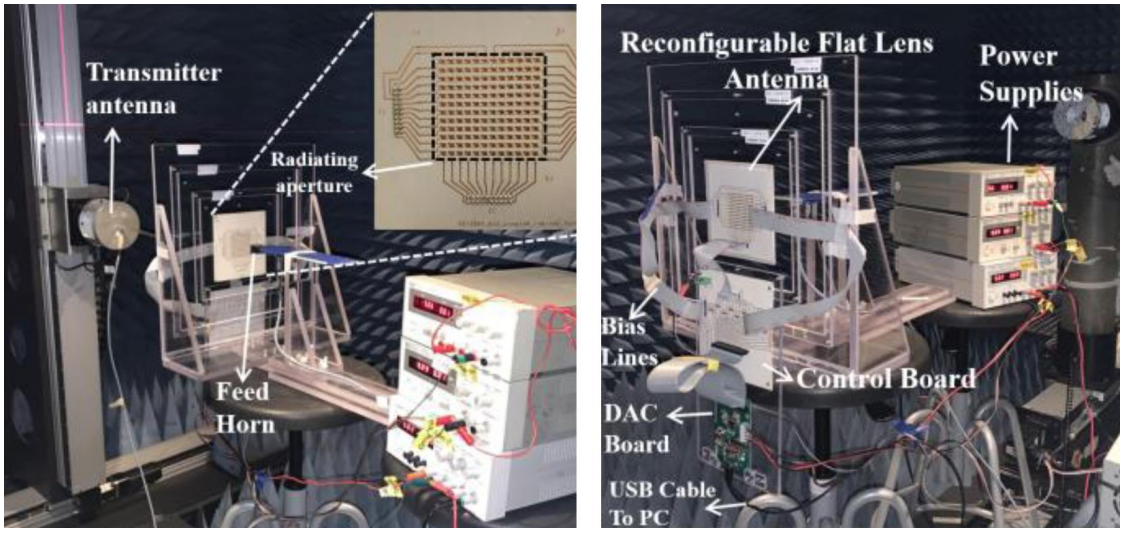

FIGURE 2.8 : Photographs of fabricated reconfigurable HMTS-based flat lens prototype [49].

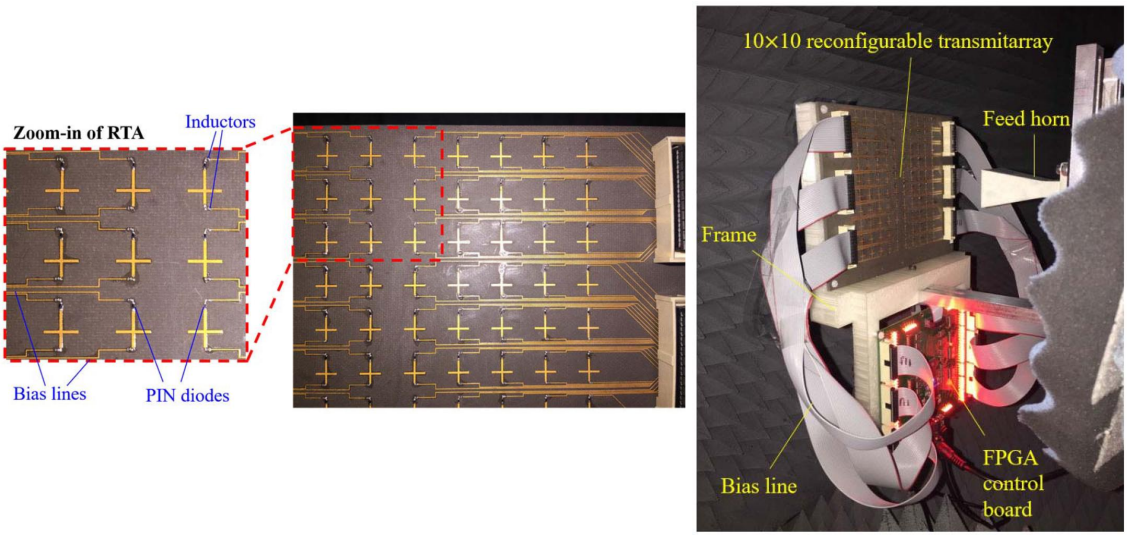

FIGURE 2.9 : Photographs of (a) fabricated reconfigurable transmitarray prototype [50].

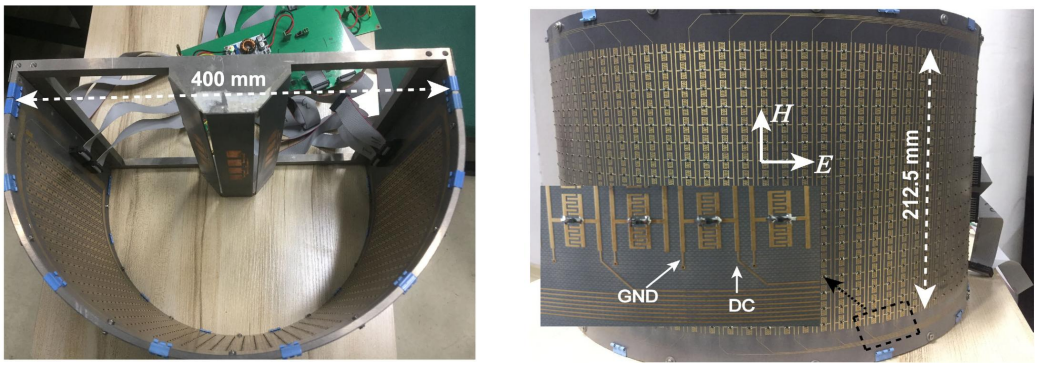

FIGURE 2.10 : Fabricated metasurface cylindrical lens antenna [51].

2.5 Key Research Trends and Developments

2.5.1 Fixed vs. Reconfigurable Transmitarrays

The design of traditional fixed transmitarrays restricts them to static beam directions which results in reduced adaptability for dynamic environments. Reconfigurable transmitarrays utilize tunable components like PIN diodes and varactors to enable instantaneous beam steering while dynamically adjusting radiation patterns. New developments show electronically reconfigurable transmitarrays that direct beams without mechanical movement which improves their usefulness in contemporary communication networks, see Figure 2.11 [52, 53].

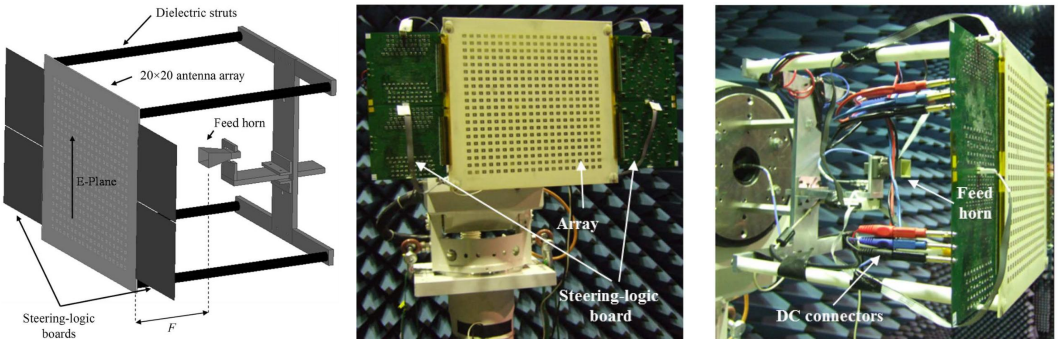

FIGURE 2.11 : Electronically reconfigurable transmitarray [52].

2.5.2 Analog vs. Digital Beam Control

Analog beamforming in transmitarrays offers continuous (or nearly continuous) phase control, enabling fine-grained beam steering. However, it often suffers from complexity in control circuitry and susceptibility to non-linearities. Digital beamforming, employing discrete phase states (e.g., 1-bit, 2-bit), simplifies the control mechanism and enhances robustness but may introduce quan-

tization errors. Hybrid approaches combining analog and digital techniques are being explored to leverage the advantages of both methods [54, 55].

2.5.3 1-Bit vs. Multi-Bit Phase Designs

The resolution of phase control in transmitarray elements significantly impacts beamforming accuracy. 1-bit designs, offering two phase states (0° and 180°), are simpler and easier to implement but provide limited beam steering capabilities. Multi-bit designs (e.g., 2-bit, 3-bit) offer finer phase resolution, enabling more precise beam control at the cost of increased complexity and potential insertion losses [56].

In [57], a broadband 1-bit reconfigurable transmitarray antenna (RTA) utilizing polarization rotation elements was proposed. Each transmitarray unit cell consisted of two split circular rings connected by narrow strips integrated with p-i-n diodes, sandwiched between orthogonal polarizers serving as DC bias lines. By switching the diode states, the polarization orientation of the emitted waves was rotated, resulting in a broadband 180° phase difference. A prototype with 16×16 elements was designed, fabricated, and measured. The measured results indicated a 3 dB gain bandwidth of 45%, a 1 dB gain bandwidth of 17%, and a peak gain of 16.8 dBi with an aperture efficiency of 18.4%. Additionally, the proposed RTA demonstrated effective beam-scanning performance within a ±40° range in two dimensions. In [58], an electronically steerable transmitarray antenna operating at Ka-band, featuring 2-bit phase quantization per cell, was reported. The transmitarray was composed of 14 × 14 unit cells, each incorporating four p-i-n diodes for phase control. Experimental results demonstrated a scanning capability over a 120° × 120° window, with a maximum gain of 19.8 dBi at broadside and a 3 dB fractional bandwidth of 16.2%. In [59], the authors presented a 2-bit electronically reconfigurable transmitarray unit cell operating at Ka-band was presented. The design consisted of six metal layers and three dielectric substrates forming an antenna-filter-antenna structure, with two p-i-n diodes integrated on each patch for 2-bit phase resolution. Fabrication and waveguide-based characterization demonstrated minimal transmission loss between 1.5–2.3 dB and achieved a 3 dB fractional bandwidth of 10.1–12.1%.

2.5.4 Material Innovations in Transmitarrays

Material advancements significantly improve transmitarray performance :

1) Graphene-based metasurfaces offer dynamic control at THz frequencies due to tunable conductivity.

In [60], a graphene-based metasurface for broadband mid-infrared cross-polarization conversion was demonstrated. The design featured periodic graphene patterns on a metal-backed silicon dioxide substrate and achieved a polarization conversion ratio exceeding 0.9 over a wide frequency

range. The structure offered a 41.98% full-width at half-maximum bandwidth centered at 5.98 THz and maintained effective performance up to a 40° incident angle for both TE and TM polarizations. Field distributions and electromagnetic parameters supported the conversion mechanism, while the ultrathin unit cell design confirmed its classification as a metasurface.

2) VO2-based metasurfaces enable thermally-triggered switching at THz applications.

In [61], a programmable vanadium dioxide (VO2) metasurface for terahertz (THz) beam steering was proposed, utilizing the phase-change property of VO2 controlled by electrical stimulation. By using a field-programmable gate array (FPGA), dynamic phase gradients were achieved across the metasurface. In 1-bit coding, both periodic and aperiodic 24 × 24 configurations enabled wide-angle beam scanning from -60° to +60°, while 2-bit coding with 18 × 18 sequences allowed finer phase control and improved 3 dB diffraction efficiency. This programmable metasurface concept offers strong potential for dynamic THz wave manipulation in future 6G wireless systems.

3) Multilayer Huygens' metasurfaces achieve broadband, low-loss transmission.

In [62], a comprehensive overview of bandwidth-limiting factors in metasurfaces was provided, and a semi-analytical broadband design methodology was also introduced. By integrating network analysis with a genetic algorithm, the approach enabled the optimization of frequency-independent circuit parameters for multi-layer transmissive metasurfaces, achieving desired complex transmission coefficients over a wide bandwidth. The method was demonstrated through the design of quarter- and half-waveplate metasurfaces, showing improved bandwidth and efficiency. The approach also showed potential for mechanically tunable or reflective metasurfaces by modifying the substrate structure or accounting for interlayer coupling effects.

2.5.5 Application-Specific Transmitarray Designs

Transmitarrays are increasingly tailored for specific applications, including :

1) Satellite communication : Compact, high-gain designs suitable for satellite terminals [63, 64].

As shown in Figure 2.12, a high-gain multi-beam transmitarray antenna operating at 30 GHz was designed using a passive metasurface composed of three Rogers 5880 layers and four etched copper layers. Beam steering was achieved through two-dimensional displacement of multiple feed radiators, allowing independent control of beams in both azimuth (0°–360°) and elevation (0°–40°) planes. The metasurface, initially synthesized with a uni-focal phase profile and later optimized using a bi-focal distribution, achieved a peak measured gain of 34.2 dBi. The passive, low-cost, and foldable design with no active components, makes it suitable for robust deployment in deep space and next-generation satellite or mmWave 5G communication systems [65].

2) Vehicular Sensing and Communication : Fast switching arrays providing real-time object detection and tracking [66, 67].

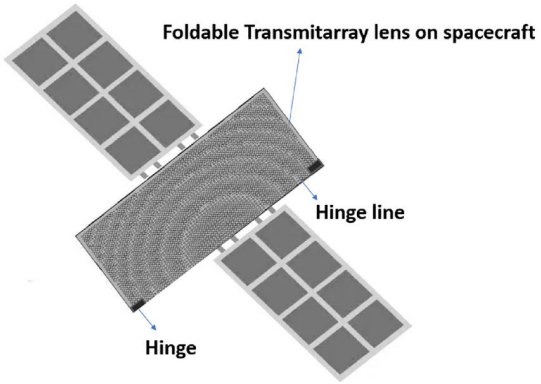

FIGURE 2.12 : Depiction of transmitarray lens mounted on satellite [65].

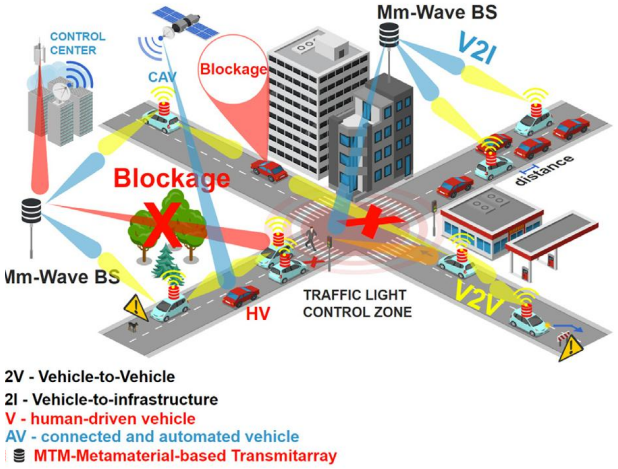

FIGURE 2.13 : Transmitarray antenna in vehicular sensing and communication [68].

In [68], a multi-bit transmitarray for Ka-band vehicular sensing applications was proposed, featuring 400 unit cells with independently controlled phase and amplitude. The beam steering was achieved through cell-specific phase compensation and amplitude tapering, optimized using a Genetic Algorithm to minimize gain loss and side-lobe levels. Simulations and measurements showed peak gains up to 27.2 dBi with side-lobe levels below -22.1 dB and cross-polarization levels below -44 dB, confirming the TA's effectiveness for high-gain, low-SLL millimeter-wave vehicular communication, see Figure 2.13.

3) Base stations : Beam-steerable and reconfigurable designs for dynamic user tracking and interference reduction in mmwave communication systems [69, 70].

Figure 2.14 illustrates a transmitarray antenna with beam scanning capability for enhancing communication in systems involving base stations. It adjusts the beam direction to maintain strong, reliable links with other base stations and communication users. This capability improves the signal strength, reduces interference, and ensures robust connectivity within cellular networks. This demonstrates the critical role of managing the beam direction for reliable communication [71].

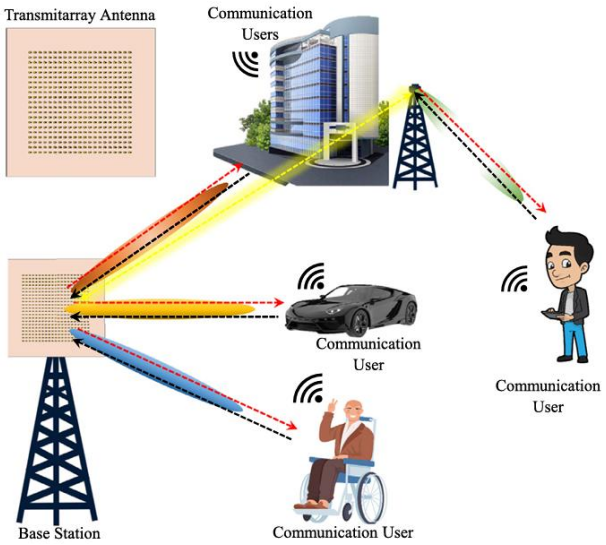

FIGURE 2.14 : Conceptual illustration of a transmit array antenna in base stations [71].

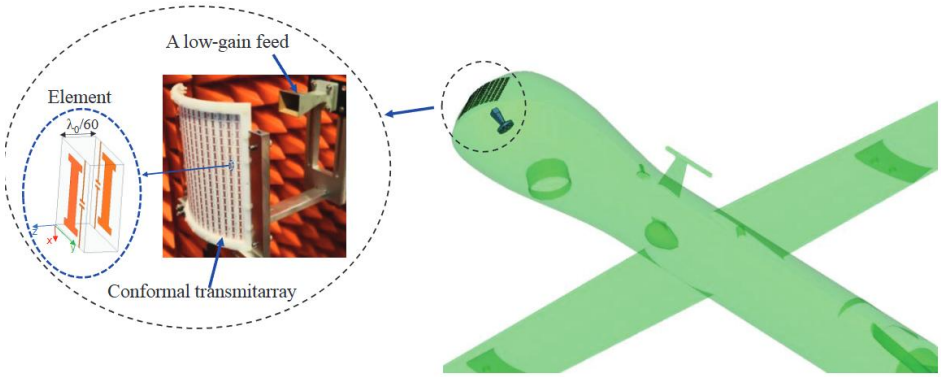

FIGURE 2.15 : Schematics of a conformal transmitarray integrated with an UAV [74].

4) UAVs and drone communication : Lightweight and low-profile antennas with beam agility for maintaining stable high-throughput links in mobile aerial platforms [72, 73].

In [74], the authors reviewed recent advances in conformal transmitarrays for UAV-based wireless communications, emphasizing their potential for high-gain, multi-beam performance in 6G networks. It highlighted design challenges and emerging solutions for integrating efficient, aerodynamic antennas on UAV platforms to support high-speed, millimeter-wave connectivity, as illustrated in Figure 2.15.

2.6 Conclusion

In this chapter, we presented a detailed literature review by exploring key papers, research studies, and recent advancements in the field of transmitarray antennas. We examined various beamforming techniques, highlighted the limitations of conventional approaches, and reviewed the

evolution of metasurface-based transmitarrays with reconfigurable and application-specific designs. This comprehensive review provides a solid foundation and highlights the importance of transmitarrays for high-performance millimeter-wave systems. With this knowledge, we now proceed to the design and development of transmitarray antennas for beamforming purposes in the following chapters.

3 FEED ANTENNA

3.1 Introduction

Based on the research objective and methodology outlined in Chapter 1, beam-steering antenna systems typically consist of two main components : a feeding antenna and a metasurface panel. This chapter focuses on the design and development of the feed antennas required for the proposed reconfigurable beamforming system operating at 28 GHz. Developing efficient and practical feed solutions is a critical first step toward realizing the complete transmitarray system, ensuring high gain, low loss, and effective excitation of the metasurface panel.

Two types of feed antennas are explored to address different design needs and implementation stages. The first is a Substrate Integrated Waveguide (SIW)-based slot antenna array, selected for its high gain, broadband operation, low loss, and excellent integration capability in millimeter-wave systems. The SIW feed is intended for the final deployment of the beamforming system, where compactness, performance, and integration are key.

The second is a 3D-printed horn antenna, designed and evaluated as a simplified, well-understood reference configuration. Thanks to its straightforward geometry and reduced meshing complexity, the horn antenna offers faster simulation times, making it a practical choice for early-stage testing and prototyping.

By leveraging these two complementary feed options, the system offers flexibility in both simulation and practical implementation. Both antennas are designed to operate in conjunction with metasurface panels composed of phase-reconfigurable unit cells, as will be discussed in the following chapters.

3.2 Proposed SIW Antenna

In the first part of this chapter, we focus on the study and investigation of SIW technology to design mm-wave antenna feeding networks with low loss and high efficiency. This section introduces the fundamental concepts of SIW , including key formulas and primary design guidelines. In alignment with the project objectives of the industrially funded project presented in Chapter 1, the target is to design an SIW antenna that achieves a gain greater than 16 dBi within the 27–29 GHz frequency band.

It is important to note that although the general performance target for the complete transmitarray system is a realized gain exceeding 16 dBi, the design goal for the SIW-based feed antenna (intended for final implementation) is set above this threshold. This ensures sufficient margin to

compensate for the potential gain reduction that may occur after integrating the feed with the metasurface panel in practical scenarios.

SIW stands for Substrate Integrated Waveguide, which is a rectangular waveguide-like structure in an integrated planar form, that is created by utilizing slots and two rows of conducting cylinders embedded in a dielectric substrate that is electrically sandwiched by two parallel metal plates [75]. The modes of the SIW practically coincide with a subset of the modes of the rectangular waveguide, namely with the TE_{n0} modes, with n =1, 2, ... In particular, the fundamental mode is similar to the TE_{10} mode of a rectangular waveguide, with vertical electric current density on the side walls. TM modes cannot exist in the SIW, due to the gaps between metal vias : in fact, transverse magnetic fields determine longitudinal surface current. Due to the presence of the gaps, the longitudinal surface current is subject to strong radiation, preventing the propagation of TM modes [76–78]. Figure 3.1.a depicts the basic structure of SIW. The key design parameters of the SIW slot antenna can be calculated by the following equations :

$$fc_{mn} = \frac{c}{2\pi\sqrt{\varepsilon_r}}\sqrt{\left(\frac{m\pi}{a_{\text{eff}}}\right)^2 + \left(\frac{n\pi}{b}\right)^2} \tag{3.1}$$

$$a_{\text{eff}} = a - \frac{{v_d}^2}{0.95 \ \cdot \ v_s} \tag{3.2}$$

$$v_d \leq \frac{\lambda_0}{10} \tag{3.3}$$

$$v_s \leq 2v_d \tag{3.4}$$

Where, fc_{mn} is the cutoff frequency for TE_{mn} mode, vd is via diameter, vs is via spacing, and a_eff is the effective SIW width. The gap between center to center of slots has been considered as λ_g/2 whereas the gap between the last slot, and the closing face has been taken as λ_g/4 [2,78,79].

The proposed SIW slot antenna is designed based on the basic configurations, as shown in Figure 3.1.b. In order to have a desired far-field characteristic, the array of four elements is formed, as given in Figure 3.1.c. Then, the feeding network is designed for the proposed structure while the elements are brought closer to each other, as just one column of vias is between elements for making a panel of the proposed SIW slot antenna smaller, as shown in Figure 3.1. d. In the last step, the designed panels are placed in a form of a hexagonal shape, as given in Figure 3.1.e.

3D Radiation patterns of the proposed antenna for different excitations are demonstrated in Figure 3.2. Note, one panel of the proposed antenna configuration is excited at a time in the hexagonal structure. This arrangement is suitable for achieving 360-degree coverage.

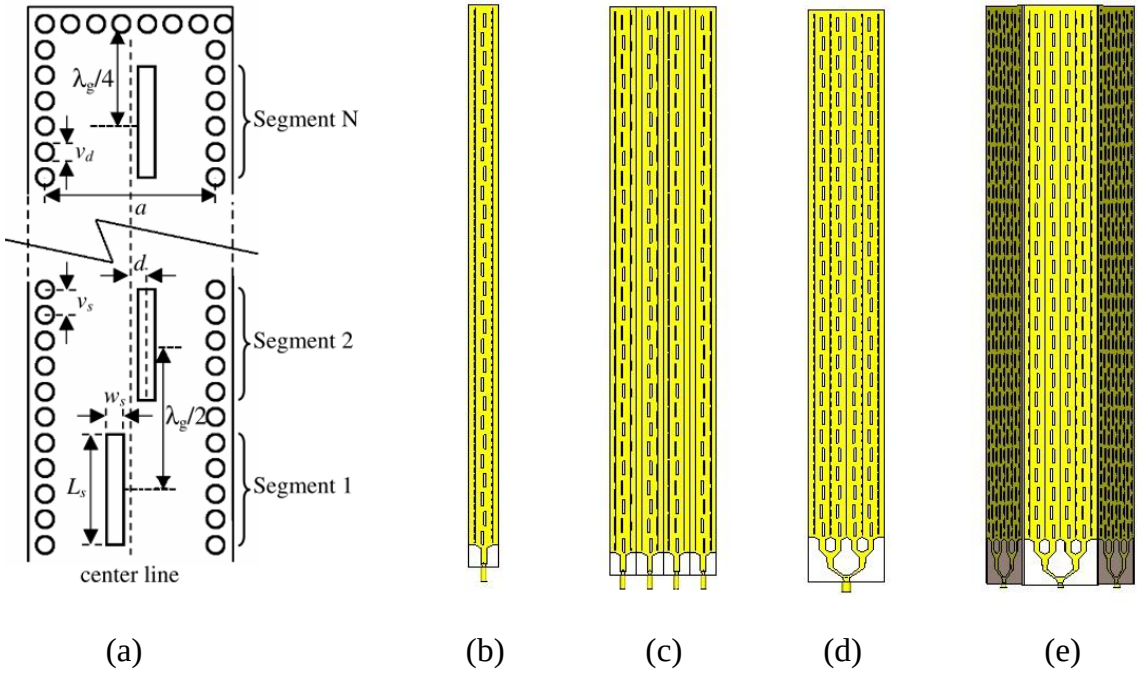

FIGURE 3.1 : (a) Basic structure of SIW slot antenna (b) step 1, (c) step 2, (d) step 3, and (e) step 4 of the proposed SIW slot antenna.

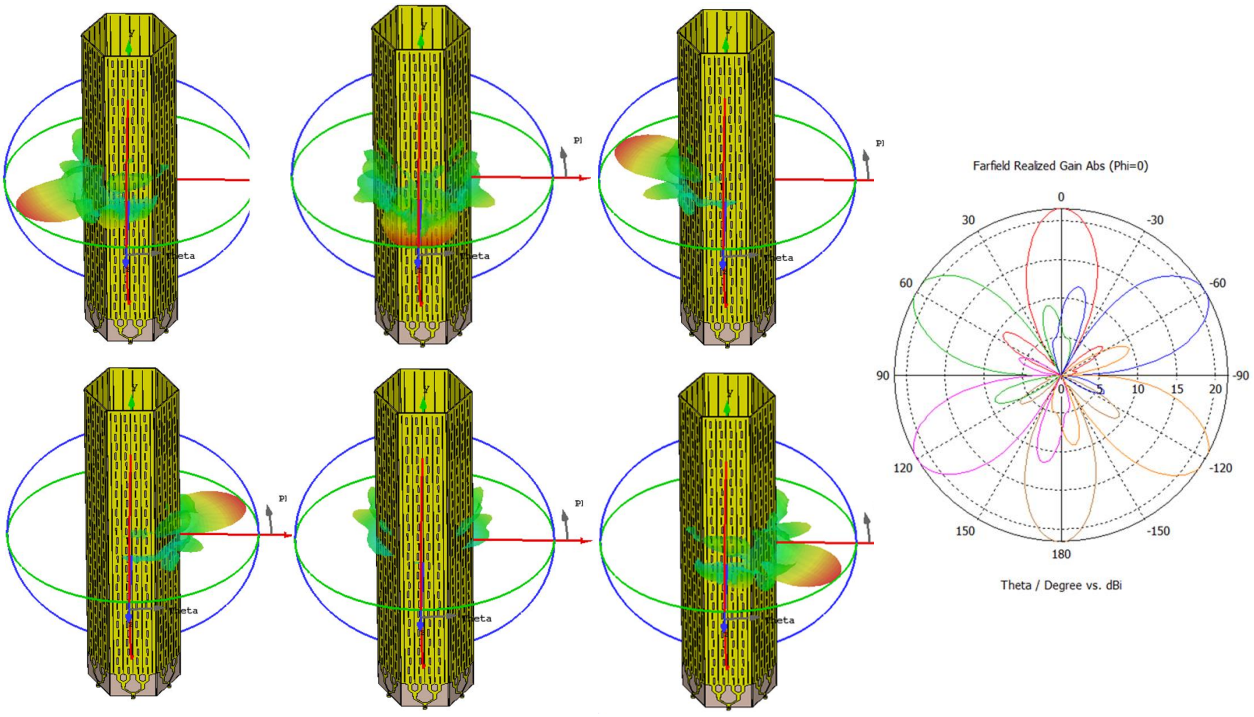

FIGURE 3.2 : Radiation patterns of the proposed SIW antenna for different excitation ports.

It should be pointed out that the conventional microstrip line has been used to feed the proposed structure. The part of the microstrip line that connects to the radiating section has been

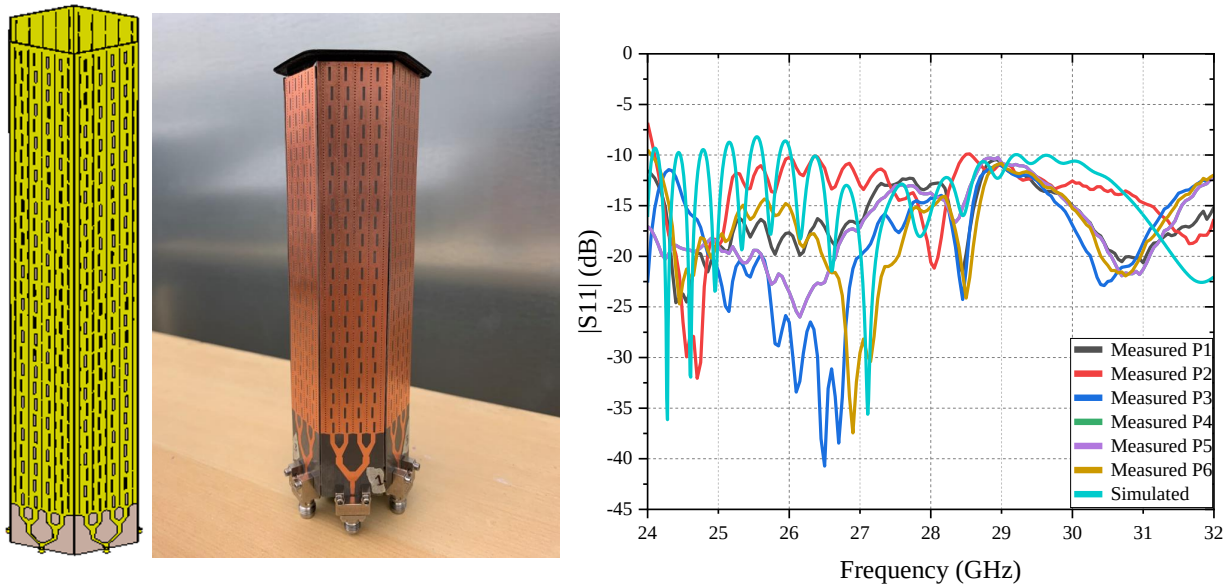

(a) (b) (c)

FIGURE 3.3 : Proposed SIW slot antenna (a) configuration (b) prototype (c) the reflection coefficient.

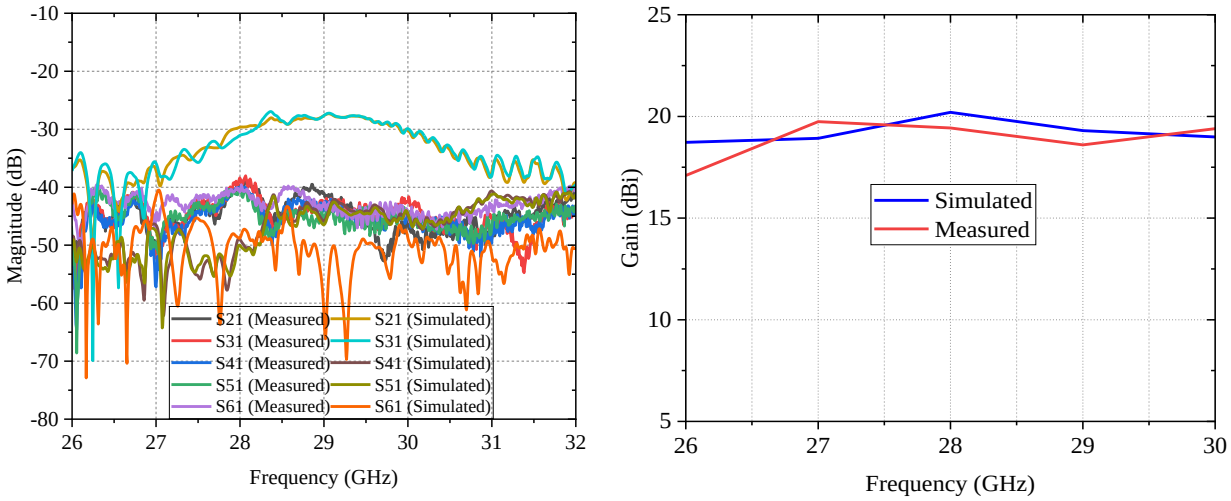

(a) (b)

FIGURE 3.4 : Proposed SIW slot antenna : (a) transmission coefficients (b) gain.

tapered to achieve better impedance matching. This design is referred to as the microstrip to SIW transition [80]. Besides, the connector's effect is considered during the design steps. To measure the antenna performance, the designed SIW slot antenna is fabricated on a Rogers 5880 with a

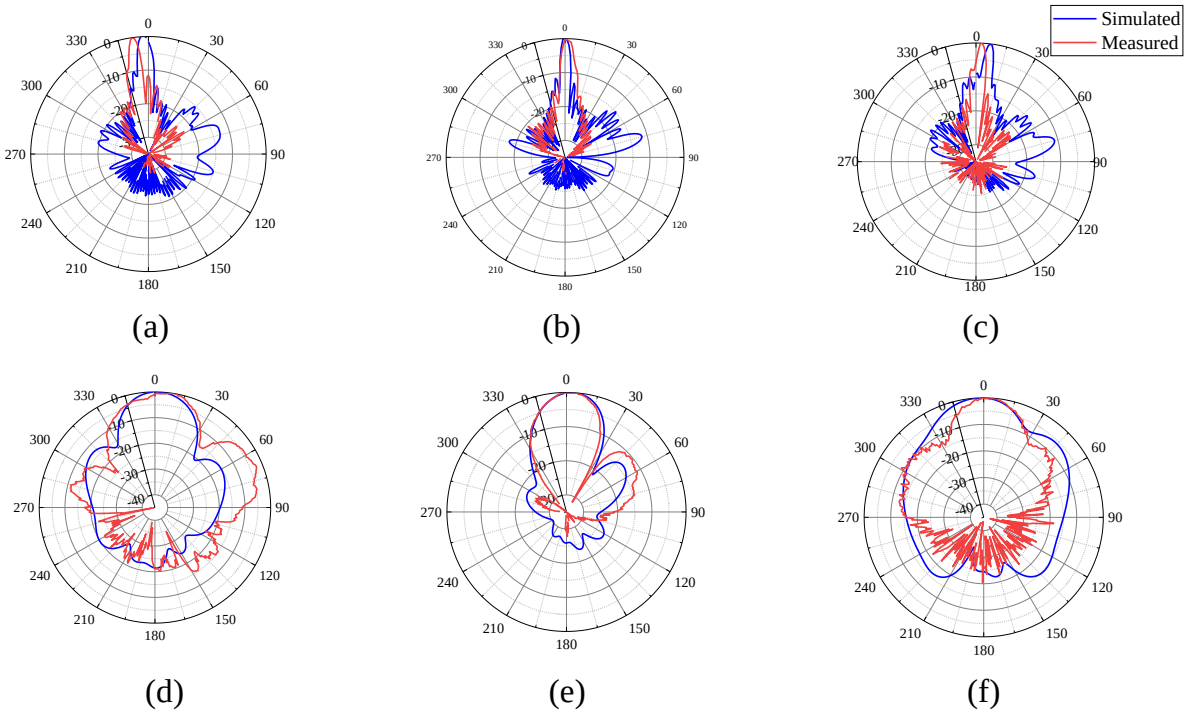

FIGURE 3.5 : Radiation pattern of the proposed SIW slot antenna in the E-plane at (a) 27 GHz, (b) 28 GHz, and (c) 29 GHz, H-plane at (d) 27 GHz (e) 28 GHz (f) 29 GHz.

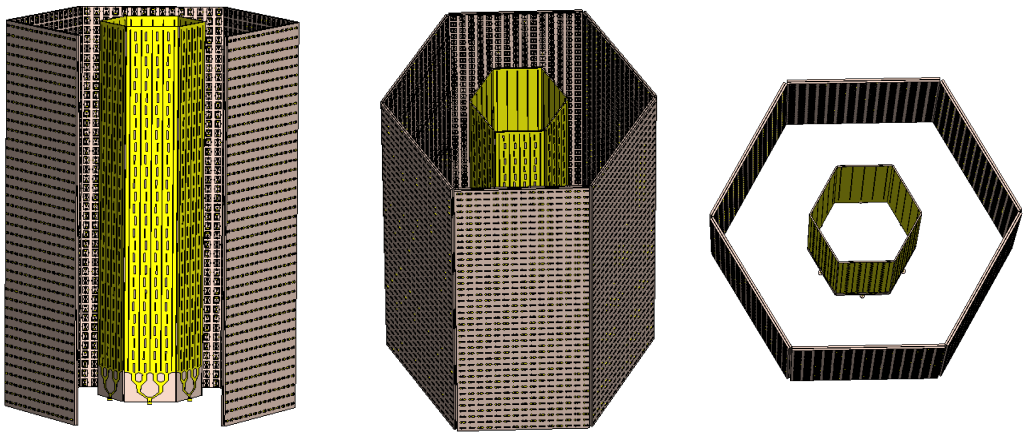

FIGURE 3.6 : Configuration of the beamforming structure using proposed SIW slot antenna.

relative dielectric constant of 2.2 and a thickness of 0.508 mm. Figure 3.3.a and Figure 3.3.b show the configuration and the prototype of the proposed SIW slot antenna, respectively.

The measured S_{11} for different panels are shown in Figure 3.3.c, along with the simulated result. Moreover, the transmission coefficients and gain are also provided in Figure 3.4.a and Figure 3.4.b, respectively. The simulated and measured results show a good agreement. Although the reflection coefficient of the proposed antenna extends from 26 GHz to higher frequencies, our focus is specifically on the 27 to 29 GHz range, as defined by the project objectives. All six panels were measured individually; each time, one panel was excited while the remaining five panels were

terminated with 50-ohm loads. Some differences between the measured results were observed, mainly due to fabrication tolerances. Additionally, the isolation between the six ports was measured and found to be better than -26 dB. Furthermore, the gain of the proposed configuration was measured and compared with the simulated results for one panel. The maximum simulated gain for a single panel is 20.2 dBi, and the gain remains above 18.7 dBi across the 27 to 29 GHz frequency range. In addition, the corresponding radiation patterns are shown in Figure 3.5, where the simulated and measured results agree well.

As explained earlier, an SIW slot antenna was designed and measured. To create the source for the beamforming system, six of these SIW antennas were arranged in a hexagonal configuration. This hexagonal assembly serves as the primary source antenna. Subsequently, a metasurface panel is placed in front of each SIW antenna, also arranged in a hexagonal layout. Together, the six SIW antennas and six metasurface panels form the complete transmitarray for beam-steering system, enabling symmetrical and efficient control over the direction of the transmitted beam, as illustrated in Figure 3.6.

3.3 Proposed Horn Antenna Configuration

In the previous section, the detailed design and validation of the SIW-based slot antenna array were presented. This antenna is intended for the final implementation of the beamforming system and serves as the primary radiating source in the proposed reconfigurable transmitarray configuration. However, due to the complex geometry of the SIW structure, full-wave simulations in CST Microwave Studio require a fine mesh and thus result in increased computational time. To address this limitation and facilitate faster and more efficient simulations, a 3D-printed horn antenna is also designed, fabricated, and evaluated. The proposed horn antenna serves as the second option and acts as a simplified and reliable reference feed. Its well-known radiation characteristics, broad bandwidth, and lower meshing complexity in CST make it an ideal candidate for early-stage simulations, rapid prototyping, and experimental testing of the metasurface panels. Later in this section, we demonstrate how six horn antennas can be used to achieve 360-degree beam control within the beamforming system.

It should be mentioned that while off-the-shelf standard horn antennas are commercially available and can be used in such test setups, their relatively large physical size poses integration challenges in compact beamforming systems. In this project, where a 360 degree beam coverage is targeted using a multi-panel transmitarray configuration, the physical footprint of the feed antenna becomes a critical factor. Therefore, a custom compact horn antenna is designed and fabricated to reduce the overall size of the complete system without compromising performance. To this end, a 3D-printed WR-series waveguide horn antenna is developed. This design provides high directivity, low insertion loss, and a well-controlled radiation pattern, ensuring effective and uniform illumination of the transmitarray aperture.

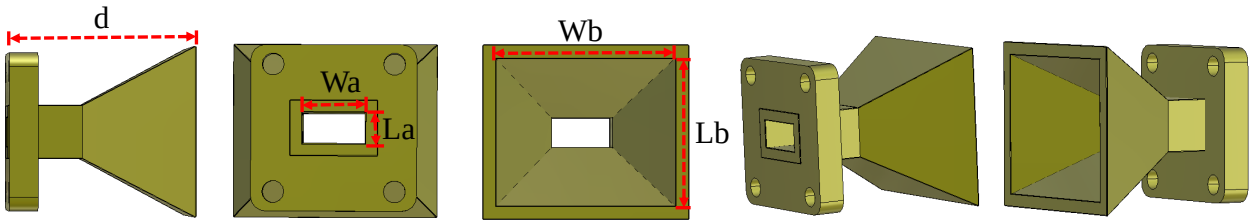

FIGURE 3.7 : Proposed 3D-printed horn antenna (d = 26.2, Wa = 8.6, La = 4.3, Wb = 24.5, Lb = 20, all in mm).

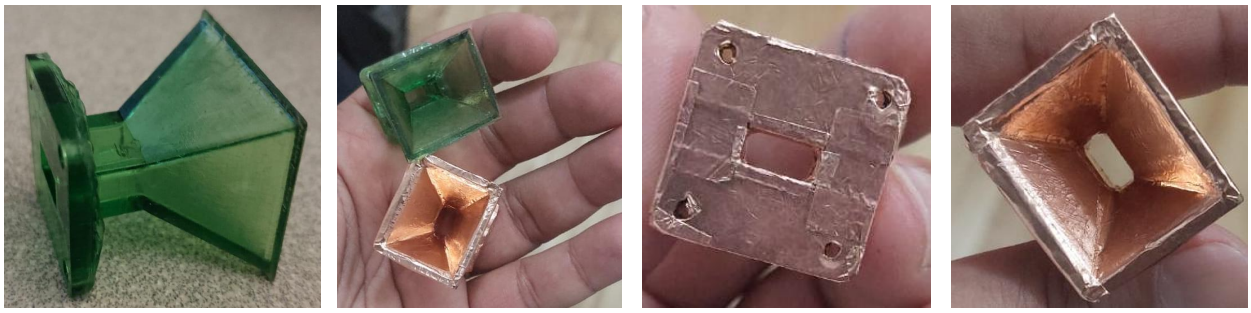

FIGURE 3.8 : Fabricated prototype of the proposed 3D-printed antenna.

TABLEAU 3.1 : Realized Gain of the proposed 3D-printed horn antenna.

	26 GHz	28 GHz	30 GHz
Simulated Realized Gain	13.2	13.9	13.8
Measured Realized Gain	13	13.3	13.1

The configuration and fabricated prototype of the proposed 3D-printed horn antenna are shown in Figure 3.7 and Figure 3.8, respectively. The proposed horn antenna is designed based on standard horn antenna principles, with specific modifications to suit the project requirements. The design process begins with the selection of a WR-series waveguide aperture. From this foundation, the flare dimensions (the width and height) are optimized to achieve the desired radiation characteristics while minimizing the overall physical length. This compact design enables fabrication using PLA material via 3D printing. After fabrication, the horn is coated with copper to ensure proper electromagnetic performance and is then connected to the WR waveguide interface. This approach allows for a reduced-size horn antenna that remains effective for beamforming applications while being suitable for integration within the limited space of the overall transmitarray system.

Figure 3.7 depicts the reflection coefficient and measurement setup of the proposed 3D-printed horn antenna. The results indicate that the simulated S_{11} is below -18 dB, while the measured one remains below -12 dB within the frequency band of interest.

The proposed antenna is specifically designed to operate at a center frequency of 28 GHz, making it suitable for applications at mm-wave frequencies. At this frequency, the feed provides a measured gain of 13.3 dBi, as given in Table 3.1, which ensures a transmitarray a narrow and

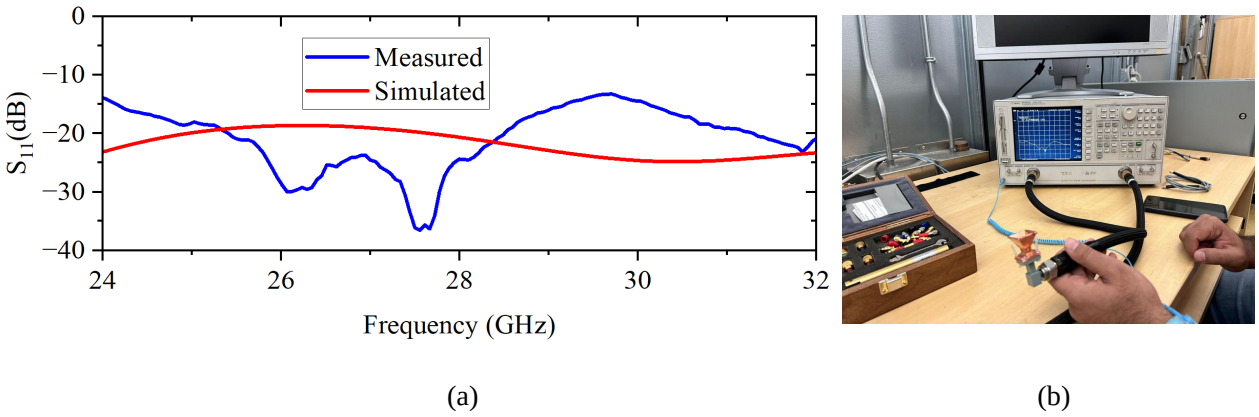

FIGURE 3.9 : (a) Reflection coefficient, and (b) measurement setup of the proposed 3D-printed horn antenna.

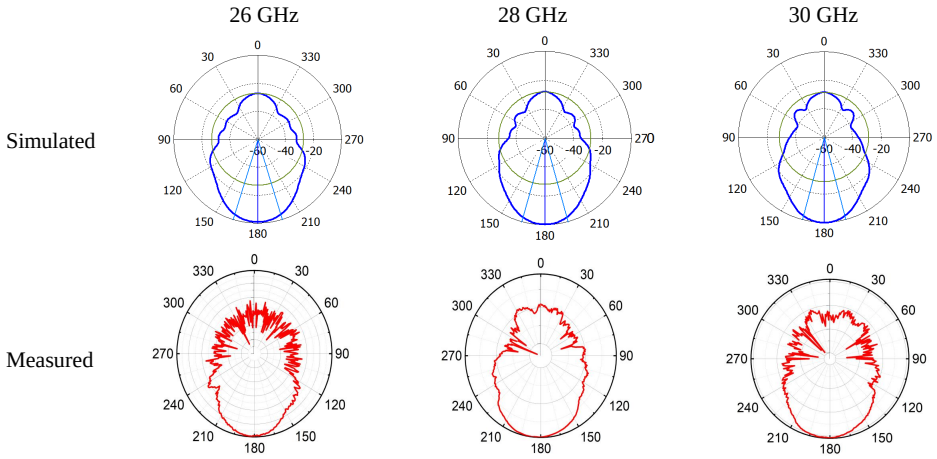

FIGURE 3.10 : The radiation pattern of the proposed 3D-printed horn antenna for different frequencies.

focused beam that can adequately illuminate the entire aperture of the transmitarray with minimal spillover. High-gain feeds are essential in transmitarray designs because they reduce the amount of energy radiated outside the aperture, thereby increasing the usable energy directed toward the main beam and improving the overall aperture efficiency. The physical length of the feed antenna is 26 mm, which reflects a compact form factor suitable for integration into planar or low-profile array structures. Despite its compact size, the antenna maintains excellent performance which can be seen from Figure 3.10. This compactness is especially valuable when space constraints are present or when the feed needs to be embedded into a conformal or portable system. One of the most important aspects of feed design is its radiation pattern, which must be tailored to match the focal geometry of the transmitarray. Uniform or properly tapered illumination is essential for minimizing amplitude taper loss and suppressing side lobe levels. In this case, the feed exhibits a very low side lobe level of –31.5 dB, indicating that the energy radiated into undesired directions is significantly suppressed. This contributes to a cleaner main beam and reduces interference or coupling with adjacent elements or devices.

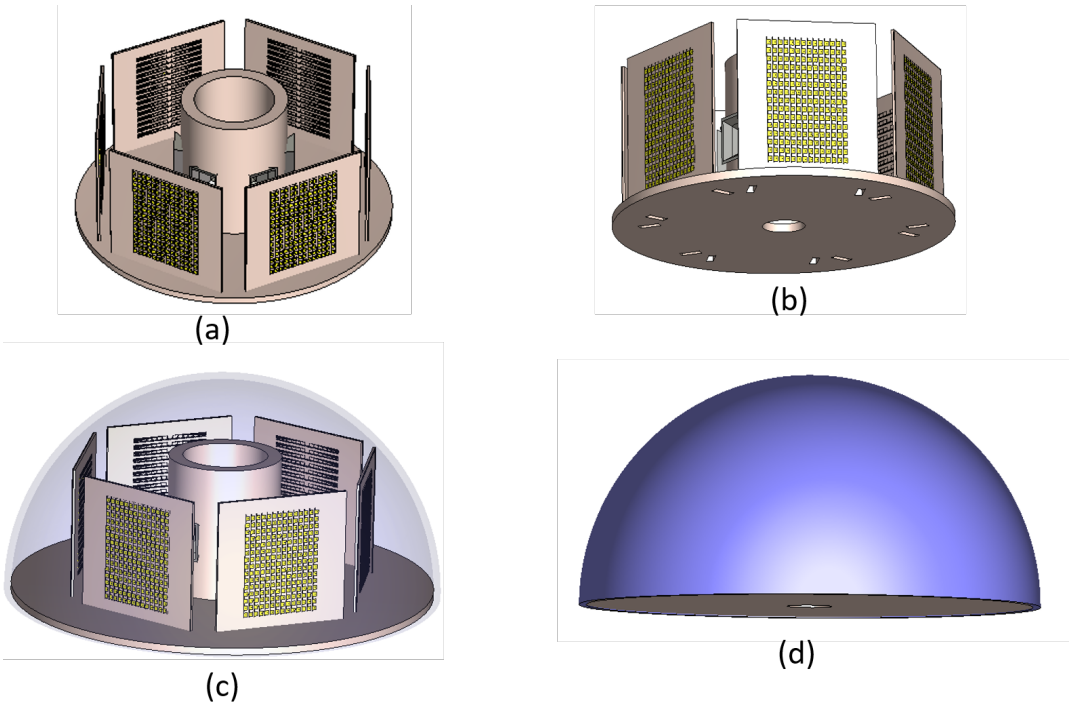

FIGURE 3.11 : (a) Proposed configuration of the transmitarray antenna, (b) etched layout for connections and wiring, (c) proposed antenna enclosed with radome, (d) standalone radome structure.

To achieve full 360° azimuthal beamsteering using a transmitarray architecture, the system is modularly designed by replicating a single panel that can steer beams within a ±30° angular range. As shown in Figure 3.11, the complete configuration is composed of six identical transmitarray panels arranged cylindrically around a central support structure. Each panel is optimized to operate independently and steer the beam within its 60° field of view, ensuring seamless 360° coverage when all six panels are integrated. The base plate provides mechanical stability and acts as a shared platform for mounting all unit cells, feed elements, and control circuits. The configuration supports electronic beamsteering across each sector, offering the potential for continuous scanning without mechanical movement.

For practical deployment, especially in outdoor or mobile environments, the system is enclosed within a hemispherical radome, as illustrated in Figure 3.11.c–d. The radome serves multiple purposes : it offers environmental protection against dust, wind, and precipitation, while also preserving the structural integrity of the transmitarray panels during operation and transport. Designed with minimal electromagnetic interference, the radome material and shape are selected to ensure negligible impact on the transmitted and received signals across the operating frequency band. The dome's geometry also supports uniform radiation across all panels by minimizing multipath effects and preserving beam shape integrity. Additionally, enclosing the system in a radome enhances its stealth and mechanical robustness, making it suitable for real-world applications such as wireless communication hubs, or satellite terminals that require both mobility and full azimuthal scanning capability.

3.4 Summary

This chapter presented the design, fabrication, and experimental validation of two feed antennas operating at a center frequency of 28 GHz : a SIW-based slot antenna array and a 3D-printed WR-series waveguide horn antenna. The SIW antenna was chosen for its compact size, low loss, and high integration potential, making it the preferred solution for final deployment in the beamforming system. Meanwhile, the 3D-printed horn antenna was developed as a reference feed, offering advantages in simulation and measurement due to its simplified geometry, broad bandwidth, and reduced meshing complexity.

Both antennas were fabricated and characterized through full-wave simulations and measurements. The results showed agreement, confirming the validity and robustness of the designs. The dual-feed approach ensures flexibility in both experimental validation and practical integration.

These feed antennas can be easily employed to excite the metasurface panels introduced in the following chapter. Next chapter (Chapter 4) will begin the design process of the reconfigurable metasurface, starting with the unit cell, which serves as the fundamental building block of the proposed beam-steering transmitarray system.

4 UNIT CELL DESIGN BASED ON USING MUTUAL COUPLING IN A CONSTRUCTIVE WAY AND CURRENT REVERSAL TECHNIQUE

Following the design and validation of the feed antennas in the previous chapter, this chapter focuses on the development of the metasurface unit cell, the fundamental element enabling phase manipulation in the proposed beamforming transmitarray system.

In this chapter, we explore a technique for unit cell design that leverages constructively mutual coupling and current reversal techniques. This approach exploits the strong electromagnetic interaction between closely spaced radiating elements to manipulate the direction of the main beam.

To systematically understand and evaluate the beamforming mechanism, we begin by designing a passive unit cell. This helps establish the baseline phase response and transmission performance without active components. Using the passive unit cell, we build a metasurface panel and validate its beamforming capability in simulation. After confirming the functionality of the passive system, we extend the design to a reconfigurable (active) unit cell by integrating tunable elements, enabling real-time beam steering. A new metasurface panel is then constructed using these active unit cells, and its performance is evaluated to demonstrate dynamic beam control. This chapter covers both stages, passive and active unit cell design, and sets the foundation for full transmitarray implementation.

4.1 1-Bit Passive Unit Cell Configuration

This section is based on the following publication :
P. PourMohammadi, H. Naseri, N. Melouki, F. Ahmed, Q. Zheng, A. Iqbal, and T. A. Denidni, “A Wideband Beam Steering Transmitarray Antenna for Ka-Band Applications,” AEU-International Journal of Electronics and Communications, 2025.

4.1.1 Introduction

Mobile communication technologies are now omnipresent in our society, thanks to the widespread adoption of smartphones and similar devices [81,82]. Hence, mobile networks face the challenge of meeting rising consumer expectations for faster data speeds while also coping with the anticipated surge in data traffic, which is rapidly growing [83,84]. As a result, cellular providers are working towards providing high-quality, low-latency video and multimedia applications for wireless devices [85], [86]. Several technological advancements are emerging independently to enhance wireless communication system performance significantly. One of these advancements involves

utilizing the millimeter-wave frequency bands, which offer more available spectrums since they are predominantly unused. In addition, the utilization of higher frequencies results in the availability of smaller antennas and circuits, thus enabling RF transceivers to become more affordable and compact [87], [88].

While high frequencies offer the potential to transmit greater amounts of data, they are limited by their inability to penetrate and provide coverage over larger areas [89]. Therefore, one way to extend coverage at longer ranges is by enhancing transmitting power without raising the cost of the communication system. One solution to accomplish this, is by using a large number of antennas that can handle multiple users simultaneously [27], [90], [91]. These antennas can be operated by smart systems that incorporate beamforming and multiple-input multiple-output (MIMO) systems techniques [92, 93]. Therefore, it is essential to design an antenna capable of multitasking by consolidating various functions into a single component. Addressing the challenge of radiation interference necessitates an element capable of directing the beam toward a specific direction while mitigating undesired beams in other directions [4], [94]. Consequently, beam steering antennas, frequently employed in reconfigurable pattern antennas, have garnered considerable attention in wireless communication systems. These antennas offer a significant reduction of interfering signals and enhancement of the system capacity. Integration of these antennas enables additional functionalities and greater flexibility, often within the same or even smaller physical footprint compared to traditional smart antenna arrays [95], [96]. Furthermore, to meet the future needs of consumers and technology, the beamforming subsystems and components must fulfill certain criteria, such as being low-loss, compact, and easy to manufacture. Additionally, they must address the challenges associated with designing cost-effectiveness and working with high frequencies [97], [98].

Transmitarray antennas, also known as discrete lenses or flat lens arrays, have emerged as a highly promising antenna architecture for a wide range of millimeter-wave applications to address the above-mentioned limitations. This is primarily due to their impressive attributes, such as high gain, beam-scanning, and beam-forming capabilities, along with their relatively low cost and seamless integration into base stations [99].

There are two primary approaches for designing transmitarray antennas : the multilayer-frequency selective surface method [100–103] and the receive/transmit method [36, 104]. The multilayer-frequency selective surface method stacks multiple frequency selective surface layers, typically more than three, which leads to a relatively high profile for the transmit array, as each layer is usually thicker than 0.1 λ_0. On the other hand, the receive/transmit approach only necessitates the receive and transmit layers, which can result in a potentially thinner unit-cell thickness [105, 106]. Also, increasing the bandwidth is predominantly accomplished through the receive/transmit method. The structure of a transmitarray antenna in the receive/transmit approach consists of two main components : a transmitter layer and a receiver layer, in which two layers are connected by a circuit that controls the direction of those signals. The entire setup is powered by a central focal source. Instead of using a separate circuit such as a phase shifter, the unit cells can be

designed to fulfill the required phase. indeed, through precise control of the transmission phase introduced by each unit cell, the transmitted signal from the focal source can be focused and manipulated, facilitating beam-forming and beam-steering functionalities. However, a significant challenge in the development of transmitarrays lies in designing unit cells capable of independently varying their transmission phase across different frequency bands while minimizing insertion loss [107], [108], [109, 110].

Transmitarray antennas have extensively been researched in the literature, focusing on their performance, design, and applications in modern communication systems. Despite significant progress in enhancing beamforming capabilities, these antennas often face limitations such as a narrow bandwidth and modest gain enhancement. Consequently, developing high-gain and beam-scanning antennas is essential for advancing millimeter-wave communication technologies. Achieving a wide bandwidth and high aperture efficiency poses considerable design challenges that must be addressed to meet the demands of modern communication systems [111]. The impedance bandwidth, -3 dB gain bandwidth, and aperture efficiency of existing transmit arrays with beam-steering capabilities are often suboptimal [112–115]. However, some research has yielded promising results, though there is room for improvement. For instance, in [116], a transmitarray antenna has been designed for intersatellite communications, using feed displacement, achieving a 3-dB gain bandwidth of 19.1% with an aperture efficiency of 35%. In [117], researchers have introduced a folded transmitarray antenna utilizing a Fabry-Perot polarizer, which exhibited an 18% 3 dB gain bandwidth and an aperture efficiency of 13.8%. The authors of [118] have presented an innovative Cassegrain-reflectarray-fed transmitarray antenna, incorporating amplitude and phase distribution synthesis, resulting in a 36.9% aperture efficiency but only a 9.5% gain bandwidth. In [119], a two-layer transmitarray antenna utilizing the mutual coupling of vias to collect the transmission phase without extra substrate layers has been proposed, achieving an aperture efficiency of 28% and a 3 dB gain bandwidth of 11.2%. In [120], a Ka-band transmitarray antenna with mechanical beam steering was designed, showing an aperture efficiency of 13%. In [121], a transmitarray developed using a unit cell featuring crossed-arrow geometry and a two-line symmetry structure achieves an aperture efficiency of 28.4% and a 3-dB gain bandwidth of 16.5%. A planar lens antenna, utilizing metamaterials, was reported for spatial beamforming and multibeam massive multiple-input multiple-output (MIMO) systems in [122]. The findings have showed that the presented antenna attained an aperture efficiency of 24.5% within its operating bandwidth of 26.6-29 GHz (12%).

Although there have been significant advancements in designing transmitarray antennas, further enhancements are still needed. Therefore, we aim to achieve a wider bandwidth with higher aperture efficiency. The proposed transmitarray antenna addresses the shortcomings and positions it as a promising candidate for future wireless communication systems. In this paper, at first, a wideband unit cell design is presented, strategically leveraging mutual coupling in a constructive manner to form a transmit array. Following this, the source antenna (horn antenna) is excited. The validity of the beamforming principle is confirmed through the utilization of a fully functional

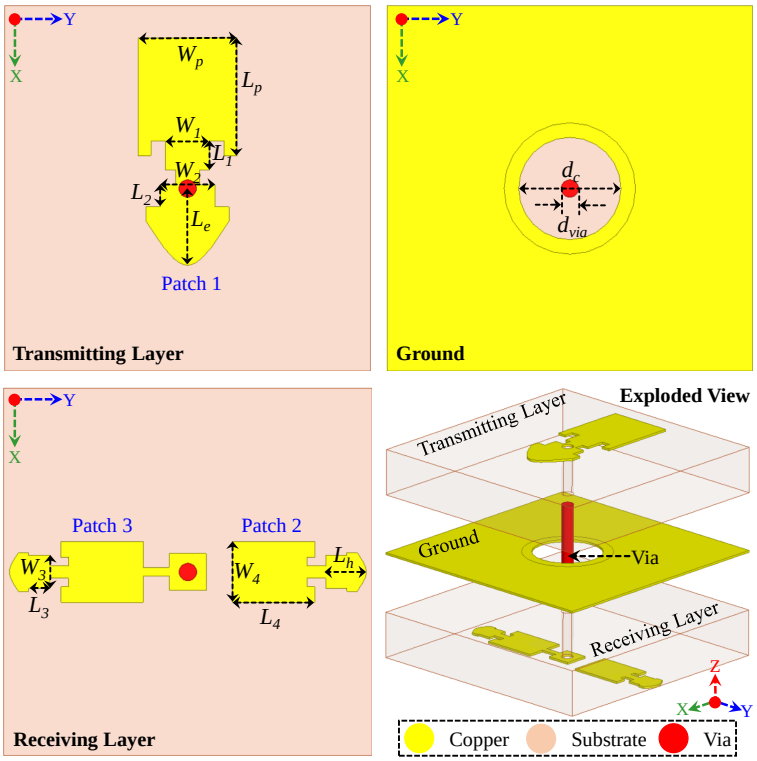

FIGURE 4.1 : Configuration of the proposed 1-bit unit cell (Wp = 1.13, Lp = 1.35, L1 = 0.34, W1 = 0.50, L2 = 0.25, W2 = 0.63, Le = 0.88, W3 = 0.38, L3 = 0.24, W4 = 0.7, L4 = 0.93, Lh = 0.46, s = 0.42, dvia = 0.2, dc = 1.17, all in mm).

metamaterial-based system. According to the results, a broad bandwidth of 33.3% is achieved, with the antenna gain surpassing that of its feed by 12.22 dBi, reaching a value of 25.52 dBi at 28 GHz.

4.1.2 Proposed Passive Unit Cell

The configuration of the proposed passive unit cell is given in Figure 4.1. The unit cell employs a 1-bit phase quantization (0° and 180°) aiming to decrease the insertion loss and minimize the overall expense of the antenna system.

The proposed unit cell's structure involves a modified patch array on top of the upper substrate (Tx) and two modified patch arrays on the bottom of the lower substrate (Rx). These layers are interconnected by a metalized via-hole with a diameter of 0.38 mm, centrally positioned within the unit cell. Both components are fabricated on identical substrates made of Rogers RO3003 material, featuring a dielectric constant of 3 and a thickness of 0.787 mm. These substrates are separated by a copper ground plane with a thickness of 0.035 mm.

The method employed to alter the patch in the proposed unit cell involves constructively leveraging mutual coupling to achieve a broader bandwidth. Initially, a conventional array, composed of two patches, is designed. Following this, adjustments are made to the patch shapes, and their

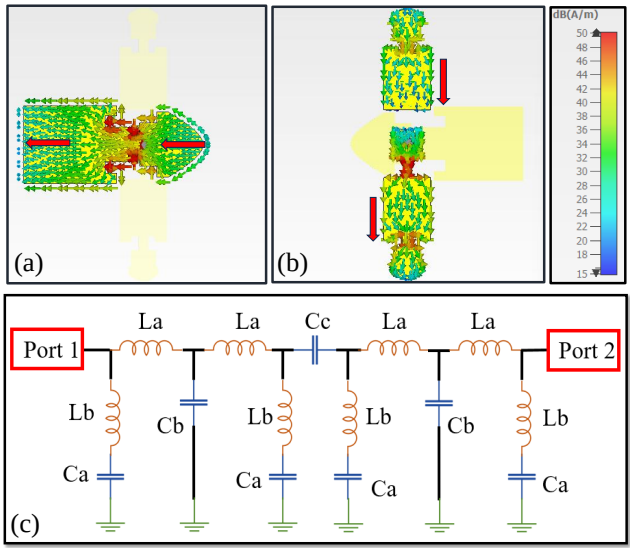

FIGURE 4.2 : Vector plot of the current distribution on the proposed unit cell (a) top layer, (b) bottom layer at 28 GHz, and (c) the equivalent circuit model of the proposed unit cell.

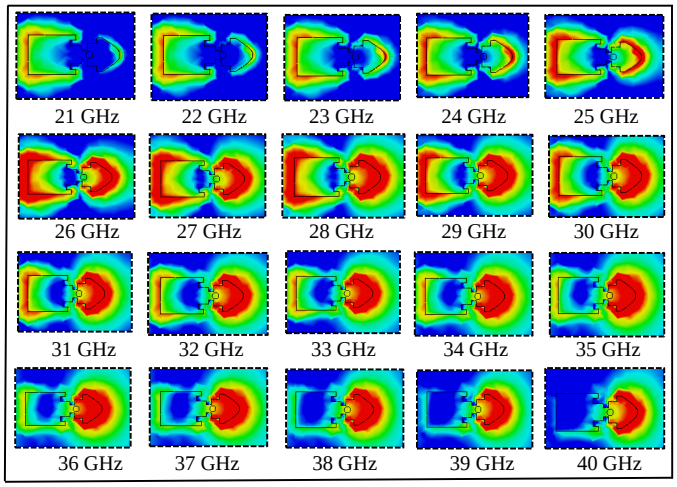

FIGURE 4.3 : Electric field on the proposed structure.

proximity to each other is fine-tuned. It is crucial to highlight the need for monitoring the surface current between the patches to achieve an optimal distribution of in-phase current in both, as shown in Figure 4.2.a and Figure 4.2.b. The equivalent circuit model of the proposed unit cell is presented in Figure 4.2.c. In the proposed design, the patches and short pins act as an inductor, and the gap acts as a capacitor. It is obvious that the direction of the current on the proposed structure in both rectangular and half-elliptical patches is the same. To comprehend the operational principles and assess the mutual coupling comprehensively, it is imperative to scrutinize the electric field within the modified patch structure. The electric field within the proposed configuration changes between rectangular and half-elliptical patches across different frequencies, as depicted in Figure 4.3. Notably, while the right patch maintains consistent intensity throughout the frequency band, the intensity of the electric field gradually increases in the left patch (rectangular patch) up to 28 GHz. This phenomenon is also controlled by significant mutual coupling, which can solely be exa-

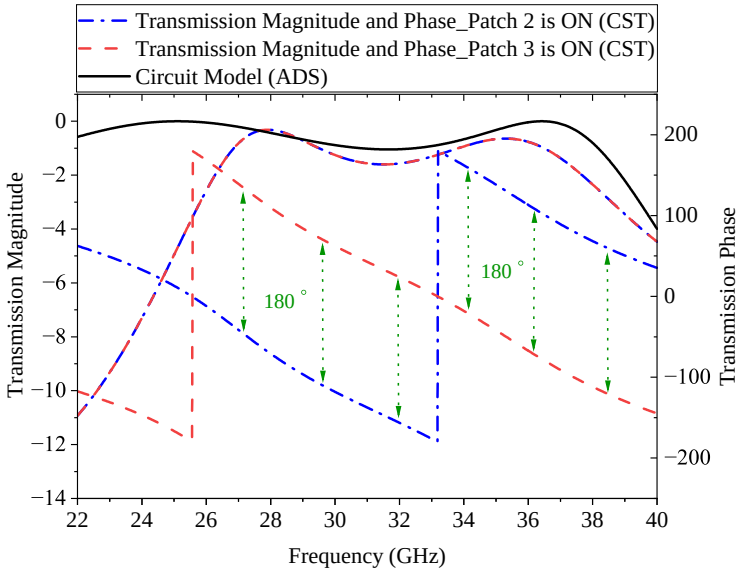

FIGURE 4.4 : Simulated transmission results.

mined through full-wave techniques. Subsequently, the electric field intensity diminishes gradually. Through the integration of these frequency-dependent amplitude variations, a broader bandwidth is achieved. Note, this enhancement stems from incorporating two unit cells in one unit cell, half-elliptical and rectangular-shaped patches, forming an array. The proposed structure is applied in the transmitting layer, while two of the optimized structures, oriented in opposite directions by 180 degrees, are utilized in the receiving layer.

It is worth noting that we devised a unit cell design that combines the receiver-to-transmitter structure with the current reversal technique. This unique architecture enables 1-bit resolution, facilitating two distinct states (0° and 180°). This is accomplished by rotating the microstrip line to patch 2 and patch 3, as shown in Figure 4.2. The unit cell directs the incoming wave from the receiving layer to the transmitting layer. By toggling the microstrip line between patch 2 and patch 3, the current direction is reversed, resulting in a phase shift from 0 to 180 degrees. Depending on the polarity of the bias current, the incident field is transmitted either in phase or with a 180° rotation, thereby generating a 1-bit phase shift (0°/180°). In other words, when patch 2 is on, the current direction results in a phase shift of 0°, and when patch 3 is on, the current direction produces a phase shift of 180°. This enables a 1-bit resolution, as the phase can either be 0° or 180°, depending on which patch is activated.

The results demonstrate a minimal insertion loss of less than -3 dB from 25.82 GHz to 38.57 GHz, equivalent to 45.53% at 28 GHz, which remains consistently low across both phase states, as shown in Figure 4.4. The simulated insertion loss for the equivalent circuit model of the proposed unit cell in ADS is also presented in Figure 4.4, validating the performance of the design. In the next section, the proposed unit cell is utilized to build a tranmsitarray antenna.

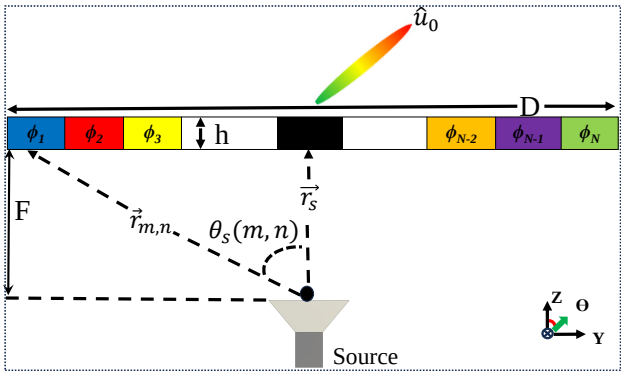

FIGURE 4.5 : The schematic of a linear transmitarray antenna.

4.1.3 Transmitarray Configuration

The general schematic of the transmitarray antenna is depicted in Figure 4.5. This structure comprises a feeding antenna (source) that emits a quasi-plane wave and a metasurface slab positioned in front of the feeding antenna with a distance of F, serving as a modifiable lens. The metasurface lens with a length of D and a thickness of h is subdivided into N sub-wavelength segments. Either the effective refractive index or the thickness of individual segments can be independently adjusted, resulting in varying phase (ϕ) shifts experienced by the transmitting electromagnetic wave within these segments. This functionality allows for precise control and radiation orientation by incorporating phase adjustments among neighboring segments in a certain pattern as needed. It means each sub-wavelength segment is viewed as a uniform substrate, and the alteration of the segment's refractive index/thickness controls the resulting phase shift. The required phase difference $\Delta\varphi$ is correlated with the refractive index difference (Δn = n_1 - n_2), as shown in (1). Similarly, the required phase difference $\Delta\varphi$ is correlated with the thickness difference of segments (Δh = h_1 - h_2), as shown in (2) :

$$\Delta\varphi = k_0.h.\Delta n \tag{4.1}$$

$$\Delta\varphi = k_0.\Delta h.n \tag{4.2}$$

in which h represents the thickness of the segments and k_0 is the free-space wave vector. Given the dielectric constant of the utilized substrate $n = \sqrt{\varepsilon_r.\mu_r}$, it suffices to ascertain for designing a three-dimensional meta-lens using commercially accessible dielectric materials [123], [51].

However, achieving 1-bit phase quantization by changing the refractive index is not ideal. Finding two substrates with exactly the desired refractive indices is challenging, as materials with exact properties are rarely available. Moreover, achieving 1-bit phase quantization by varying the

thickness necessitates the use of two different material thicknesses. This approach results in a non-planar transmitarray antenna, which is bulky and costly to manufacture [124].

Instead of relying on altering the refractive index and varying the thickness, a more practical approach involves designing metasurface unit cells that provide 1-bit phase quantization (0 and 180 degrees) by utilizing mutual coupling and current reversal techniques. With this design, the transmitarray antenna structure employs the same material and thickness for all unit cells, simplifying the configuration and maintaining a planar structure. The desired phase shifts are achieved through the interactions between neighboring cells, offering a more practical and efficient solution.

A transmitarray antenna aperture is made up of a planar array with N $\times$ N transmitting unit cells and a source (feeding antenna), which is positioned on the z-axis at the point $z = -\vec{r}_s$. Unit cells are utilized as passive phase shifters to steer the beam in the desired direction, thereby controlling the incident beam produced by the source. Based on the array theory presented in [125] and [126], the far-field radiation pattern for the transmission mode of the transmitarray antenna can be represented as

$$\mathbf{E}(\theta,\varphi) = \sum_{m=1}^{N}\sum_{n=1}^{N} \frac{f_e\left(\theta,\varphi\right) f_s\left(\theta,\varphi\right)\left|T_{m,n}\right|}{\left|\vec{r}_{m,n}-\vec{r}_s\right|} \times \exp\left(-jk(\left|\vec{r}_{m,n}-\vec{r}_s\right| - \vec{r}_{m,n}\cdot\hat{u}) + j\varphi_{m,n}\right), \tag{4.3}$$

where $\hat{u} = \hat{x}\sin\theta\cos\varphi + \hat{y}\sin\theta\sin\varphi + \hat{\mathrm{z}}\cos\theta$. The terms $f_e\left(\theta,\varphi\right)$ and $f_s\left(\theta,\varphi\right)$ denote the unit cell and source radiation pattern, respectively. The vectors $\vec{r}_{m,n}$ and $\vec{r}_s$ represent the positions of the mn-th unit cell and the source, respectively. k stands for the free space wave number. $|T_{m,n}|$ refers to the transmission magnitude of the mn-th element as determined from unit cell analysis.

To direct a beam to the intended angles $\hat{u_0}(\theta_0,\varphi_0)$, the phase of each unit cell must be adjusted accordingly, as given by

$$\varphi_{m,n} = k(\left|\vec{r}_{m,n}-\vec{r}_s\right| - \vec{r}_{m,n}\cdot\hat{u}_0) + \varphi_c, \tag{4.4}$$

where φ_c is the phase constant, an optimized value for a 1-bit transmitarray antenna. Besides, this highlights that the design of a transmitarray antenna relies on relative transmission phases instead of absolute ones. In the proposed 1-bit unit cell design, if $\varphi_{m,n} \in [-90^\circ, 90^\circ]$, the phase of each unit cell is *zero*, and is 180° for $\varphi_{m,n} \notin [-90^\circ, 90^\circ]$.

It should be pointed out that the phase obtained for each unit cell may change as φ_c changes, leading to phase quantization errors. Therefore, selecting an optimized value for φ_c is essential for the 1-bit transmitarray antenna radiation performance. By adjusting the phase differences between rays passing through various segments, the outgoing wave can be aligned to travel in the desired direction [21], [127], [128].

4.1.3.1 Verifying the Beamforming Mechanism

To verify the beamforming mechanism, first two-dimensional simulations are carried out in COMSOL software, where a linear metasurface lens with a length of L = 75 mm, and an array of N = 15 dielectric unit cells with the size of P = 3 mm (less than $\lambda_0/2$ at 28 GHz). A transverse magnetic (TM) polarized wave is used to illuminate the proposed meta-lens, with a pyramidal horn antenna acting as the EM source. It should be mentioned that in this step, different refractive indexes are defined in simulations for each dielectric unit cell column which will be realized later by DC voltages applied to the PIN diodes in metasurface unit cells, see Eq. 4.1. As an example, the desired achieved direction of the main beam (Theta = 25 deg.) is given in Figure 4.6.

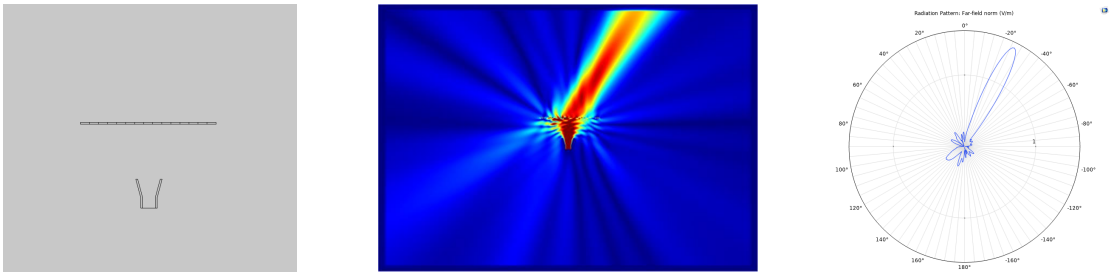

(a) (b) (c)

FIGURE 4.6 : (a) Linear Metasurface Lens using single feed antenna (b) electric field at 28 GHz and (c) steering the beam to Theta = 25 degree, in COMSOL.

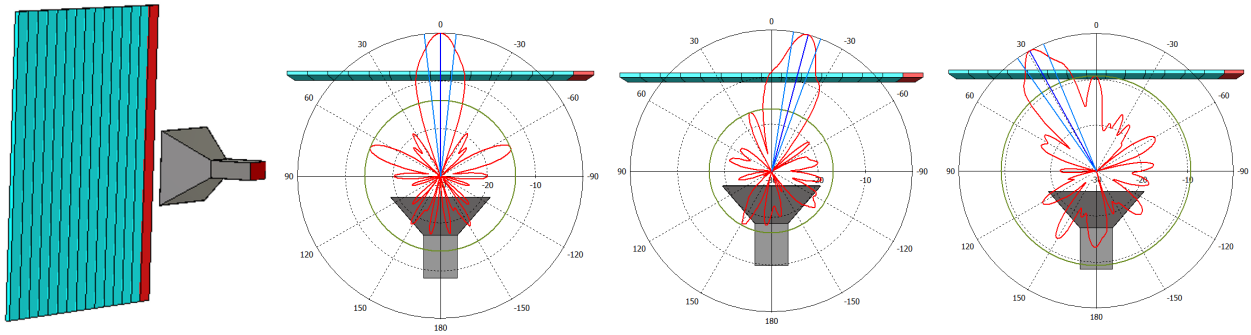

(a) (b) (c) (d)

FIGURE 4.7 : (a) Linear metasurface lens using the proposed horn antenna as a feed antenna, (b) steering the beam to Theta = 0 degree, (c) steering the beam to Theta = 15 degree, (d) steering the beam to Theta = -30 degree.

Next, three-dimensional full-wave simulations of a linear metasurface lens are carried out using the two feed antennas designed in Chapter 3 : the proposed horn antenna and the SIW-based slot antenna. As shown in 4.7 and Figure 4.8, the simulations were performed in CST Microwave Studio to evaluate the beamforming performance at various angles. With the horn antenna as the feed, simulations were conducted for 0°, +15°, and –30° to demonstrate directional beam steering. For the SIW slot antenna, simulations were performed at 0° and –30°. The results confirm the

beamforming principle and validate the operation of the metasurface lens composed of dielectric unit cell columns, each exhibiting a different effective refractive index. Although both feed antennas confirm the beam steering concept, the SIW slot antenna requires significantly finer meshing in CST, resulting in longer simulation times. Therefore, to optimize computational resources and prototyping efficiency, the horn antenna is used in subsequent simulations. However, the SIW antenna remains a suitable candidate for final hardware implementation of the complete beamforming system, ensuring design consistency with the project's intended goals.

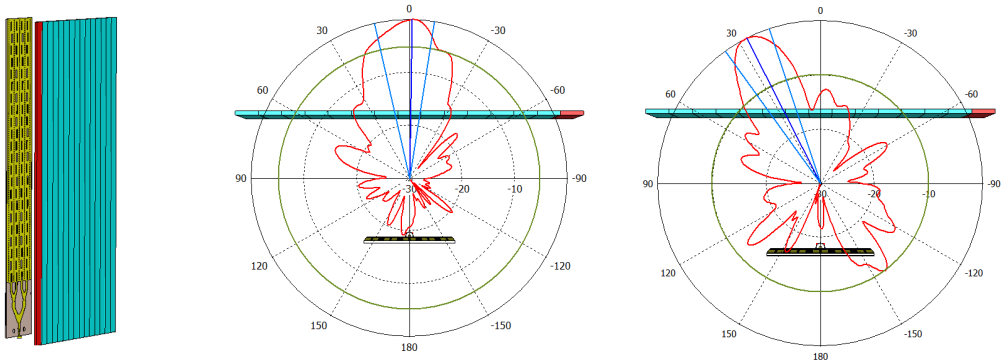

(a) (b) (c)

FIGURE 4.8 : (a) Linear metasurface lens using the proposed SIW slot antenna as a feed antenna, (b) steering the beam to Theta = 0 degree, (c) steering the beam to Theta = 30 degree.

4.1.4 Results and Discussions

After validating the beamforming concept, custom beam-steering software is employed to generate specific phase distributions for beam-steering angles of 0, 30 and 50 degrees, as depicted in Figure 4.9. Then, a complete transmitarray antenna, sized at 21 × 21 (88.2 × 88.2 mm), is considered and constructed using CST Microwave Studio 2022.

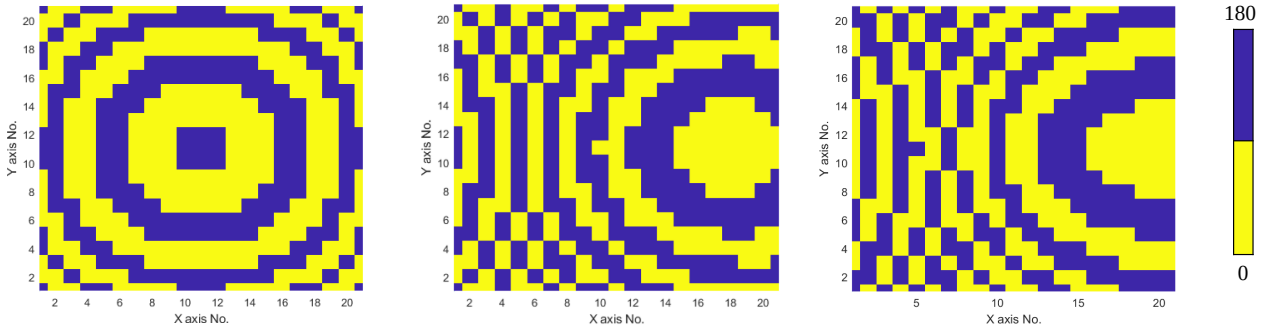

(a) (b) (c)

FIGURE 4.9 : Initial phase distributions at (a) 0°,(b) 30°, and (c) 50°.

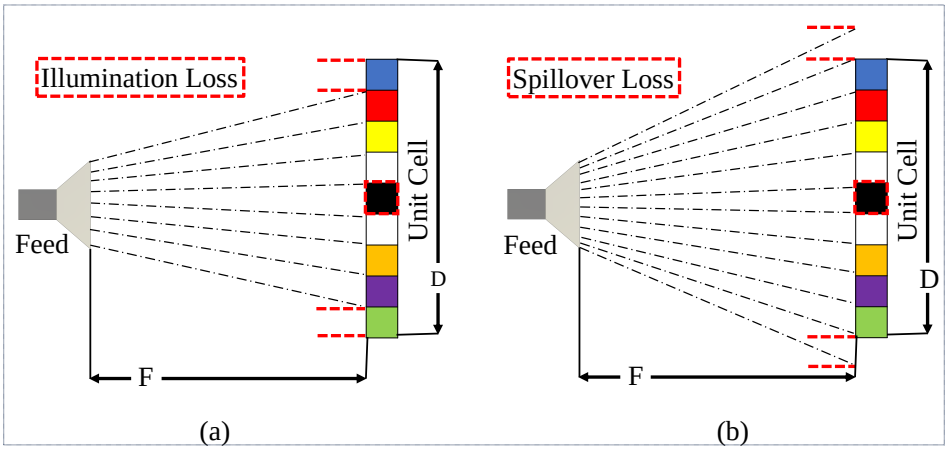

FIGURE 4.10 : Illustration of (a) illumination loss, (b) spillover loss.

Therefore, a linear metasurface lens with a length of d = 88.2 mm, and an array of N = 21 unit cells with the size of Ws = 4.2 mm is employed. A transverse magnetic (TM) polarized wave is used to illuminate the proposed transmitarray antenna, with a pyramidal horn antenna with a gain of 13.3 dBi at 28 GHz acting as an EM source. To enable beam steering at a specific angle, a focal distance of 63 mm is set. By adjusting the phase differences among distinct rays traversing segmented portions, the resultant wave can be precisely directed to the intended beam-steering orientation.

It should be pointed out that the focus to the diameter ratio (F/D) is a crucial parameter for a transmitarray antenna. Here, F represents the distance from the phase center of the antenna feed to the center of the array's aperture surface, while D denotes the size of the aperture surface. As the focal distance changes, the value for φ_c also changes, resulting in quantization error. Thus, the beam direction, gain, aperture efficiency, and side lobes are also affected. The parameters that affect the efficiency of the transmitarray antenna are illumination losses and spillover losses. Therefore, the F/D value should be selected carefully by considering low illumination and spillover losses. Both excessively large and excessively small F/D values can negatively impact the transmitarray's performance. To determine the appropriate F/D, the electromagnetic waves from the feed antenna should reach the aperture surface's edge at about -10 dB relative to the center of the surface. As shown in Figure 4.10.a, the illumination loss increases as the focal distance decreases from the optimized value of F = 63 mm, and vice versa. Similarly, as depicted in Figure 4.10.b, the spillover loss increases as the focal distance increases from the optimized value of F = 63 mm and vice versa. To achieve high gain, low side lobes, good aperture efficiency, and to minimize the illumination and spillover losses, the optimized F/D = 0.7 value is chosen (at F/D = 0.7, the edge illumination level is -10 dB).

It should be noted that the focal distance-to-metasurface diameter ratio F/D directly affects the phase distribution required for each unit cell in the transmitarray, as determined by Eq. 4.4. A custom MATLAB code has been developed to calculate these phase values, taking design parameters such as the number of rows and columns, unit cell size and thickness, and focal point as

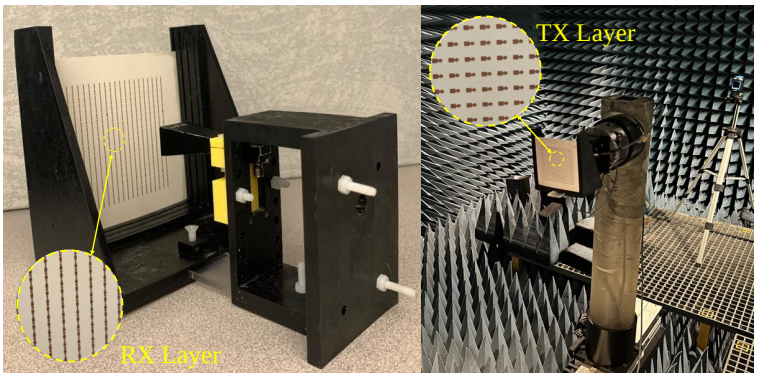

FIGURE 4.11 : (a) Fabricated prototype with mounting block, (b) the measurement setup in the anechoic chamber.

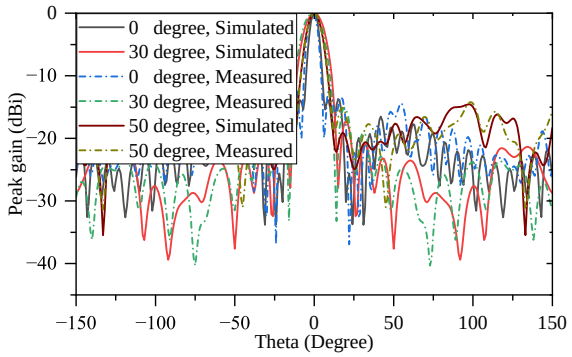

(a)

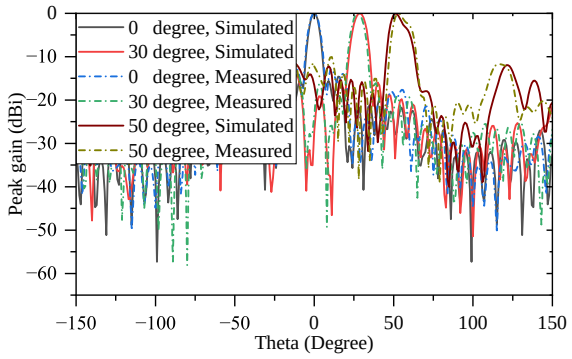

(b)

FIGURE 4.12 : Simulated and measured normalized radiation patterns of the proposed TA at 28 GHz (a) E-planes, and (b) H-planes for beam-steered at 0°, 30°, and 50°.

inputs. When the focal point is adjusted (i.e., the F/D ratio changes), the software recalculates the phase distribution for all unit cells to accommodate the new focal point. This iterative process ensures precise compensation for feed phase delay, optimizing beam-steering performance. Therefore, the F/D ratio significantly impacts both the phase distribution and the overall transmitarray performance by influencing illumination and spillover loss.

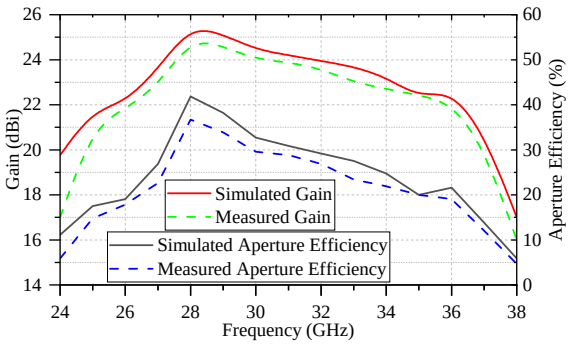

FIGURE 4.13 : Simulated and measured peak gains and the corresponding aperture efficiencies.

The proposed transmitarray was fabricated, as illustrated in Figure 4.11.a, and subsequently measured in an anechoic chamber, as depicted in Figure 4.11.b. The outcome reveals that the proposed unit cell effectively achieved precise beam-steering angles (0°, 30°, 50°) with only a 1-bit resolution. The findings from both measurements and simulations are in a good agreement, as shown in Figure 4.12 and Figure 4.13.

At 28 GHz, the maximum peak gains recorded for 0°, 30°, and 50° beam-deflection angles are 25.52 dBi, 22.94 dBi, and 21.18, respectively. Furthermore, the measurement indicates maximum peak gains of 24.95, 22.40, and 20.79 at 0°, 30°, and 50°, respectively. The -3dB gain bandwidths range from 26.8 to 36.1 GHz (9.3 GHz) in simulation and from 26.4 to 35.3 GHz (8.9 GHz) in measurement. This corresponds to approximately 33.3% and 31.7% -3dB bandwidth around 28 GHz for simulation and measurement results, respectively. In addition, the simulated/measured levels of side lobes maintain values for the E-plane and H-plane are lower than -15.2/-14.1 dB and -14.5/-12.5 dB for 0 degree, -13.8/-13.1 dB and -14.1/-13.5 for 30 degree, and -14.8/-14.2 dB and -12.3/-11.1 for 50 degree, respectively.

A crucial parameter in the performance of antennas, especially in a transmit array antenna, is aperture efficiency. The aperture efficiency of the proposed transmitarray antenna is calculated as follows [129, 130] :

$$\varepsilon_{ap} = \frac{A_e}{A_p} \tag{4.5}$$

$$A_e = \frac{\lambda^2 G}{4\pi} \tag{4.6}$$

e_{ap} is the aperture efficiency, G is the antenna gain, and A_e and A_p are the effective and physical area of the aperture, respectively.

The study presents the aperture efficiency achieved through simulation and measurement, with values of 41.67% and 36.29% at 28 GHz for 0° beam steering, 23.11 % and 20.41 % for a 30° beam deflection angle, and 15.41 % and 14.09 % for a 50° beam deflection angle. These findings high-

light excellent, effective radiation performance. Both simulation and measurement results closely align, with minor deviations attributed to fabrication and substrate tolerance errors. These findings validate the underlying principle and functionality of the proposed beamforming concept.

TABLEAU 4.1 : Performance Comparison Between the Proposed Transmit Array Antenna and State-of-the-art Transmit Array Antennas (λ_L = Free Space Wavelength at the Lowest Frequency)

Ref.	Phase Distribution Range	Operating Frequency (GHz)	Maximum Gain (dBi)/ G.E. (dBi)	TA Thickness (λ_0)	Aperture Efficiency (%)	-3 dB Gain Bandwidth (%)	Beam Steering Capability?/ Range
[117] (2018)	2-bit	28	25.2 / 11.2	0.1	13.8	18	No / 0
[118] (2019)	360°	12	22.8 / N.G.	1.53	36.9	9.5	No / 0
[119] (2020)	360°	28	27 / 12.5	0.14	28	11.2	No / 0
[120] (2023)	360°	30	25 / N.G.	1.6	13	N.G.	Yes / 50
[121] (2024)	1-bit	28	20.8 / 15.6	0.08	28.4	16.5	Yes / 60
This work	1-bit	**28**	**25.5** / **12.2**	**0.14**	**41.6**	**33.3**	**Yes** / **50**

Table 4.1 provides a detailed comparison of the proposed transmitarray antenna (TA) against state-of-the-art TAs, focusing on several key performance metrics. The comparison is based on the phase distribution range, operating frequency, maximum gain (dBi)/gain enhancement (G.E.), TA thickness, aperture efficiency, 3 dB gain bandwidth, and beam steering capability. The results show that the proposed transmitarray antenna demonstrates superior performance across multiple metrics. It excels in aperture efficiency and 3 dB gain bandwidth, indicating a more effective use of its aperture and a wider operational bandwidth. While its maximum gain and gain enhancement are competitive, its TA thickness is well-balanced, providing a compact design without compromising performance. Additionally, its beam steering capability further enhances its applicability in various advanced communication scenarios.

4.1.5 Conclusion

An innovative wideband 1-bit transmitarray antenna has been presented in this Section. The key feature of this design is the strategic use of the current reversal technique and mutual coupling in a constructive way, which significantly enhances the bandwidth within a compact metasurface unit cell measuring 4.2 × 4.2 mm^2. The design incorporates a microstrip line in the receiving layer, positioned in opposite directions across two patches, to achieve a 180° phase difference. This ensures the unit cell maintains a strong linear phase response throughout the operational bandwidth. The effectiveness of this unit cell design has been demonstrated through a 21 × 21 transmitarray antenna, which successfully enables beam scanning capabilities. The antenna has an aperture efficiency of 41.6%, with a -3 dB gain spanning from 26.8 to 36.1 GHz (a range of 9.3 GHz), resulting in a bandwidth of 33.3% at a center frequency of 28 GHz. These features mark the high reported aperture efficiency and gain bandwidth for a transmitarray antenna in the literature. This system can adjust the beam direction, highlighting its potential as an ideal solution for advanced radar and satellite communication applications.

In the next section, we will design the active unit cell based on the proposed passive unit cell. By "active unit cell", we refer to a configuration that includes PIN diodes, allowing for dynamic phase control by simply switching the diodes on and off.

4.2 Active Unit Cell Design and Implementation

This section is based on the following publication :
P. PourMohammadi, H. Naseri, N. Melouki, and T. A. Denidni, “A 1-Bit Wideband Electronically Beam Steering Transmitarray for 5G Communication Systems,”in 2024 IEEE International Symposium on Antennas and Propagation and USNC-URSI Radio Science Meeting (USNC-URSI), 2024.

As demonstrated in the previous section, we successfully designed and proposed a 1-bit passive unit cell. Using this passive unit cell, the beamforming concept was verified, and we were able to steer the beam toward the desired direction angles, confirming the feasibility of the proposed approach. In this section, building upon the validated passive unit cell, we present the design of an active unit cell. The proposed active configuration incorporates PIN diodes to enable dynamic phase control by toggling the diodes between On and Off states.

Before designing the proposed active unit cell, it is essential to accurately characterize the PIN diode that will be integrated into the structure. The active metasurface performance relies on diode impedance which varies with biasing conditions making precise modeling essential before simulations and implementation.

4.2.1 PIN Diode Characterization

Two operational modes exist for the diode, ON and OFF states, which align with forward-biased and reverse-biased conditions respectively. Every state generates a specific complex impedance that influences both the phase and amplitude of the transmitted signal. To capture this behavior accurately in CST Microwave Studio, the PIN diode is modeled using an equivalent RLC circuit. This equivalent circuit is extracted based on the manufacturer’s datasheet specifications and verified through S-parameter measurements where available.

Accurate diode characterization ensures that the simulated phase shift and transmission loss closely match practical performance, enabling reliable full-wave design of the active unit cell. This step is thus critical to ensure proper beam-steering functionality in the final reconfigurable transmitarray system. In this work, the MACOM MA4AGFCP910 PIN diode is selected as the switching element to enable binary phase control within each unit cell. To evaluate the suitability of the selected PIN diode for high-frequency switching applications in reconfigurable metasurfaces a detailed

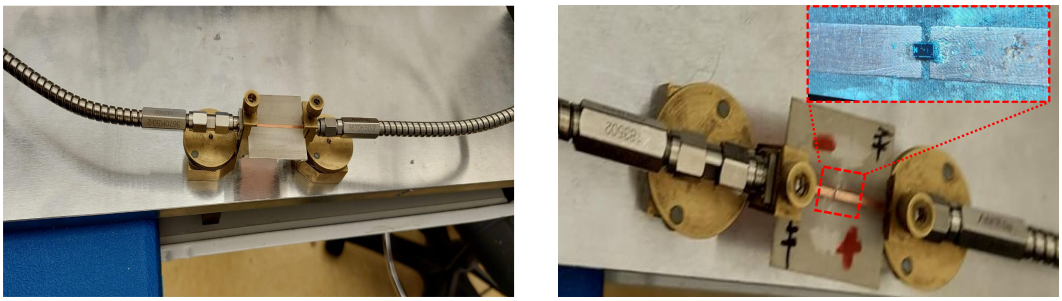

(a) (b)

FIGURE 4.14 : (a) microstrip line with gap, (b) micro stripline with diode installed.

characterization is conducted in the K-band (26–30 GHz). The objective is to assess the diode's performance in terms of insertion loss (On state) and isolation (Off state), both of which are critical parameters in dynamic beam-steering structures.

Step 1 : Fabrication and Baseline Measurement A microstrip transmission line was designed and fabricated with a central gap to accommodate the PIN diode, as shown in Figure 4.14.a. This initial configuration, without the diode, served as the reference structure. Its S-parameters are measured using a Vector Network Analyzer (VNA) to establish a baseline for subsequent comparisons.

Step 2 : Diode Integration and Performance Measurement The MA4AGFCP910 diode is carefully soldered into the central gap, as depicted in Figure 4.14.b, with appropriate biasing circuitry implemented to toggle the diode between On (forward-biased) and Off (reverse-biased) states. The same test structure is re-measured under both biasing conditions.

Insertion Loss (ON State) : The diode demonstrated an average insertion loss of -0.9 dB across the 26–30 GHz frequency range. This indicates excellent conductivity in the forward-biased condition, with minimal signal attenuation.

Isolation (OFF State) : In the reverse-biased state, the diode achieved an isolation of approximately -12 dB, effectively attenuating signal transmission.

4.3 Proposed Active Unit Cell

As shown in Figure 4.15 and Figure 4.16, the proposed active unit cell is a modified version of the proposed passive unit cell in the previous section. The proposed unit cell consists of a modified patch array located on the top side of the upper substrate (Tx) and two modified patch arrays on the bottom side of the lower substrate (Rx). These layers are interconnected via a central metallized via-hole with a diameter of 0.38 mm. Both substrates are fabricated using Rogers RO3003 material, which features a dielectric constant of 3 and a thickness of 0.787 mm.

Additionally, several structural and functional modifications are introduced in the active unit cell to enable electronic reconfigurability. On Layer 1 (the lower substrate), the bottom side hosts two

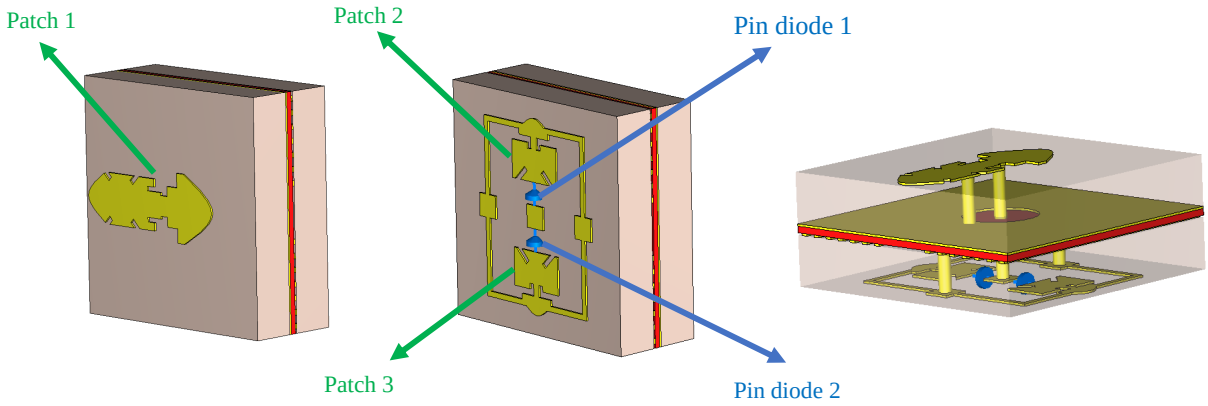

FIGURE 4.15 : The proposed active unit cell : (a) top view, (b) bottom view, (c) 3D view.

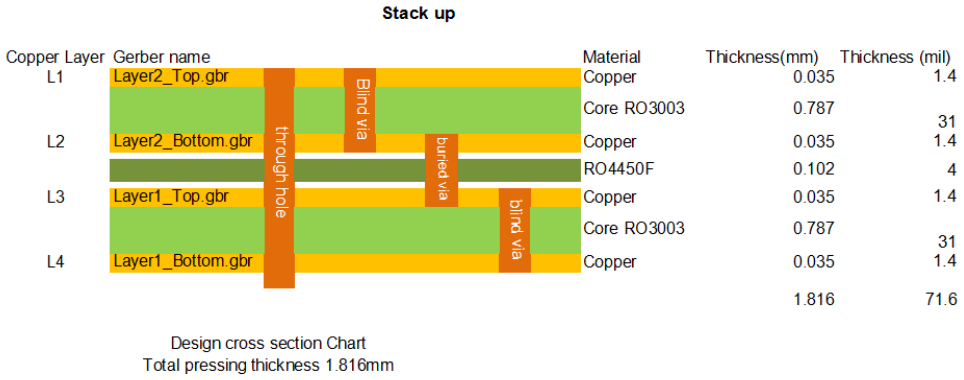

FIGURE 4.16 : The stack-up of the proposed active unit cell.

modified patch arrays, each integrated with a PIN diode. The top side of this layer contains all RF biasing lines. A square biasing pad is placed on the bottom side, and two blind vias connect this pad to the top side for bias control. The two PIN diodes are oriented in the same direction and are connected diagonally to the bias pad. The top corner of the square is connected to the cathode (bottom terminal) of PIN diode 1, and its anode (top terminal) is connected to Patch 2. Similarly, the bottom corner of the square is connected to the anode (top terminal) of PIN diode 2, whose cathode is connected to Patch 3. When a voltage is applied from the bottom to the top of Layer 1, one of the PIN diodes becomes forward-biased (ON) while the other becomes reverse-biased (OFF), due to their uniform orientation and shared biasing network. This configuration enables a current reversal mechanism, in which the current is directed either toward Patch 2 or Patch 3, resulting in a phase shift of 0° or 180°, respectively.

The proposed active unit cell builds upon the Rx-to-Tx topology of the passive design. However, unlike the passive unit cell, where 1-bit phase modulation (0°/180°) was achieved by rotating the microstrip connections between Patch 2 and Patch 3, the active unit cell realizes the same functionality electronically using PIN diodes. This design eliminates the need for rotation and offers fast,

compact reconfigurability. The unit cell transmits the incoming electromagnetic wave from the receiving layer (Layer 1 bottom) to the transmitting layer (Layer 2 top). When Patch 2 is activated, the current flows in one direction, producing a 0° phase shift. Conversely, when Patch 3 is activated, the current flows in the opposite direction, producing a 180° phase shift. This approach enables electrical switching between two phase states by simply changing the polarity of the applied bias, supporting reconfigurable 1-bit beamforming within the metasurface array. Layer 2 (the upper substrate) contains a modified patch array on its top side, while the bottom side is fully copper-clad to serve as a ground plane. A through-hole via connects the top of Layer 2 to the bottom of Layer 1, providing a direct signal path. Additional blind vias are used to connect the top and bottom sides of Layer 2 for grounding, to connect the bottom of Layer 2 to the top of Layer 1, and to connect the bottom and top of Layer 1 for biasing purposes. To ensure structural and electrical integrity, an adhesive bonding layer made of Rogers RO4450F with a thickness of 0.1 mm is used to join the bottom side of Layer 2 to the top side of Layer 1.

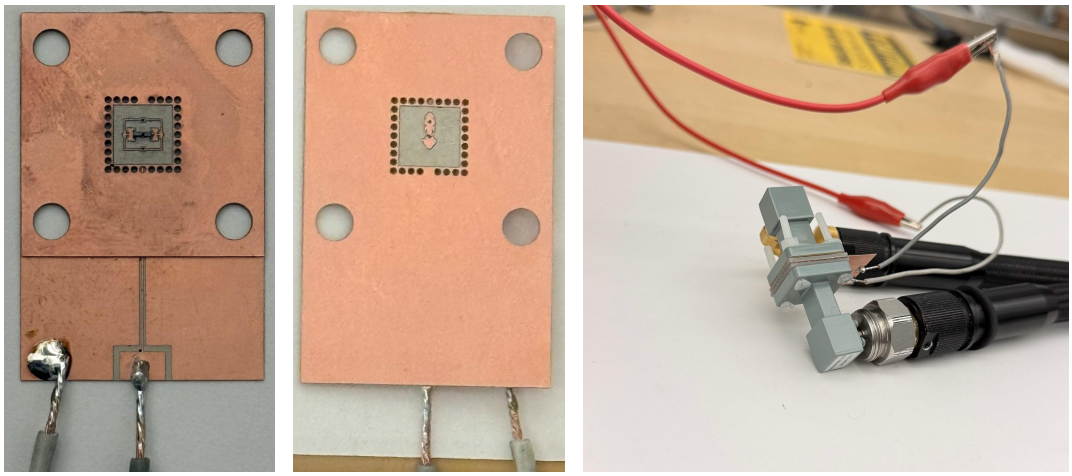

(a) (b) (c)

FIGURE 4.17 : Prototype of the proposed active unit cell (a) front side, (b) back side, (c) measurement setup to measure the unit cell in the Wr34 waveguide.

Following the simulation step, the unit cell was fabricated using standard PCB manufacturing techniques and subsequently tested to verify its electromagnetic performance. Measurements were conducted using a WR34 waveguide setup, covering the target frequency range with high precision as shown in Figure 4.17. The measured transmission and reflection coefficients showed strong agreement with the simulated results, indicating accurate realization of the design. The unit cell successfully achieved the desired phase and amplitude characteristics, confirming the effectiveness of the structure and the proper integration of its active components. Specifically, in the desired frequency range from 26 to 30 GHz, the measured transmission magnitude remained above -2.35 dB in both switching states : when PIN 1 is ON and PIN 2 is OFF, and vice versa. Furthermore, a 180 degree phase difference between the two states was observed in the same frequency band, verifying the intended 1-bit phase functionality of the proposed active unit cell. The

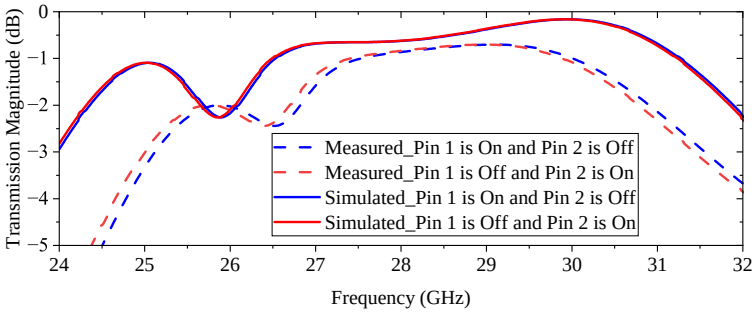

FIGURE 4.18 : Transmission magnitude of the proposed active unit cell.

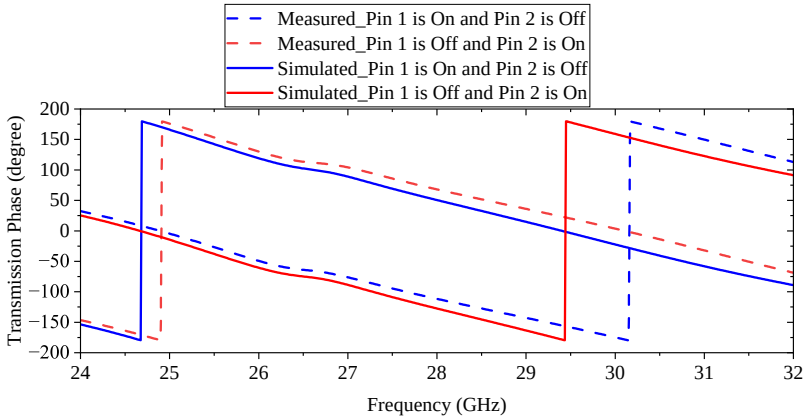

FIGURE 4.19 : Transmission phase of the proposed active unit cell.

results of the transmission coefficient (magnitude and phase) are given in Figure 4.18 and Figure 4.19.

The discrepancy between simulation and measurement results can be attributed to fabrication tolerances and connector alignment, which remained within acceptable limits. Overall, the experimental validation confirms the robustness, repeatability, and practical viability of the proposed unit cell for high-frequency beam-steering and reconfigurable antenna applications.

To verify the beamforming concept employing the proposed active unit cell, a metasurface panel consisting of a 14 × 14 array of unit cells is built. All unit cells in a row share the feeding lines located on the top side of Layer 1. Each row is divided into two halves, where seven unit cells are connected to the control board from the right side, and the other seven are connected from the left side. Two blind vias from the bottom to the top of Layer 1 are employed for biasing. The via on the right side biases the seven unit cells on the right half of the row, while the via on the left side biases the seven unit cells on the left. This layout allows for independent and efficient control of each half of the metasurface row using a minimal number of bias lines, as depicted in Figure 4.20. The combination of uniform diode orientation and the current reversal technique provides a compact and scalable solution for 1-bit electronically reconfigurable beamforming. The complete metasurface panel with biasing lines are shown in Figure 4.21 and Figure 4.22, illustrating the front and back views, respectively.

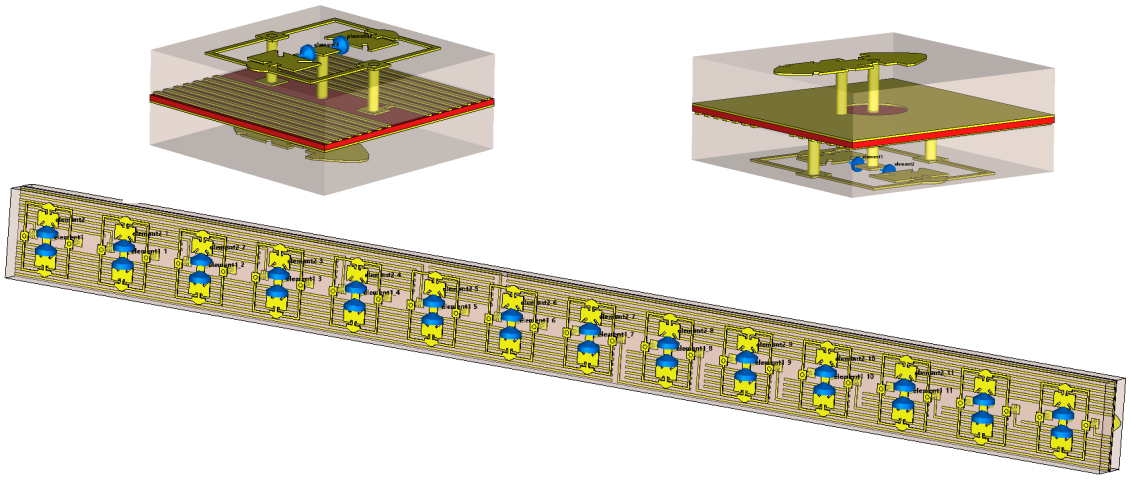

FIGURE 4.20 : The biasing lines in the proposed unit cell.

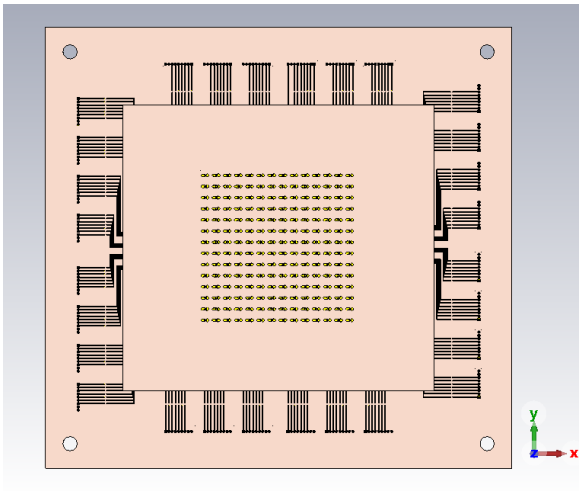

Front side View

FIGURE 4.21 : The front side view of the proposed beamfroming structure.

The proposed active unit cell was implemented in a 14 × 14 array configuration and simulated accordingly. The resulting 3D far-field radiation patterns are presented in Figure 4.23, along with the corresponding phase distributions. The phase distribution map illustrates which unit cells in the 14 × 14 array are assigned a phase shift of either 0° or 180°, thereby forming the metasurface panel based on the required phase profile for beamforming. Table 4.2 summarizes the simulation results for two beam directions : 0° and 30°. At 0°, the structure achieved a peak gain of 19 dBi with a side lobe level (SLL) of –13.8 dB. For the 30° beam direction, the gain and SLL were 17.4 dBi and –10.7 dB, respectively. The feeding source in these simulations is a horn antenna with a nominal gain of 13 dBi.

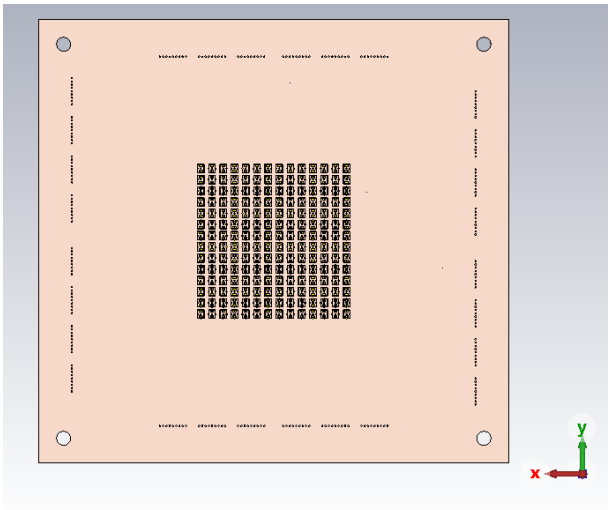

Backside View

FIGURE 4.22 : The back side view of the proposed beamfroming structure.

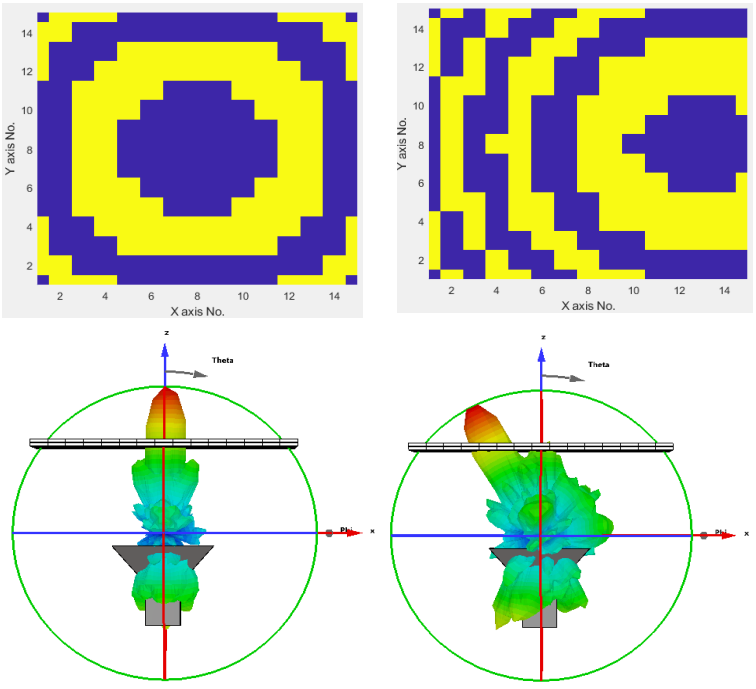

(a) (b)

FIGURE 4.23 : (a) Phase distributions and corresponding 3D radiation pattern beam at (a) 0° beam direction and (b) 30° beam direction.

Furthermore, for practical implementation, two control board options have been considered for biasing the PIN diodes : the EVAL-AD5370 evaluation board and a custom-designed control board developed at INRS. After the fabrication of the proposed structure, one of these control boards will be selected and employed during the measurement phase.

The fabrication files for the proposed metasurface panel have already been prepared. However, as this project is funded by an industrial partner, financial constraints have delayed the fabrication of the complete metasurface panel at the time of writing this thesis. Nevertheless, the measured results of the active unit cell validate both the simulation outcomes and the underlying concept. Additionally, since the passive version of the proposed transmitarray was successfully designed, fabricated, and measured (as demonstrated in Section 4.1), we are confident that the active version of the metasurface panel will also function as intended.

Once fabrication is complete, the structure will be integrated with the chosen control board, followed by full measurement and evaluation.

TABLEAU 4.2 : Performance metrics for intended vs. achieved angles in simulation.

Intended Angle (degree)	**0**	**30**
Achieved Angle (degree)	0	28
Gain (dBi)	19	17.4
SLL (dBi)	-13.8	-10.7

4.4 Summary

In this chapter, we investigated a beamforming approach based on mutual coupling and current reversal techniques. We began by designing and validating a passive unit cell capable of directional radiation through controlled coupling effects. Building upon this foundation, an active 1-bit reconfigurable unit cell was developed by integrating PIN diodes to enable dynamic phase switching between 0° and 180°.

Both unit cells were implemented in full transmitarray panels, 21 × 21 for the passive and 14 × 14 for the active design. Simulation results confirmed the beam-steering capabilities of both configurations, achieving high gain and low sidelobe levels at targeted angles. The horn antenna was used as the feed to simplify system integration during validation.

The PIN diode was accurately characterized and modeled, and options for practical biasing control were discussed. Fabrication files for the active metasurface panel were prepared, with hardware prototyping and measurement planned for the next phase. These results validate the feasibility of the proposed design and highlight its potential for compact, cost-effective, and high-performance mm-wave beamforming systems suitable for 5G and future wireless networks.

A complete transmitarray composed of the proposed active unit cells has achieved directional beams at 0° and 30° with peak gains of 19 dBi and 17.4 dBi, and side lobe levels of –13.8 dB and –10.7 dB, respectively. The horn antenna served as the feeding source during the verification phase to reduce system complexity and minimize the number of PIN diodes required. The performance comparison confirmed the effectiveness of the proposed structure in achieving high gain, wide bandwidth, and beam steering with low complexity.

Figures 4.21 to 4.28 illustrate the configuration of the proposed metasurface panel using the proposed active unit cell.

In the next chapter, we explore an alternative approach to unit cell design by Huygens principle, offering a different perspective for achieving efficient beamforming.

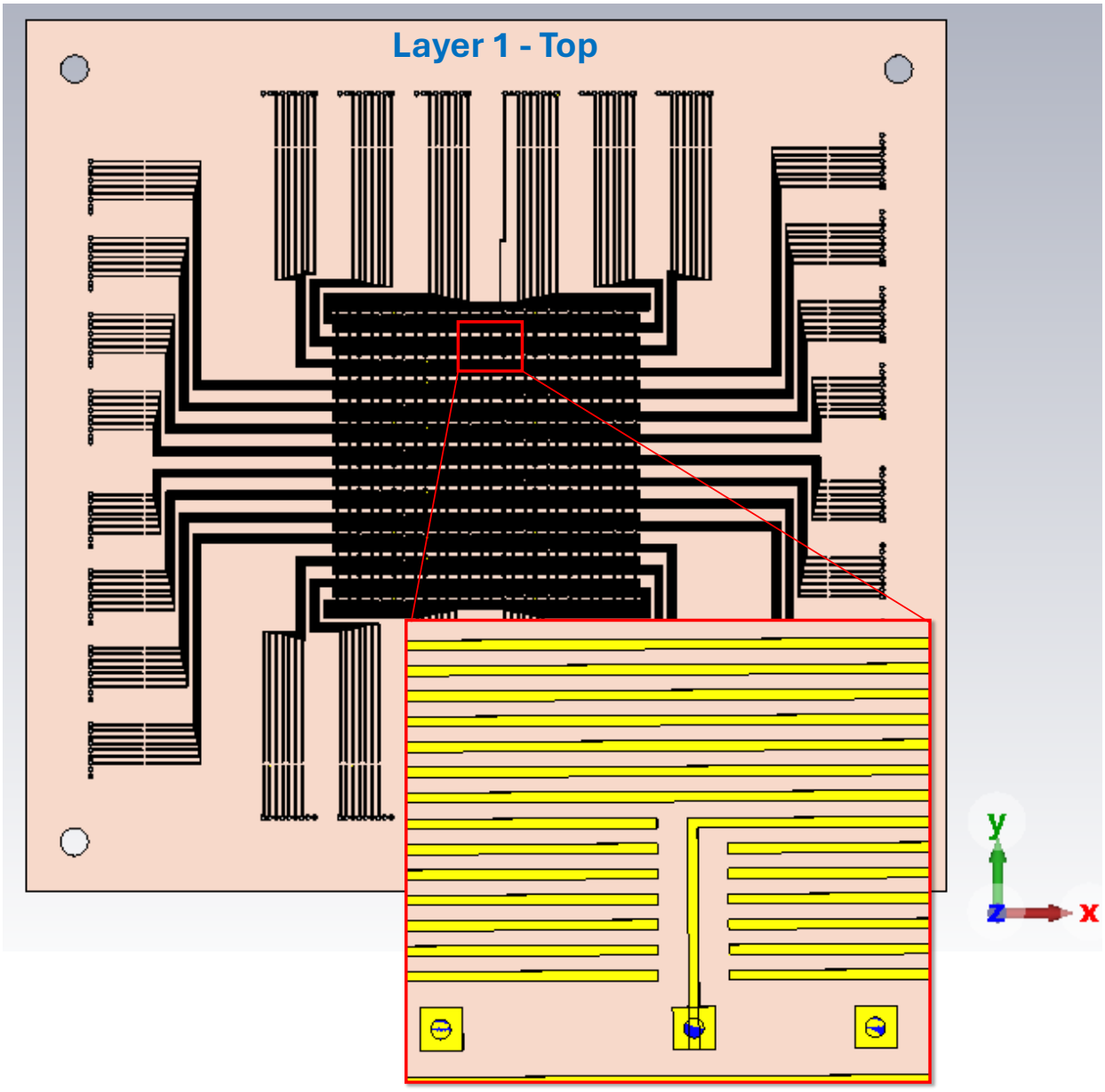

FIGURE 4.24 : The placement of the biasing lines in the proposed active unit cell in layer 1-top.

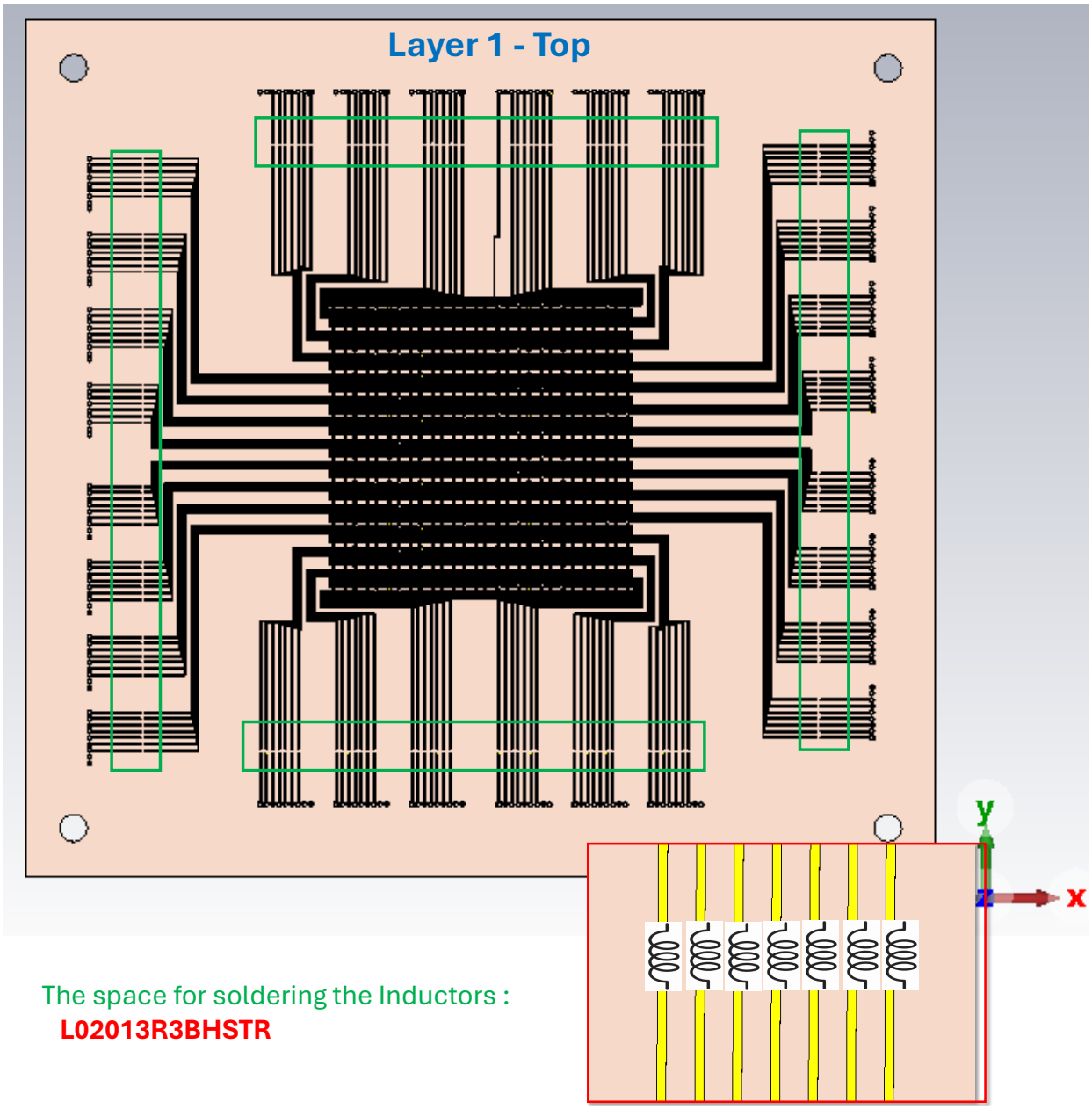

FIGURE 4.25 : The placement of inductors in the proposed active unit cell in layer 1-top.

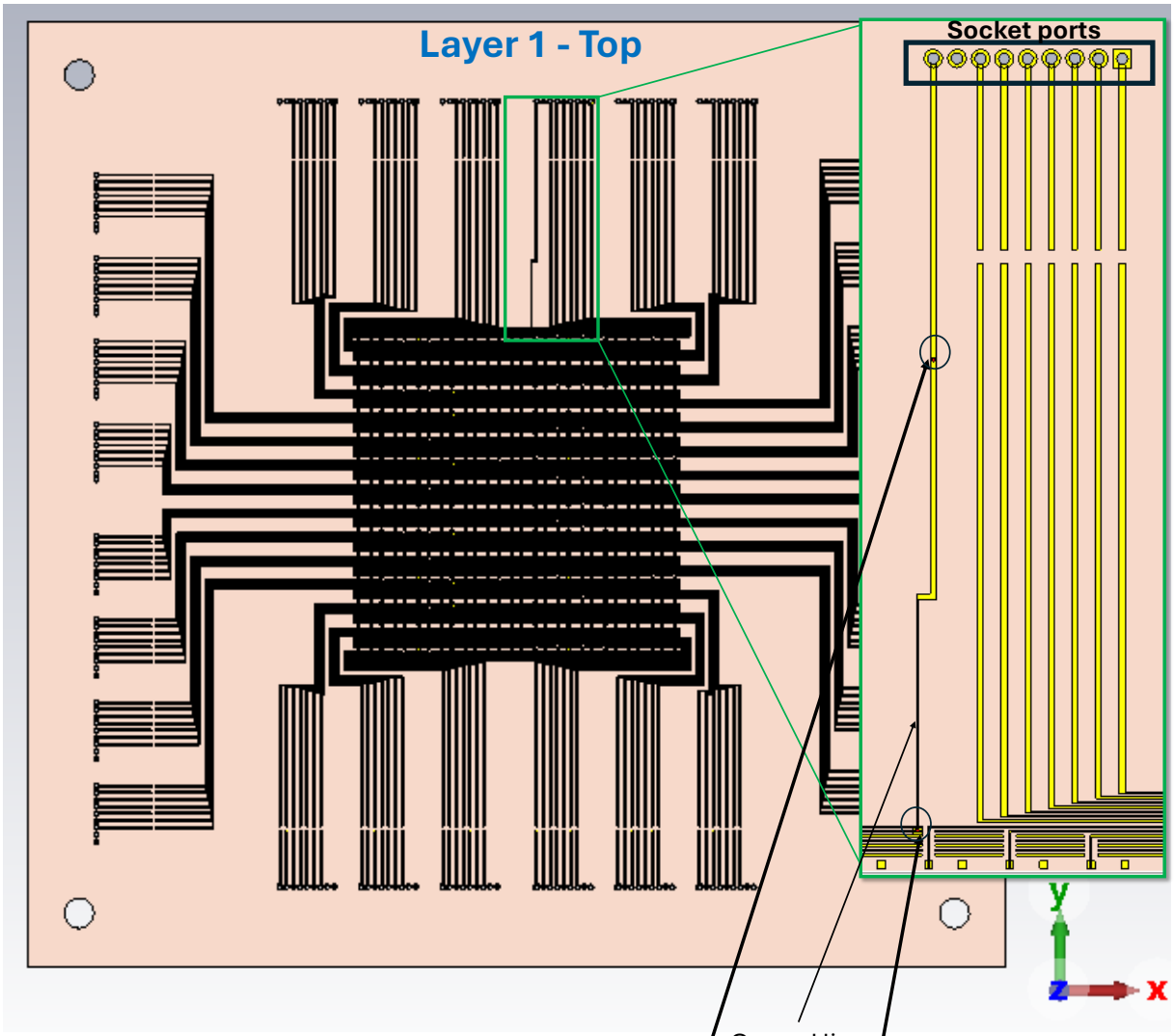

FIGURE 4.26 : The socket ports and ground line in the layer 1-top.

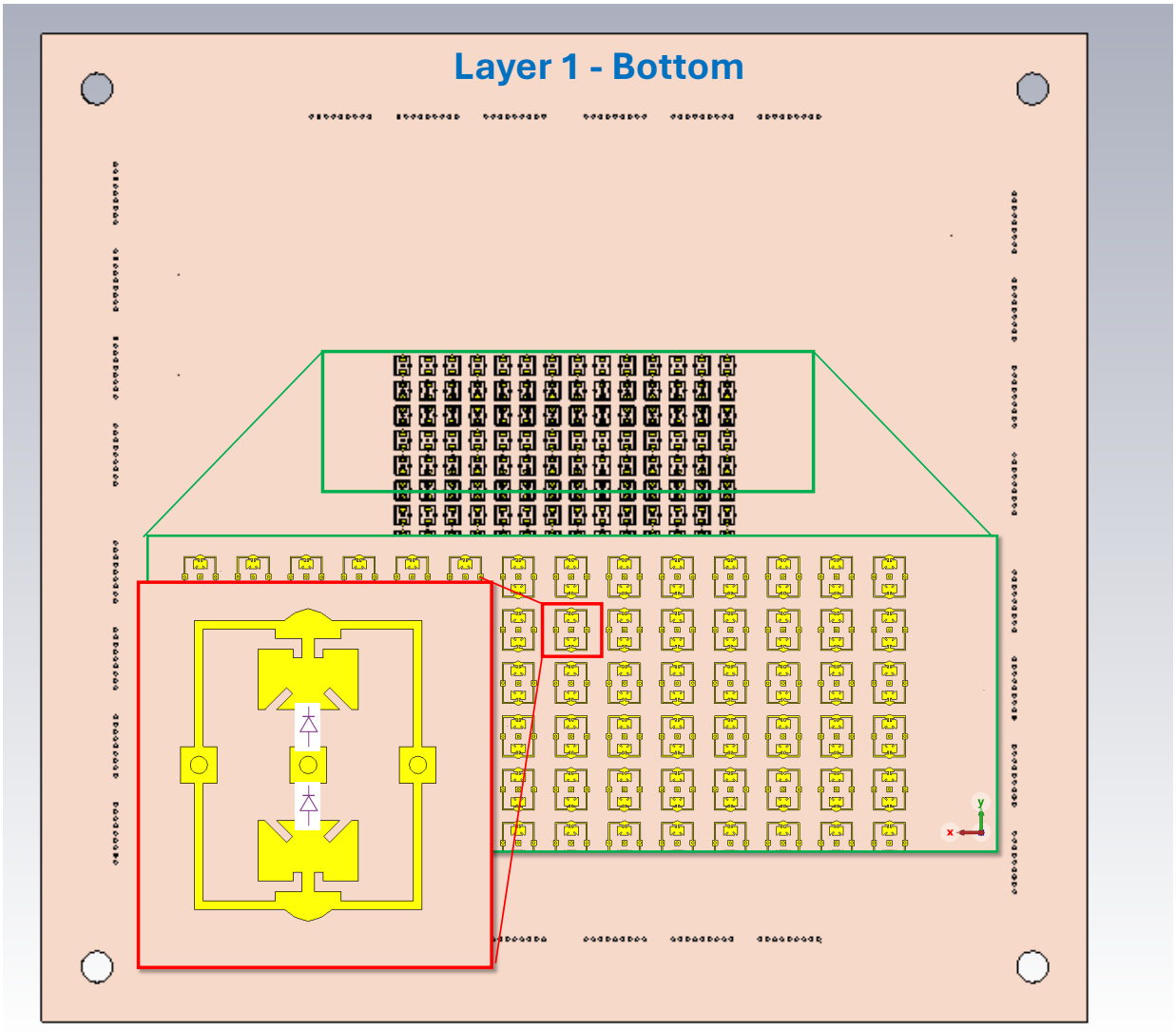

The space for soldering the PIN Diodes: **MACOM MA4AGFCP910**

FIGURE 4.27 : The layer 1-bottom in the proposed active unit cell.

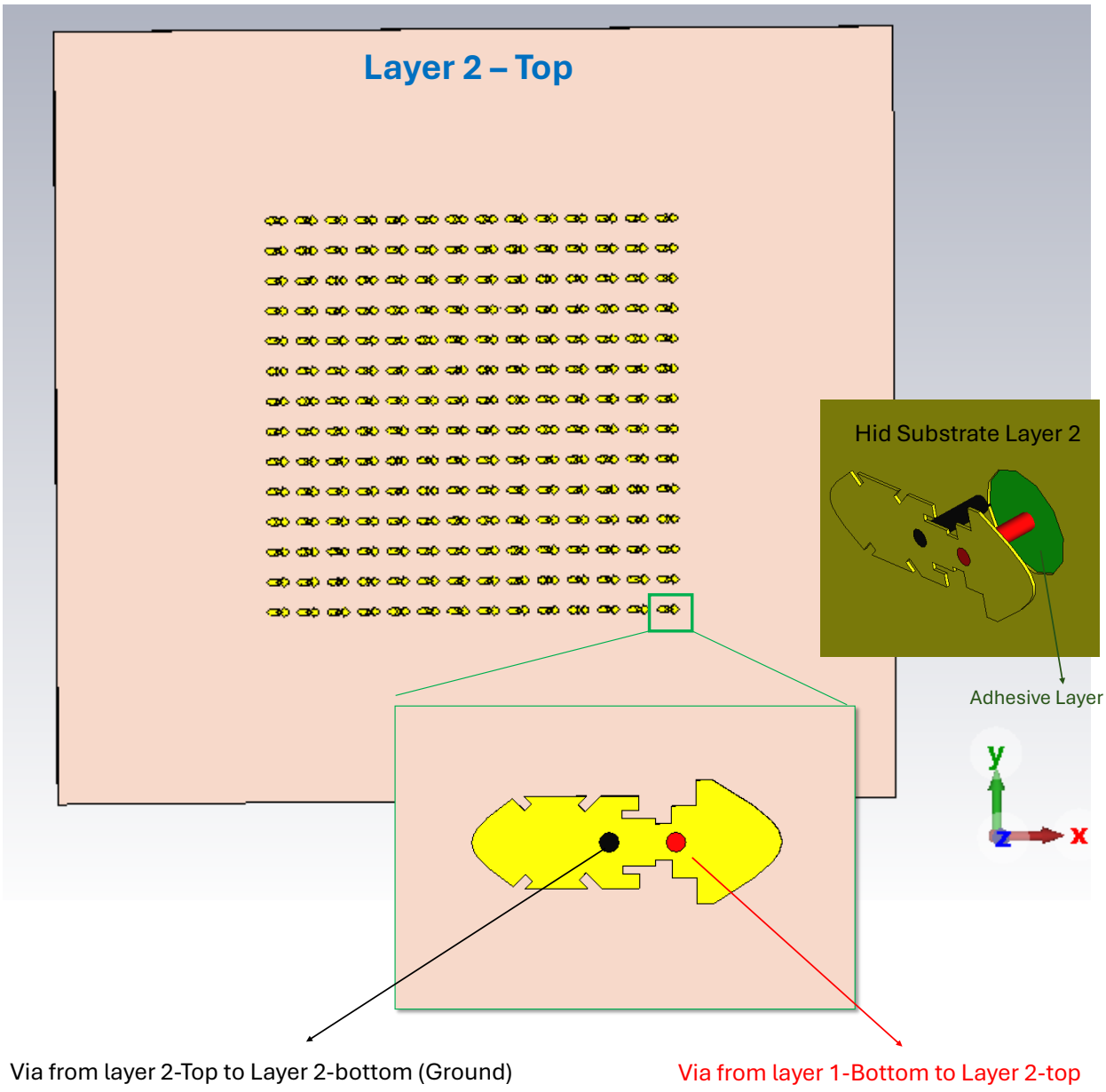

FIGURE 4.28 : The layer 2-top in the proposed active unit cell.

5 DESIGN OF HUYGENS-BASED METASURFACE UNIT CELLS

In Chapter 4, we designed and analyzed metasurface unit cells (passive and active) based on using mutual coupling in a constructive way and current reversal technique, enabling effective control of transmitted phase while maintaining high transmission efficiency. That approach formed the basis for both passive and active transmitarray implementations with promising beam-steering capabilities.

In this chapter, unit cells will be designed based on Huygens' principle, which allows for full transmission and controllable phase shifts by balancing electric and magnetic responses, making it highly suitable for millimeter-wave applications. We begin by designing a passive unit cell that demonstrates beam control. After validating its performance, we extend the concept to an active configuration by incorporating tunable components to enable dynamic beamsteering. For both passive and active designs, full transmitarray panels are constructed and evaluated to verify their beamforming capabilities.

5.1 Passive Unit Cell Design and Implementation

This section is based on the following publication :
P. PourMohammadi, H. Naseri, F. Ahamed and T. Denidni, "A Wideband Transmit Array based on Huygens' Metasurface for Millimeter-Wave Applications," in 2024 IEEE International Symposium on Antennas and Propagation and USNC-URSI Radio Science Meeting (USNC-URSI), 2024.

This section presents a transmit array antenna employing a wideband metasurface with high gain for effective beamsteering at millimeter-wave frequencies. The proposed unit cell design is based on Huygens' principle. The unit cell exhibits minimal insertion loss, consistently maintained across different phase states, and a transmission bandwidth spanning from 24 GHz to 30 GHz. Subsequently, a transmit array antenna is constructed. The results indicate successful control of the beam at desired angles with low sidelobe levels.

5.1.1 Introduction

In the dynamic landscape of modern communication systems, the demand for efficient and high-performance antennas is ever-growing. Transmit array antennas have emerged as key players in meeting this requirement, offering a transformative approach to wireless communication. These antennas are designed to transmit electromagnetic waves in a controlled and precise manner,

improving beamforming and enabling the antenna to focus its radiation pattern in specific directions [119]. Moreover, recent advancements in antenna technology have introduced the incorporation of metasurfaces to further enhance the capabilities of transmit array antennas. Metasurfaces are engineered structures composed of sub-wavelength elements that manipulate electromagnetic waves with unprecedented precision. By integrating metasurfaces into transmit array antennas, we can tailor the antenna's characteristics to achieve even greater efficiency and performance. The utilization of metasurfaces allows for the fine-tuning of electromagnetic wave interactions, enabling advanced control over the transmitted signals. This breakthrough technology enhances the antenna's beamforming capabilities, enabling it to adapt to specific communication needs with exceptional accuracy [95, 131]. The result is a synergy between transmit array antennas and metasurfaces, leading to heightened signal strength, increased coverage, and enhanced communication reliability. This innovative combination not only meets the needs of modern communication systems but also paves the way for future developments in wireless technology [132].

To this end, the principal objective of this study is to improve and advance beamforming antennas by employing metasurface, thereby facilitating the integration of 5G applications. In this section, a wideband unit cell is proposed based on Huygens' Metasurface to construct a transmit array. Subsequently, the source antenna (horn antenna) is excited, and the validation of the beamforming principle is conducted through a fully operational metamaterial-based system. This validation employs ray-tracing theory alongside the electromagnetic (EM) metamaterial technique.

5.1.2 Proposed Passive Unit Cell

The configuration of the proposed unit cell of Huygens' metasurface is depicted in Figure 5.1. Based on the Huygens' theory, a square double-layer metallic unit structure is proposed to construct the Huygens' metasurface with both electric and magnetic dipole resonances at the same time. It includes asymmetric square split rings and circular patches printed on two sides of a Rogers RO5880 substrate with a dielectric constant of 2.2 and a thickness of 1.57 mm. The frequency response of the unit cell is obtained by employing the frequency-domain solver in the CST Microwave Studio 2022. The unit cell is exposed to a plane wave incident at a normal angle.

It should be mentioned that Huygens' surface is created with the intention of controlling electromagnetic wavefronts through the manipulation of surfaces, achieved by engineering orthogonal subwavelength electric and magnetic dipoles [133]. According to the Huygens theory, a Huygens resonance can be excited with a total transmission when the orthogonally induced electric and magnetic currents are in-phase [50]. This requirement forms the basis of the Huygens' metasurface concept, which is governed by two key surface parameters : the normalized electric surface admittance ($Y_{ES} \cdot \eta_0$) and the normalized magnetic surface impedance (Z_{MS}/η_0). An ideal Huygens'

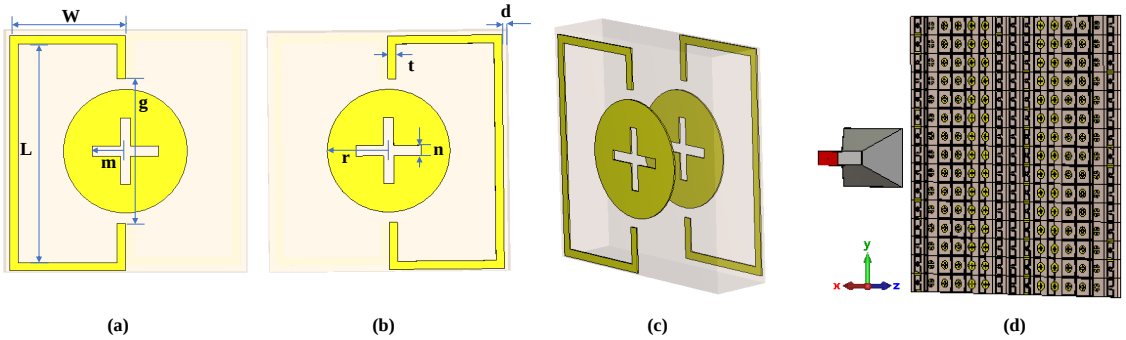

FIGURE 5.1 : The proposed unit cell (a) top view, (b) bottom view, (c) 3D view (d) transmit array based on the proposed unit cell.

surface is realized when these two quantities are equal, satisfying the condition :

$$Y_{ES} \cdot \eta_0 = \frac{Z_{MS}}{\eta_0}$$

This condition ensures that the electric and magnetic dipole responses are phase-aligned and radiate constructively in the forward direction while suppressing backward reflection, enabling full transmission with controllable phase.

To verify this condition, the surface parameters were extracted from full-wave electromagnetic simulations by evaluating the reflection (S_{11}) and transmission (S_{21}) coefficients of the unit cell. The normalized admittance and impedance were calculated using the following expressions :

$$Y_{ES} \cdot \eta_0 = \frac{2(1 - S_{21} - S_{11})}{1 + S_{21} + S_{11}}, \quad \frac{Z_{MS}}{\eta_0} = \frac{2(1 - S_{21} + S_{11})}{1 + S_{21} - S_{11}}$$

These formulas describe the effective boundary response of the metasurface to normally incident plane waves. At the design frequency of 28 GHz, the extracted values show strong agreement : the real parts of $Y_{ES} \cdot \eta_0$ and Z_{MS}/η_0 were found to be 0.12 and 0.11, respectively, confirming low-loss performance. The imaginary parts, $2.45j$ and $2.47j$, demonstrate excellent phase balance between electric and magnetic responses. This close alignment confirms that the unit cell satisfies the Huygens' condition at 28 GHz, enabling high-efficiency, reflectionless transmission and full-phase control across the aperture, which are essential for applications such as flat-lens antennas and reconfigurable beamforming systems.

Transmission amplitudes for different transmission phases are illustrated in Table 5.1. These simulated phases are used to construct the 2-bit transmit array antenna. It shows that by varying the parameters of the geometry, the proposed unit cell provides 360-phase shift variation with low transmission loss, as given in Figure 5.2. The configuration used to simulate the transmission characteristics (both magnitude and phase responses) of the unit cell is based on periodic unit cell boundaries and Floquet ports. The results indicate minimal insertion loss, which remains consis-

TABLEAU 5.1 : Unit cells with transmission performance.

Unit cell	Tran. Phase	Tran. Amp.	W	L	g	m	n	r	t	d
#1	0	-0.03	2.8	5.3	3.5	0.8	0.2	1.5	0.2	0.1
#2	-90	-0.24	2.8	4.9	1	0.8	0.4	0.7	0.4	1.5
#3	90	-0.31	5.7	5.3	2.5	0.8	0.4	1.3	0.2	0.1
#4	180	-1.36	2.8	5.3	3.5	0.8	0.4	1.5	0.2	2.9

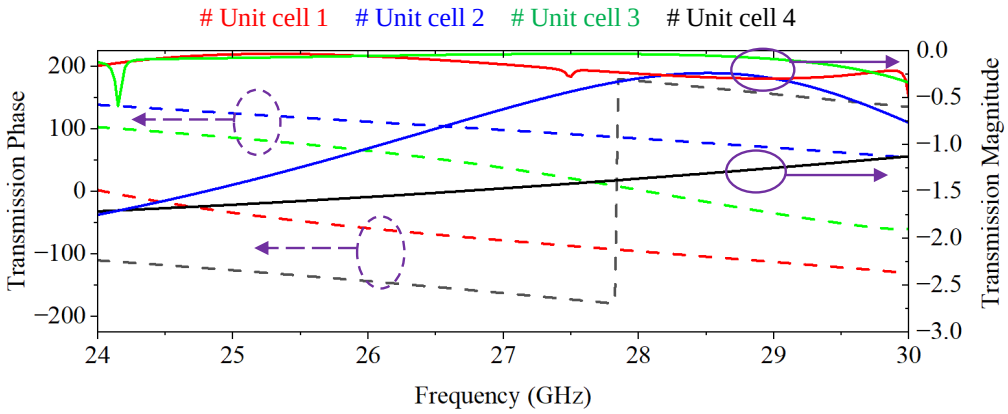

FIGURE 5.2 : Simulated transmission results.

tently low across four phase states. Additionally, the unit cell exhibits a broad 3-dB transmission bandwidth spanning from 24 GHz to 30 GHz. Note that all the necessary phase compensation, ranging from 0 to 360 degrees, can be achieved. Since our objective is to implement beamforming using a 2-bit transmit array, this leads to the acquisition of phases at 0, 90, -90, and 180 degrees. In the next section, the proposed unit cell is used to construct the transmit array.

5.1.3 Transmitarray Configuration

As discussed earlier in Section 4.1.3, the schematic of a generalized transmitarray antenna is illustrated in Fig. 5.3. It consists of a source antenna that generates a quasi-plane wave and a metasurface slab located at a distance F from the source antenna, acting as a tunable lens. The aperture of a transmitarray antenna consists of a planar array containing N$\times$N transmitting unit cells, along with a source antenna located on the z-axis at $z = -\vec{r}_s$. The unit cells act as phase shifters, enabling the beam to be directed toward the desired direction by manipulating the incident beam generated by the source. According to the array theory outlined in [125] and [126], the far-field radiation pattern of the transmitarray antenna in transmission mode can be expressed as

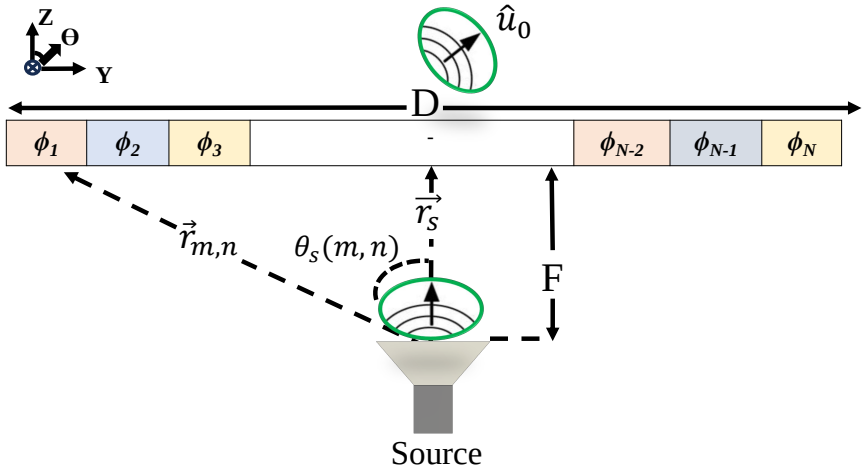

FIGURE 5.3 : Schematic of a generalized transmitarray antenna.

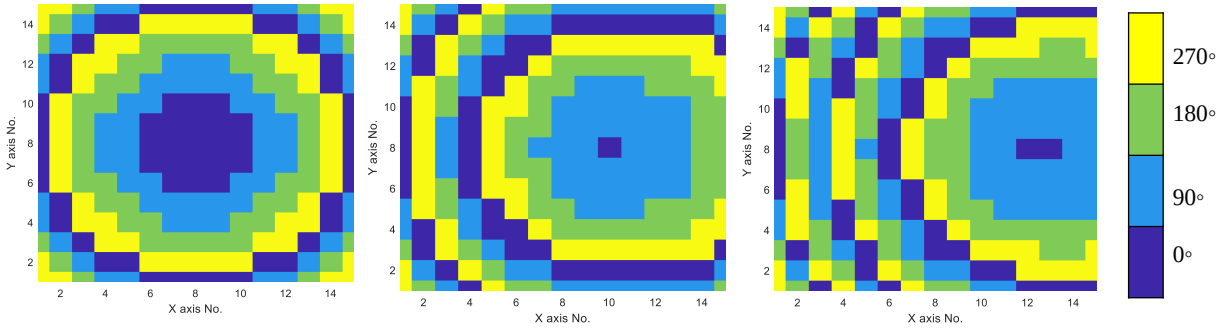

(a) (b) (c)

FIGURE 5.4 : Phase distributions at (a) 0°, (b) 10°, (c) 20°, (d) 30°.

$$\mathbf{E}(\theta,\varphi) = \sum_{m=1}^{N}\sum_{n=1}^{N} \frac{f_e(\theta,\varphi) f_s(\theta,\varphi) |T_{m,n}|}{|\vec{r}_{m,n} - \vec{r}_s|} \times \exp\left(-jk(|\vec{r}_{m,n} - \vec{r}_s| - \vec{r}_{m,n}\cdot\hat{u}) + j\varphi_{m,n}\right), \tag{5.1}$$

where $\hat{u} = \hat{x}\sin\theta\cos\varphi + \hat{y}\sin\theta\sin\varphi + \hat{z}\cos\theta$.

$f_e(\theta,\varphi)$ and $f_s(\theta,\varphi)$ represent the radiation patterns of the unit cell and the source, respectively. The vectors $\vec{r}_{m,n}$ and $\vec{r}_s$ denote the positions of the mn-th unit cell and the source. The symbol k refers to the wave number in the free space. $|T_{m,n}|$ indicates the transmission magnitude of the mn-th element, derived from unit cell analysis.

To steer a beam in the desired direction $\hat{u_0}(\theta_0,\varphi_0)$, the phase of each unit cell must be appropriately adjusted according to the following expression :

$$\varphi_{m,n} = k\left(|\vec{r}_{m,n} - \vec{r}_s| - \vec{r}_{m,n}\cdot\hat{u}_0\right) + \varphi_c, \tag{5.2}$$

where φ_c represents a phase constant optimized for a 1-bit transmitarray antenna. This emphasizes that the design of a transmitarray antenna depends on relative transmission phases rather than absolute ones. In the proposed 1-bit unit cell configuration, if $\varphi_{m,n} \in [-90°, 90°]$, the phase of the unit cell is set to $0°$, whereas it is set to $180°$ for $\varphi_{m,n} \notin [-90°, 90°]$. It is important to note that the phase of each unit cell can vary with changes in φ_c, potentially causing phase quantization errors. Hence, selecting an optimal value for φ_c is crucial to ensuring the radiation performance of the 1-bit transmitarray antenna. By fine-tuning the phase differences between rays passing through different segments, the outgoing wave can be directed to propagate in the desired direction [127], [128], [21].

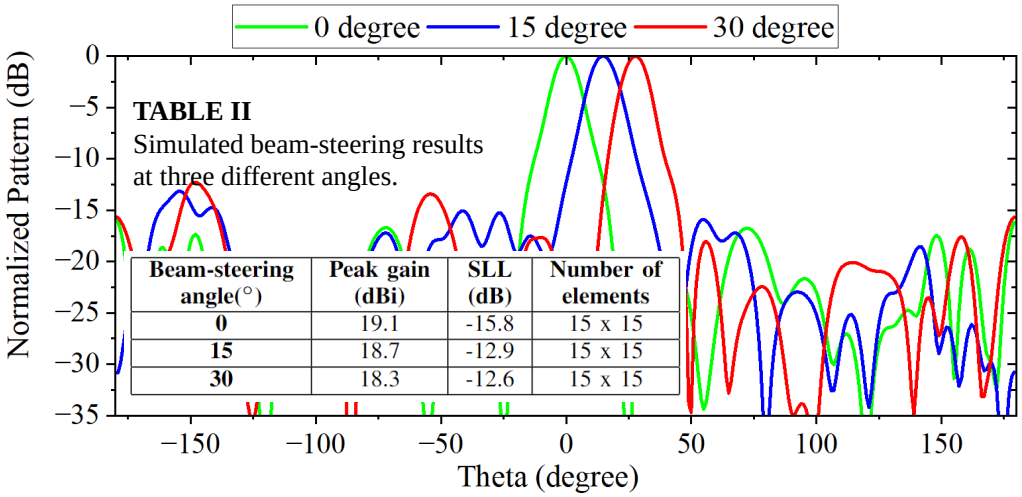

TABLE II
Simulated beam-steering results at three different angles.

Beam-steering angle(°)	Peak gain (dBi)	SLL (dB)	Number of elements
0	19.1	-15.8	15 x 15
15	18.7	-12.9	15 x 15
30	18.3	-12.6	15 x 15

FIGURE 5.5 : Beamsteering performance at three different angles at 28 GHz in simulation.

A transmitarray employing a full metasurface structure with a size of 15 × 15 is constructed using the proposed unit cell. The entire array covers an area of 88.5 mm × 88.5 mm, as illustrated in Figure 5.1.d. To verify the effectiveness of the proposed design, the array is subjected to TM-polarized radiation from a horn antenna in experimental testing. To manipulate the phase distributions for steering the beam at three different angles (0°, 15°, and 30°), we established a focal distance of 61.5 mm and adjusted key parameters using CST Microwave Studio 2022. Custom beam- steering software generates phase distributions for various beam-steering angles, as illustrated in Figure 5.4. The transmitarray based on the proposed unit cell achieved precise beam-steering angles with only a 2-bit resolution, as depicted in Figure 5.5. The summary provided in Table II (shown in Figure 5.5) confirms these findings, validating the fundamental principle and operational mechanism underlying the proposed beamforming concept. Notably, the antenna achieves a gain of 19.1 dBi at 28 GHz when the beam is steered to broadside (0°), which is 6.1 dBi higher than that of the feed antenna. The corresponding sidelobe level is –15.8 dB, indicating strong suppression of undesired radiation. When the beam is steered to 15°, the peak gain slightly decreases to 18.7 dBi with an SLL of –14.2 dB. At a steering angle of 30°, the gain remains relatively high at 18.3 dBi, while the SLL is –12.6 dB. These results confirm the transmitarray's capability to maintain high gain and low sidelobe performance across a range of beam-steering angles, demonstrating the effectiveness of the proposed Huygens metasurface unit cell design.

5.1.4 Conclusion

In this section, a novel transmissive unit cell has been designed using Huygens' metasurface. The proposed unit cell exhibits complete 360° phase control while maintaining high transmission levels. Simulation results confirm its strong performance across the desired frequency band. This passive unit cell was then used to construct a transmitarray antenna, demonstrating effective beamsteering capability, making it a promising candidate for practical applications such as radar and wireless communication systems.

In the next section, we extend this design to an active unit cell by integrating tunable components. Based on this reconfigurable unit cell, a new active transmitarray will be built and evaluated to enable dynamic, real-time beamsteering.

5.2 Active Unit Cell Design and Implementation

This section is based on the following publication :
P. PourMohammadi, H. Naseri, N. Melouki, F. Ahamed, and T. Denidni, "Single-Layer Electronically BeamSteering Transmitarray Antenna for the Ka-band Applications," in 2025 IEEE International Symposium on Antennas and Propagation and USNC-URSI Radio Science Meeting (USNC-URSI), 2025.

This section introduces a novel 1-bit single-layer transmitarray antenna that utilizes a wideband metasurface to enhance gain and enable efficient beamsteering at millimeter-wave frequencies. The unique design of the unit cell is based on Huygens' principle and incorporates two metallic T- and E-shaped patches, printed on both sides of a dielectric substrate. The E-shaped patches are rotated 90 degrees and positioned above the T-shaped patches. Furthermore, 44 holes are employed to lower the permittivity of the substrate and improve the transmission efficiency. In addition, PIN diodes are integrated into the T-shaped patches, and two microstrip lines are added to the sides of the patches. The microstrip lines act as biasing lines for the PIN diodes, with one connected to the arm and the other to the bottom of the T-shaped patches. The design exhibits consistently low insertion loss across two-phase states and supports a broad transmission bandwidth from 26 GHz to 30 GHz. Next, the transmitarray antenna (15×15) is constructed using the proposed unit cell, showing effective beamsteering toward the intended angles. The antenna design achieves low sidelobe levels, which minimizes interference and improves overall performance. The proposed structure offers a compact and efficient solution for applications requiring high gain, wide bandwidth, and accurate beam control in a single-layer configuration.

5.2.1 Introduction

The increasing demand for dynamic radiation control in modern wireless communications has driven the development of beam-steerable transmitarray antennas. These antennas are specifically designed to transmit electromagnetic waves with high precision and control, which also enhances the beamforming process. By optimizing the directionality of the antenna's output, the design allows the antenna to focus its radiation pattern toward specific directions, thereby improving its overall performance and efficiency. Furthermore, these antennas surpass the limitations of fixed-beam designs by providing real-time adaptability and improved performance. In addition, high-gain transmitarray antennas with electronic beam-steering are ideal for next-generation wireless base stations [124, 134, 135]. Operating at millimeter-wave frequencies, they enable high data rates, greater bandwidth, and less interference. This helps ensure reliable coverage and makes the most efficient use of available frequency bands [136].

However, conventional phased array antennas are employed for beamsteering, but they are often constrained by high costs and losses due to their complex feeding and phase-shifting networks [137]. To overcome these challenges, beam-steering transmitarray antennas have emerged as a promising alternative. These systems offer advantages such as precise phase control over the aperture of the array, reduced losses, and cost-effective spatial feeding techniques. Using active components like PIN diodes, these antennas efficiently manipulate incident electromagnetic waves, achieving superior adaptability and performance [138, 139].

Metasurfaces, composed of engineered sub-wavelength structures, have recently been employed in transmitarray antenna design to enhance performance. These artificial surfaces are designed to manipulate electromagnetic waves with high precision, enabling to optimize the efficiency, directivity, and overall functionality of antennas. By tailoring the phase, amplitude, and polarization of the transmitted waves at a sub-wavelength scale, metasurfaces provide a flexible and compact solution for advanced beamforming, low-sidelobe levels, and wide bandwidth operations, making them invaluable in modern wireless communication systems and applications. This technology enhances antenna beamforming by enabling precise signal direction and adjustment to meet specific communication needs [140]. By combining transmit array antennas with advanced metasurfaces, it optimizes signal transmission and reception, improving strength, coverage, and reliability. Metasurfaces offer fine control over radiation patterns, ensuring more efficient use of bandwidth and energy. This technology supports the growing demands of 5G, IoT, and future wireless systems, enabling high-speed data transfer, better network efficiency, and improved connectivity for emerging applications [141–143].

Thus, the goal of this section is to enhance the beamforming functionality of transmitarray antennas using a metasurface-based approach. To achieve this, a novel unit cell based on Huygens' Metasurface is designed. This unit cell is then utilized to construct the transmitarray. A horn an-

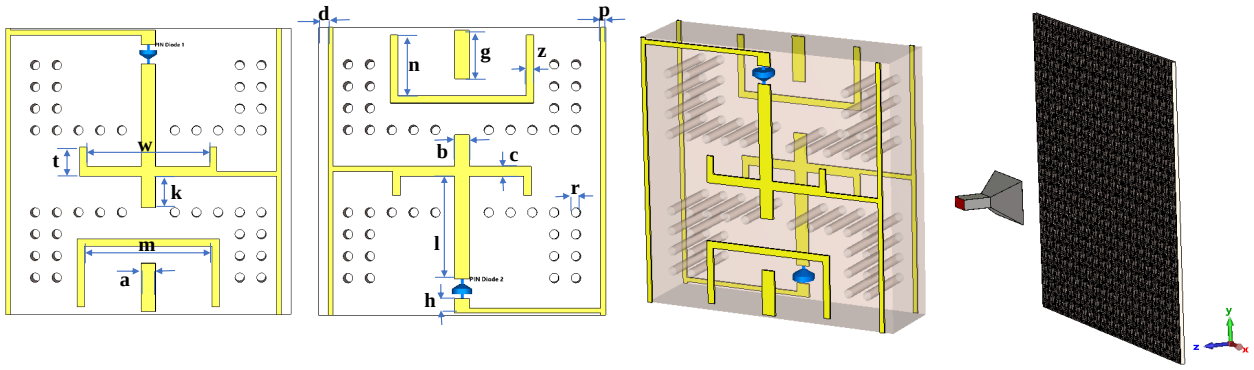

FIGURE 5.6 : The proposed unit cell (a) top view, (b) bottom view, (c) 3D view, and (d) transmitarray antenna based on the proposed unit cell (w = 2.55, k = 0.65, t = 0.60, a = 0.3, b = 0.3, m = 2.65, l = 2.12, n = 1.25, g = 1, z = 0.15, c = 0.2, h = 0.3, r = 0.2, d = 0.2, p = 0.1, all in mm).

tenna serves as the source antenna, and the beamforming concept is validated through testing to confirm the system's performance.

5.2.2 Proposed Active Unit Cell

The configuration of the proposed unit cell with dimensions of 5.92 × 5.92 mm^2 is given in Fig. 5.6. a-c. Based on Huygens' theory, two metallic T-shaped and E-shaped patches are printed on the top and bottom sides of a Rogers RO5880 substrate with a dielectric constant (ϵ_r) of 2.2 and a thickness of 1.57 mm. The E-shaped patches are rotated by 90 degrees and positioned above the T-shaped patches. The integration of active elements allows for real-time beam reconfiguration and enhances the overall adaptability of the beamforming system. In addition, two microstrip lines are added on the sides of the patches. The microstrip lines act as biasing lines for the pin diodes, with one connected to the arm and the other to the bottom of the T-shaped patches. The selected PIN Diode (MACOM MA4AGFCP910) has been characterized in Section 4.2.2. Moreover, 44 holes are employed to lower the permittivity of the substrate and increase the transmission efficiency. This structure is proposed to construct a Huygens' metasurface with simultaneous electric and magnetic dipole resonances. Note, a Huygens' surface is designed to control electromagnetic wavefronts by manipulating surfaces, accomplished through the engineering of orthogonal subwavelength electric and magnetic dipoles. As per Huygens' theory, a Huygens resonance achieves total transmission when the induced orthogonal electric and magnetic currents are in phase [99, 133].

The unit cell's frequency response is analyzed using the frequency-domain solver in CST Microwave Studio 2022. The configuration used to simulate the transmission characteristics (both magnitude and phase responses) of the unit cell is based on periodic unit cell boundaries and Floquet ports. A plane wave is applied with normal incidence to the unit cell during the simulation.

Fig. 5.7 shows that by turning ON and OFF two PIN diodes, the proposed unit cell provides 0 and 180-degree phase variation with low transmission loss below -2.4 dB in the Ka-band at the

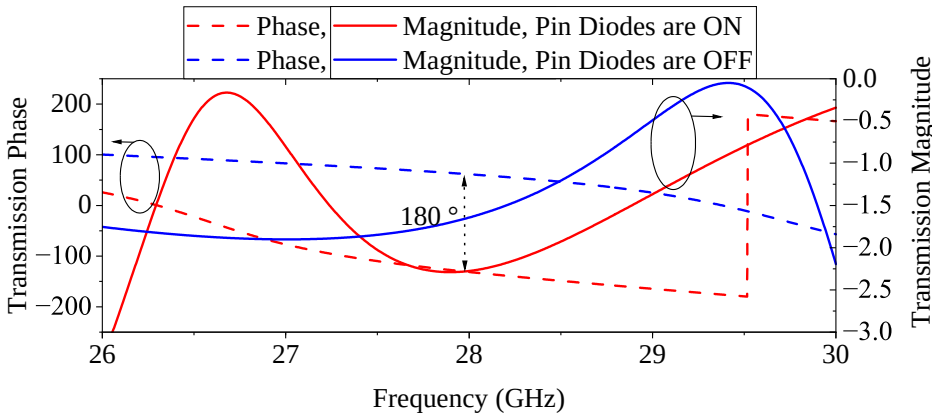

FIGURE 5.7 : Simulated transmission results of the proposed unit cell with both PIN diodes in the ON state and both PIN diodes in the OFF state.

center frequency of 28 GHz. The results indicate minimal insertion loss, which remains consistently low across two phase states. Since the objective is to implement beamforming using a 1-bit transmitarray, this leads to the acquisition of phases at 0, 180 degrees. The proposed unit cell is utilized in the building of a metamaterial-based transmitarray antenna in the next section, as depicted in Figure 5.6.d.

As explained in the previous section, a metasurface must simultaneously support both tangential electric and magnetic dipole moments within each unit cell to achieve high transmission efficiency and minimal reflection. This requirement defines the operational foundation of a Huygens' metasurface, where the electromagnetic behavior is governed by two equivalent surface parameters : the normalized electric surface admittance $Y_{ES} \cdot \eta_0$ and the normalized magnetic surface impedance Z_{MS}/η_0. A metasurface behaves as an ideal Huygens surface when these two parameters are equal, satisfying the condition $Y_{ES} \cdot \eta_0 = Z_{MS}/\eta_0$. This equality ensures that the electric and magnetic responses are in phase and balanced in magnitude, which leads to constructive interference in the forward direction and destructive interference in the backward direction. As a result, the metasurface enables full-power transmission with low reflection, which are essential characteristics for beam-steering antenna applications.

To verify this condition, full-wave electromagnetic simulations are conducted, and the relevant surface parameters were extracted using the reflection and transmission coefficients of the unit cell, denoted by S_{11} and S_{21}, respectively. The normalized surface admittance and impedance were calculated using the standard expressions $Y_{ES} \cdot \eta_0 = \frac{2(1-S_{21}-S_{11})}{1+S_{21}+S_{11}}$ and $Z_{MS}/\eta_0 = \frac{2(1-S_{21}+S_{11})}{1+S_{21}-S_{11}}$, which characterize the metasurface boundary response under normal plane-wave excitation. At the design frequency of 28 GHz, the extracted values for the proposed unit cell were $Y_{ES} \cdot \eta_0 = 0.13 + j2.36$ and $Z_{MS}/\eta_0 = 0.14 + j2.34$. The close agreement between these values confirms that the electric and magnetic responses are both well-matched and in phase. The small real parts indicate minimal loss, while the closely aligned imaginary components confirm that the structure exhibits strong reactive behavior, consistent with low-reflection and high-transmission performance.

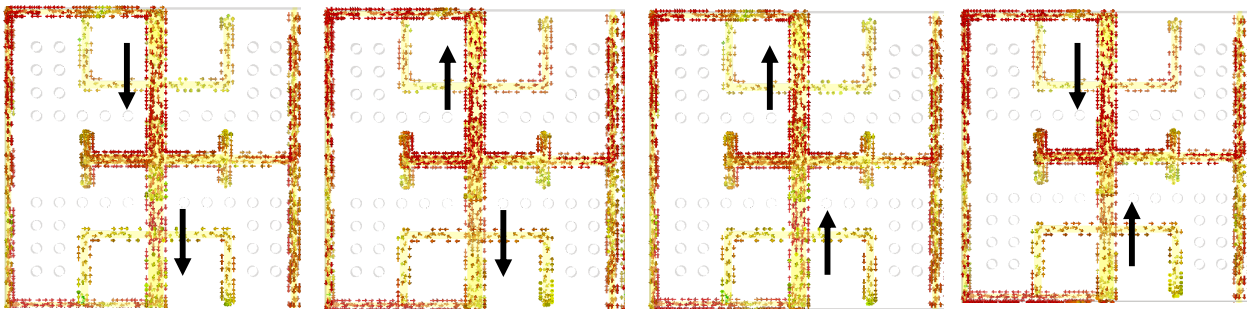

(a) (b) (c) (d)

FIGURE 5.8 : Current distributions on the proposed unit cell (a) t = 0, (b) t = T/4, (c) t = T/2 and (d) t = 3T/4.

This alignment demonstrates that the unit cell satisfies the Huygens condition at 28 GHz and is capable of providing efficient wavefront manipulation with broadband phase control.

To further validate the electromagnetic behavior of the unit cell, the time-domain evolution of surface currents was analyzed as shown in Figure 5.8. Over one complete sinusoidal period T, the direction of surface currents on the top and bottom metallic layers alternates in a manner consistent with Huygens metasurface operation. At time instants $t = 0$ and $t = T/2$, the surface currents on the top and bottom layers flow in the same direction. This in-phase current configuration results in the accumulation of surface charges on opposite layers, thereby establishing a strong electric dipole moment across the metasurface. In contrast, at time instants $t = T/4$ and $t = 3T/4$, the surface currents flow in opposite directions between the two layers, creating a closed-loop pattern characteristic of a magnetic dipole. This temporal alternation between electric and magnetic dipole dominance, occurring every quarter cycle, ensures the necessary 90-degree phase shift between the two contributions. The presence of both dipole types confirms that the unit cell exhibits the defining properties of a Huygens' metasurface. This behavior enables the structure to operate with high transmission efficiency and accurate phase control, making it well-suited for integration into advanced millimeter-wave beam-steering and flat-lens antenna systems.

5.2.3 Transmitarray Configuration

Building on the beamsteering principles outlined in section 5.1.3, a complete transmitarray antenna with dimensions of 15 × 15 is designed and simulated using CST Microwave Studio 2022 to validate the beamforming mechanism, incorporating the proposed unit cell. A linear metasurface lens, with a length of $D = 88.8$ mm, is used, and custom beam-steering software generates phase distributions for various beam-steering angles, as illustrated in Fig. 5.9. For proof of concept, simulations are performed at angles of 0°, 10°, 20°, and 30°. A transverse magnetic (TM) polarized wave is employed to illuminate the transmitarray antenna, with a pyramidal horn antenna (15 dBi gain) serving as the EM source. To facilitate beamsteering at specific angles, a focal distance

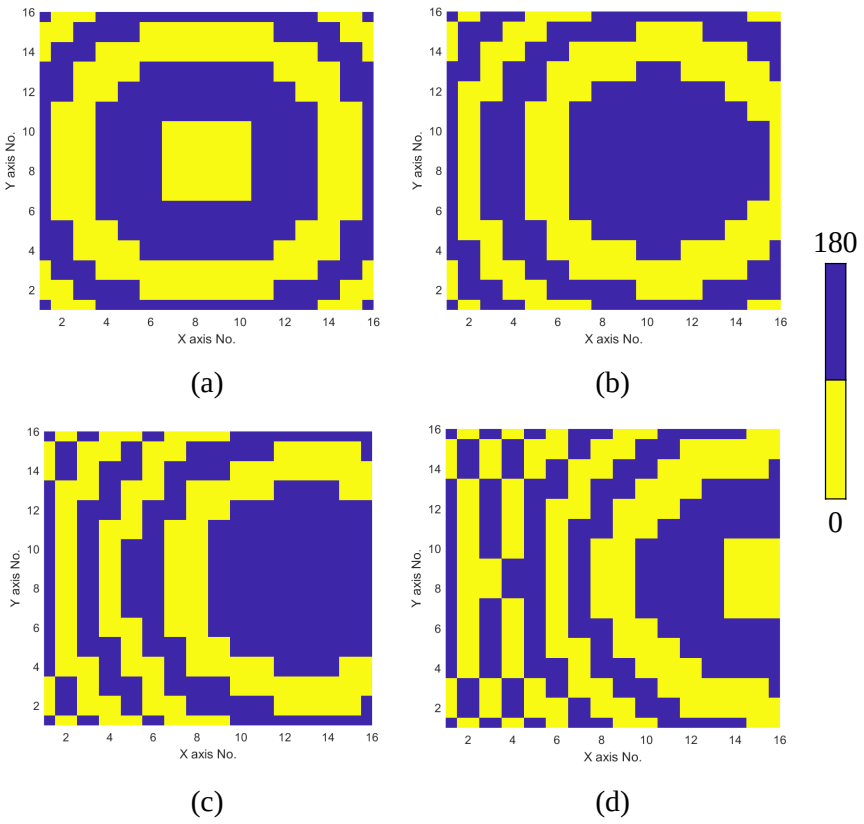

FIGURE 5.9 : Phase distributions at (a) 0°, (b) 10°, (c) 20°, (d) 30°.

of 65 mm is chosen. By adjusting the phase differences between rays passing through different segments, the resulting wave can be precisely directed to the desired beam-steering direction.

It should be pointed out that a key factor in the performance of a transmitarray antenna is the ratio of the focal distance to the aperture diameter (F/D). Here, F is the distance between the phase center of the source antenna and the center of the array's aperture, while D refers to the size of the aperture. Variations in the focal distance affect the value of the phase constant (φ_c), leading to quantization errors. This, in turn, impacts the beam direction, gain, aperture efficiency, and side lobes. Factors such as illumination and spillover losses influence the efficiency of the transmitarray antenna. Therefore, it is important to carefully select the F/D ratio to minimize these losses. Both very large and very small F/D values can harm the antenna's performance. To optimize the F/D ratio, the electromagnetic waves from the feed antenna should ideally illuminate the edge of the aperture at a level of around -10 dB relative to the center. Reducing the focal distance from the optimal increases the illumination loss while increasing it leads to higher spillover losses. For optimal performance, the F/D ratio of 0.7 is chosen, where the edge illumination level is -10 dB [144].

As shown in Fig. 5.10, the radiation patterns in the H-plane and E-plane demonstrate that the transmitarray antenna utilizing the proposed unit cell successfully achieved accurate beam-steering angles with just a 1-bit resolution. Beamsteering was achieved for the desired angles of 10°, 20°,

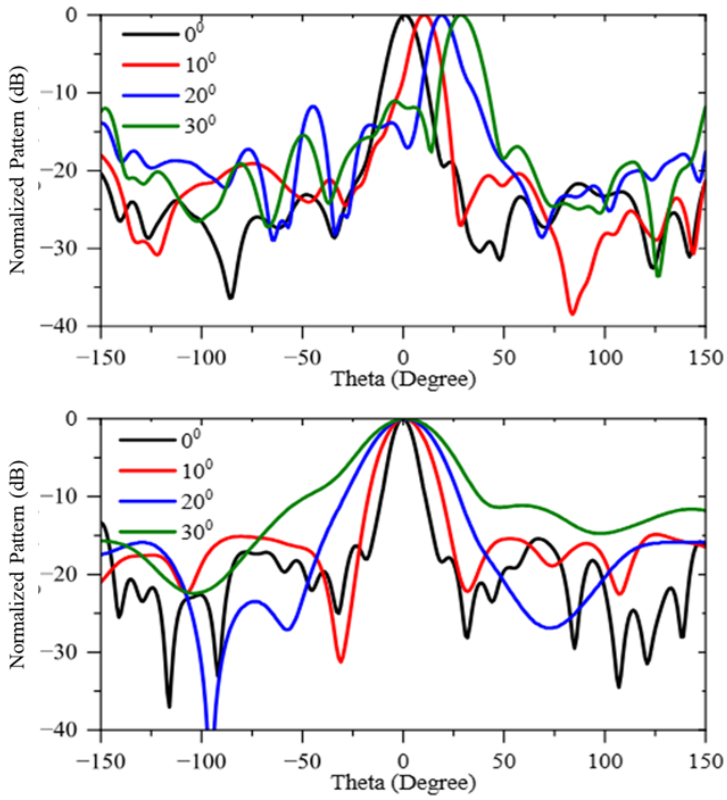

FIGURE 5.10 : Radiation patterns of the proposed transmitarray antenna in the H-plane and E-plane.

TABLEAU 5.2 : Beamsteering performance at four different angles of 0°, 10°, 20°, 30° at the center frequency of 28 GHz in simulation.

Beam Steering Angle (degree)	Peak Gain (dBi)	Side Lobe Level (dB)	Number of Elements
0	21.2	-17.6	15 × 15
10	20.7	-15.8	15 × 15
20	18.9	-12.5	15 × 15
30	18.1	-12.1	15 × 15

and 30°. Additionally, the antenna's gain exceeds that of its feed by 6.2 dBi, reaching a peak value of 21.2 dBi with a low side lobe level of -17.6 dB at 28 GHz. The gains for the beam-steering angles of 10°, 20°, and 30° are 20.7 dBi, 18.9 dBi, and 18.1 dBi, respectively. Corresponding side lobe levels are -15.8 dB, -12.5 dB, and -12.1 dB, respectively. The data summarized in Table 5.2 supports these findings, confirming the core principles and operational mechanism behind the beamforming process.

5.2.4 Conclusion

A novel single-layer 1-bit transmitarray antenna has been presented in this section. The design is based on Huygens' principle and utilizes a metasurface unit cell with dimensions of 5.92 × 5.92 mm^2. To achieve a 180° phase difference, two PIN diodes are integrated into the design, ensuring a linear phase response across the operational bandwidth. Simulation results confirm the excellent performance of the proposed unit cell. This unit cell is then implemented in the construction of a 15 × 15 transmitarray antenna, demonstrating effective beam-scanning capabilities.

5.3 Summary

In this chapter, we explored the design and development of Huygens-based metasurface unit cells for use in beamforming transmitarray antennas. The chapter began with the design of a 2-bit passive transmissive unit cell, which demonstrated full 360° phase coverage and high transmission efficiency. A transmitarray panel was constructed using this unit cell, and simulation results confirmed its effectiveness in achieving fixed-beamsteering, validating the feasibility of the passive design for mm-wave applications. Building on this foundation, we then developed an active reconfigurable unit cell using PIN diodes to enable 1-bit phase control. This design was integrated into a 15 × 15 transmitarray panel and shown to provide dynamic beam-steering functionality in simulation. The structure maintained strong transmission characteristics while achieving a 180° phase shift, making it suitable for real-time directional control. Together, these two stages, passive and active metasurface designs, lay the groundwork for the realization of a complete, reconfigurable transmitarray antenna system.

6 CONCLUSION AND FUTURE WORK

6.1 Conclusions

This thesis presented a comprehensive design and analysis of reconfigurable transmitarray antennas operating at 28 GHz for millimeter-wave beamforming applications. The proposed system addresses key challenges in 5G and future wireless communications by combining compact design, high gain, and reconfigurable functionality.

Two types of feed antennas were developed and analyzed : a compact Substrate Integrated Waveguide (SIW)-based slot antenna, and a 3D-printed horn antenna for validation and simplified simulation. For the metasurface panel, two distinct design approaches were explored : one based on Huygens' principle and another based on mutual coupling and current reversal techniques. These complementary methods demonstrate the versatility of unit cell design strategies in achieving efficient phase control and beam steering.

Each approach began with the design of a passive unit cell, which was optimized for transmission performance and phase response. Building upon these designs, active unit cells were developed by integrating PIN diodes, enabling dynamic 1-bit phase modulation between 0° and 180°. Full transmitarray panels were constructed and simulated using these active unit cells. The results confirmed effective beam steering, achieving directional radiation with high gain and acceptable sidelobe levels. The horn antenna was employed as the feed during simulation and verification phases to simplify the system and reduce the number of active components required.

To support practical realization, the PIN diode was accurately characterized and modeled in the CST environment. The EVAL-AD5370 evaluation board was considered for biasing control, with final integration decisions to be made during the hardware implementation phase. Although the fabrication files for the metasurface panels have been fully prepared, financial constraints (due to the nature of the industrial funding) have delayed the fabrication of the complete active metasurface panel at the time of writing this thesis. Nonetheless, the passive version of the proposed transmitarray was successfully designed, fabricated, and experimentally validated, as detailed in Section 4.1. Additionally, the measured results of the active unit cell closely match the simulation outcomes, reinforcing confidence that the full active metasurface panel will perform as intended once fabrication and integration are completed.

At a higher level, this work delivers several original contributions to the field of millimeter-wave antenna design :

- A dual-strategy methodology was employed for unit cell design, leveraging two distinct electromagnetic principles : Huygens' principle and mutual coupling with current reversal. This

approach provided two effective and complementary design pathways for realizing phase-reconfigurable metasurface unit cells tailored for dynamic beamforming applications.

- Both passive and active reconfigurable transmitarrays were developed and analyzed, offering a complete path from fundamental unit cell design to full array implementation.
- A systematic integration of feed types, active switching elements, and phase modeling strategies was conducted, with attention to practical implementation and simulation fidelity.
- This research also provides theoretical insight into how mutual coupling and current reversal can be leveraged as design tools for simplified beamforming architectures; an area less explored in conventional transmitarray literature.

From a broader perspective, the work advances the state-of-the-art in compact, reconfigurable mm-wave antenna systems that are well-suited for next-generation wireless technologies such as 5G and 6G. The proposed transmitarray designs are not only cost-effective and highly directional but also scalable and adaptable, making them viable candidates for intelligent communications infrastructure, smart radar, and emerging high-data-rate applications like autonomous vehicles.

In addition, the simulation models, design methodologies, and performance results presented in this thesis offer valuable benchmarks for future researchers and serve as a practical foundation for hardware prototyping and real-world integration.

6.2 Future Work

The outcomes of this thesis provide a solid foundation for the continued development of high-performance reconfigurable transmitarray antennas for millimeter-wave applications. While the proposed designs have demonstrated strong beamforming capabilities through simulation, several research directions can be pursued to extend the impact, applicability, and functionality of the system.

The most immediate next step is the fabrication and experimental validation of the designed active transmitarray structures. This includes hardware realization of the metasurface panel, integration of the biasing network, and complete radiation characterization in an anechoic environment. These measurements will serve to verify simulation results and identify any discrepancies due to manufacturing tolerances, parasitics, or environmental factors.

Beyond experimental validation, several strategic research directions are proposed :

- **Enhanced Phase Resolution :** Future work may explore multi-bit unit cell designs like 2-bit and 3-bit to enhance beam-steering precision while minimizing sidelobe intensity and achieving better angular resolution. Advanced applications like user tracking systems and high-precision radar imaging depend on this technology.

- **Alternative Tuning Mechanisms :** Research should explore alternative reconfigurable technologies including MEMS devices, liquid crystals, tunable dielectrics and phase-change materials such as VO_2. The materials provide benefits for switching speed efficiency while maintaining low insertion loss and power consumption together with precise phase control.

- **Machine Learning-Based Beamforming :** Real-time feedback and data-driven strategies in intelligent control systems improve system responsiveness and adaptability. Dynamic beam management becomes feasible through learning-based approaches in environments with high variability.

- **Wideband and Multi-Band Operation :** Expanding the metasurface design to support broadband or multi-band operation will increase its utility in heterogeneous wireless systems and frequency-agile platforms required for 5G and emerging 6G applications.

- **Energy-Aware Control Architectures :** To enable deployment in energy-constrained platforms such as IoT nodes or UAVs, low-power control schemes and energy-harvesting-enabled systems should be explored. These can extend operational lifetime and reduce reliance on external power supplies.

- **System-Level Integration :** Moving beyond antenna-level validation, future research may involve co-designing the transmitarray with RF front-end circuits, including amplifiers, mixers, and digital control logic, to develop a fully functional reconfigurable antenna module.

- **Compact and Conformal Implementations :** Miniaturization of control circuitry and integration into flexible or conformal substrates can expand deployment to new application domains such as wearable electronics, automotive platforms, and aerospace systems.

- **Security and Multifunctionality :** The reconfigurable nature of the system can be exploited for advanced applications such as physical-layer security (e.g., beam randomization), multi-beam generation, and joint communication–sensing functionalities.

- **Software-Defined Metasurfaces (SDMs) :** Enabling software-driven control over unit cell states through programmable interfaces can transform static designs into intelligent, adaptable platforms. This would allow centralized beam control and real-time reconfiguration in response to network demands.

- **Exploration of New Unit Cell Architectures :** While this thesis focused on Huygens-based and mutual coupling-based designs, future work could explore hybrid configurations, tunable metamaterials, or optimization-driven inverse design to achieve improved performance metrics such as reduced loss, wider scanning range, and enhanced gain.

- **Real-World Deployment and Field Testing :** Finally, extensive evaluation in realistic operating environments including urban, vehicular, and industrial settings, is essential to assess the

robustness of the system under multipath, blockage, temperature variations, and interference scenarios.

By addressing these directions, the proposed reconfigurable transmitarray system can be evolved into a scalable, cost-effective, and intelligent beamforming solution, aligned with the performance and adaptability requirements of next-generation wireless technologies in the 5G, 6G, and beyond landscape.

BIBLIOGRAPHIE

[1] C. A. Balanis, *Antenna theory : analysis and design*. John wiley & sons, 2016.

[2] D. M. Pozar, *Microwave engineering*. John wiley & sons, 2011.

[3] T. S. Rappaport, S. Sun, R. Mayzus, H. Zhao, Y. Azar, K. Wang, G. N. Wong, J. K. Schulz, M. Samimi, and F. Gutierrez, "Millimeter wave mobile communications for 5g cellular : It will work!," *IEEE access*, vol. 1, pp. 335–349, 2013.

[4] J. C. Gallagher and M. E. DeVine, "Fifth-generation (5g) telecommunications technologies : issues for congress," *Congressional Research Service*, vol. 1, no. 30, pp. 1–39, 2019.

[5] J. R. Hoehn, K. M. Sayler, and J. C. Gallagher, "Overview of department of defense use of the electromagnetic spectrum," LIBRARY OF CONGRESS WASHINGTON DC, 2021.

[6] M. Series, "Minimum requirements related to technical performance for imt-2020 radio interface (s)," *Report*, pp. 2410–0, 2017.

[7] B. Ai, K. Guan, M. Rupp, T. Kurner, X. Cheng, X.-F. Yin, Q. Wang, G.-Y. Ma, Y. Li, L. Xiong, *et al.*, "Future railway services-oriented mobile communications network," *IEEE Communications Magazine*, vol. 53, no. 10, pp. 78–85, 2015.

[8] G. H. Elzwawi, H. H. Elzwawi, M. M. Tahseen, and T. A. Denidni, "Frequency selective surface-based switched-beamforming antenna," *IEEE Access*, vol. 6, pp. 48042–48050, 2018.

[9] M. M. Tahseen, T. A. Denidni, and A. A. Kishk, "Proof of concept low-loss reconfigurable reflectarray for beam steering," in *2018 18th International Symposium on Antenna Technology and Applied Electromagnetics (ANTEM)*, pp. 1–2, IEEE, 2018.

[10] J. T. Bernhard, "Bernhard, reconfigurable antennas, synthesis lectures on antennas and propagation series," 2007.

[11] A. Hakkarainen, J. Werner, N. Gulati, D. Patron, D. Pfeil, H. Paaso, A. Mämmelä, K. Dandekar, and M. Valkama, "Reconfigurable antenna based doa estimation and localization in cognitive radios : Low complexity algorithms and practical measurements," in *2014 9th International Conference on Cognitive Radio Oriented Wireless Networks and Communications (CROWNCOM)*, pp. 454–459, IEEE, 2014.

[12] A. Mozharovskiy, A. Artemenko, A. Sevastyanov, V. Ssorin, and R. Maslennikov, "Beam-steerable integrated lens antenna with waveguide feeding system for 71–76/81–86 ghz point-to-point applications," in *2016 10th European Conference on Antennas and Propagation (EuCAP)*, pp. 1–5, IEEE, 2016.

[13] A. Abbaspour-Tamijani, L. Zhang, G. Pan, H. K. Pan, and H. Alavi, "Lens-enhanced phased array antenna system for high directivity beam-steering," in *2011 IEEE International Symposium on Antennas and Propagation (APSURSI)*, pp. 3275–3278, IEEE, 2011.

[14] T. Ueda, S. Yamamoto, Y. Kado, and T. Itoh, "Pseudo-traveling-wave resonator with magnetically tunable phase gradient of fields and its applications to beam-steering antennas," *IEEE transactions on microwave theory and techniques*, vol. 60, no. 10, pp. 3043–3054, 2012.

[15] Y. Yokohama and T. Kodera, "Voltage beam-steerable leaky-wave antenna using magnetless non-reciprocal metamaterial (mnm)," in *2015 International Symposium on Antennas and Propagation (ISAP)*, pp. 1–3, IEEE, 2015.

[16] T. A. Denidni and G. Y. Delisle, "A nonlinear algorithm for output power maximization of an indoor adaptive phased array," *IEEE transactions on electromagnetic compatibility*, vol. 37, no. 2, pp. 201–209, 1995.

[17] V. S. Rao, V. Srinivasan, and S. Pal, "Generation of dual beams from spherical phased array antenna," *Electronics letters*, vol. 45, no. 9, p. 1, 2009.

[18] G. Poilasne, P. Pouliguen, K. Mahdjoubi, L. Desclos, and C. Terret, "Active metallic photonic band-gap materials (mpbg) : Experimental results on beam shaper," *Ieee Transactions on antennas and propagation*, vol. 48, no. 1, pp. 117–119, 2000.

[19] A. Clemente, F. Diaby, L. Di Palma, L. Dussopt, and R. Sauleau, "Experimental validation of a 2-bit reconfigurable unit-cell for transmitarrays at ka-band," *IEEE Access*, vol. 8, pp. 114991–114997, 2020.

[20] D. Kong, H. Li, Q. Luo, and S. Gao, "Electronically beam-scanning antenna with active slot frequency selective surface for 5g base stations," in *2020 IEEE MTT-S International Wireless Symposium (IWS)*, pp. 1–3, IEEE, 2020.

[21] L. Han, G. Cheng, G. Han, R. Ma, and W. Zhang, "Electronically beam-steering antenna with active frequency-selective surface," *IEEE Antennas and Wireless Propagation Letters*, vol. 18, no. 1, pp. 108–112, 2018.

[22] C. Gu, S. Gao, B. Sanz-Izquierdo, E. A. Parker, F. Qin, H. Xu, J. C. Batchelor, X. Yang, and Z. Cheng, "3-d coverage beam-scanning antenna using feed array and active frequency-selective surface," *IEEE transactions on antennas and propagation*, vol. 65, no. 11, pp. 5862–5870, 2017.

[23] L. Zhang, Q. Wu, and T. A. Denidni, "Electronically radiation pattern steerable antennas using active frequency selective surfaces," *IEEE Transactions on Antennas and Propagation*, vol. 61, no. 12, pp. 6000–6007, 2013.

[24] A. Edalati and T. A. Denidni, "High-gain reconfigurable sectoral antenna using an active cylindrical fss structure," *IEEE Transactions on antennas and propagation*, vol. 59, no. 7, pp. 2464–2472, 2011.

[25] J. Li, T. A. Denidni, and Q. Zeng, "A dual-band reconfigurable radiation pattern antenna based on active frequency selective surfaces," in *2016 IEEE International Symposium on Antennas and Propagation (APSURSI)*, pp. 1245–1246, IEEE, 2016.

[26] A. Edalati and T. A. Denidni, "Frequency selective surfaces for beam-switching applications," *IEEE Transactions on Antennas and Propagation*, vol. 61, no. 1, pp. 195–200, 2012.

[27] M. Niroo-Jazi and T. A. Denidni, "Electronically sweeping-beam antenna using a new cylindrical frequency-selective surface," *IEEE Transactions on Antennas and Propagation*, vol. 61, no. 2, pp. 666–676, 2012.

[28] S. M. Mahmood and T. A. Denidni, "Pattern-reconfigurable antenna using a switchable frequency selective surface with improved bandwidth," *IEEE Antennas and Wireless Propagation Letters*, vol. 15, pp. 1148–1151, 2015.

[29] J. Li, T. A. Denidni, and Q. Zeng, "Beam switching antenna based on active frequency selective surfaces," in *2015 IEEE MTT-S International Conference on Numerical Electromagnetic and Multiphysics Modeling and Optimization (NEMO)*, pp. 1–3, IEEE, 2015.

[30] J. Li, Q. Zeng, R. Liu, and T. A. Denidni, "A compact dual-band beam-sweeping antenna based on active frequency selective surfaces," *IEEE Transactions on Antennas and Propagation*, vol. 65, no. 4, pp. 1542–1549, 2017.

[31] A. H. Abdelrahman, F. Yang, A. Z. Elsherbeni, P. Nayeri, and C. A. Balanis, "Analysis and design of transmitarray antennas," 2017.

[32] Y. J. Guo and R. W. Ziolkowski, *Advanced antenna array engineering for 6G and beyond wireless communications*. John Wiley & Sons, 2021.

[33] C. Pfeiffer and A. Grbic, "Metamaterial huygens' surfaces : tailoring wave fronts with reflectionless sheets," *Physical review letters*, vol. 110, no. 19, p. 197401, 2013.

[34] Y. Cao, M. Zhang, C. Fan, and J.-X. Chen, "A broadband transmitarray antenna using a metasurface-based element for millimeter-wave applications," *Micromachines*, vol. 15, no. 3, p. 383, 2024.

[35] Z. Pourgholamhossein, M. N. Jazi, and T. A. Denidni, "Broadband flat-lens antenna design using ultrathin huygens' metasurface for millimeter-wave applications," *IEEE Transactions on Antennas and Propagation*, vol. 71, no. 12, pp. 9914–9919, 2023.

[36] H. Kaouach, L. Dussopt, J. Lanteri, T. Koleck, and R. Sauleau, "Wideband low-loss linear and circular polarization transmit-arrays in v-band," *IEEE Transactions on Antennas and Propagation*, vol. 59, no. 7, pp. 2513–2523, 2011.

[37] Q. Cheng, H. F. Ma, and T. J. Cui, "Broadband planar luneburg lens based on complementary metamaterials," *Applied Physics Letters*, vol. 95, no. 18, 2009.

[38] C. G. M. Ryan, M. R. Chaharmir, J. Shaker, J. R. Bray, Y. M. M. Antar, and A. Ittipiboon, "A wideband transmitarray using dual-resonant double square rings," *IEEE Transactions on Antennas and Propagation*, vol. 58, no. 5, pp. 1486–1493, 2010.

[39] C. A. Fernandes, R. C. Martins, T. Radil, P. M. Ramos, E. B. Lima, C. R. Medeiros, and J. R. Costa, "Low-cost mechanically steered millimeter-wave lens antenna system for indoor lans," in *2010 International Workshop on Antenna Technology (iWAT)*, pp. 1–4, IEEE, 2010.

[40] J. R. Costa, E. B. Lima, and C. A. Fernandes, "Compact beam-steerable lens antenna for 60-ghz wireless communications," *IEEE Transactions on Antennas and Propagation*, vol. 57, no. 10, pp. 2926–2933, 2009.

[41] J. R. Costa, E. B. Lima, C. R. Medeiros, T. Radil, R. C. Martins, P. M. Ramos, and C. A. Fernandes, "Development of an indoor wireless personal area network based on mechanically steered millimeter-wave lens antenna," in *2010 IEEE Instrumentation & Measurement Technology Conference Proceedings*, pp. 1202–1206, IEEE, 2010.

[42] K. Zarb-Adami, A. Faulkner, J. G. B. de Vaate, G. W. Kant, and P. Picard, "Beamforming techniques for large-n aperture arrays," in *2010 IEEE International Symposium on Phased Array Systems and Technology*, pp. 883–890, 2010.

[43] F. Gholam, J. Via, and I. Santamaria, "Beamforming design for simplified analog antenna combining architectures," *IEEE Transactions on Vehicular Technology*, vol. 60, no. 5, pp. 2373–2378, 2011.

[44] H. Steyskal, "Digital beamforming," in *1988 18th European Microwave Conference*, pp. 49–57, IEEE, 1988.

[45] A. Artemenko, A. Maltsev, A. Mozharovskiy, A. Sevastyanov, V. Ssorin, and R. Maslennikov, "Millimeter-wave electronically steerable integrated lens antennas for wlan/wpan applications," *IEEE Transactions on Antennas and Propagation*, vol. 61, no. 4, pp. 1665–1671, 2012.

[46] J. Romeu, S. Blanch, L. Pradell, A. Barlabé, J.-M. Rius, M. Albert-Gali, L. Jofre-Roca, C. Mazzucco, and R. Flamini, "Lens-based switched-beam antenna for a 5g smart repeater," *IEEE Antennas and Wireless Propagation Letters*, vol. 22, no. 10, pp. 2482–2486, 2023.

[47] G. V. Eleftheriades, M. Kim, V. G. Ataloglou, and A. H. Dorrah, "Prospects of huygens' metasurfaces for antenna applications," *Engineering*, vol. 11, pp. 21–26, 2022.

[48] C. Pfeiffer and A. Grbic, "Metamaterial huygens' surfaces," in *2013 IEEE MTT-S International Microwave Symposium Digest (MTT)*, pp. 1–4, IEEE, 2013.

[49] Z. Pourgholamhossein and T. A. Denidni, "Reconfigurable huygens' metasurface-based unit-cell and electronically steerable active flat-lens antenna at the ka-band," *IEEE Transactions on Antennas and Propagation*, pp. 1–1, 2024.

[50] X. Wang, P.-Y. Qin, A. T. Le, H. Zhang, R. Jin, and Y. J. Guo, "Beam scanning transmitarray employing reconfigurable dual-layer huygens element," *IEEE Transactions on Antennas and Propagation*, vol. 70, no. 9, pp. 7491–7500, 2022.

[51] H. Li, C. Ma, F. Shen, K. Xu, D. Ye, J. Huangfu, C. Li, L. Ran, and T. A. Denidni, "Wide-angle beam steering based on an active conformal metasurface lens," *IEEE Access*, vol. 7, pp. 185264–185272, 2019.

[52] A. Clemente, L. Dussopt, R. Sauleau, P. Potier, and P. Pouliguen, "Wideband 400-element electronically reconfigurable transmitarray in x band," *IEEE Transactions on Antennas and Propagation*, vol. 61, no. 10, pp. 5017–5027, 2013.

[53] F. Diaby, A. Clemente, L. Di Palma, L. Dussopt, K. Pham, E. Fourn, and R. Sauleau, "Design of a 2-bit unit-cell for electronically reconfigurable transmitarrays at ka-band," in *2017 47th European Microwave Conference (EuMC)*, pp. 1321–1324, 2017.

[54] Q. Ali, W. Shahzad, I. Ahmad, S. Safiq, X. Bin, S. M. Abbas, and H. Sun, "Recent developments and challenges on beam steering characteristics of reconfigurable transmitarray antennas," *Electronics*, vol. 11, no. 4, p. 587, 2022.

[55] B. Rana, I.-G. Lee, and I.-P. Hong, "Digitally reconfigurable transmitarray with beam-steering and polarization switching capabilities," *IEEE Access*, vol. 9, pp. 144140–144148, 2021.

[56] N. Melouki, F. Ahmed, H. Nasseri, P. Pourmohammadi, A. Iqbal, and T. A. Denidni, "Multi-bit wideband transmitarray aperture with independent phase and amplitude control for high gain with low sidelobe mm-wave applications," in *2024 18th European Conference on Antennas and Propagation (EuCAP)*, pp. 01–04, IEEE, 2024.

[57] C.-W. Luo, G. Zhao, Y.-C. Jiao, G.-T. Chen, and Y.-D. Yan, "Wideband 1 bit reconfigurable transmitarray antenna based on polarization rotation element," *IEEE Antennas and Wireless Propagation Letters*, vol. 20, no. 5, pp. 798–802, 2021.

[58] F. Diaby, A. Clemente, R. Sauleau, K. T. Pham, and L. Dussopt, "2 bit reconfigurable unit-cell and electronically steerable transmitarray at ka -band," *IEEE Transactions on Antennas and Propagation*, vol. 68, no. 6, pp. 5003–5008, 2020.

[59] A. Clemente, F. Diaby, L. D. Palma, L. Dussopt, and R. Sauleau, "Experimental validation of a 2-bit reconfigurable unit-cell for transmitarrays at ka-band," *IEEE Access*, vol. 8, pp. 114991–114997, 2020.

[60] V. S. Yadav, S. K. Ghosh, S. Bhattacharyya, and S. Das, "Graphene-based metasurface for a tunable broadband terahertz cross-polarization converter over a wide angle of incidence," *Applied optics*, vol. 57, no. 29, pp. 8720–8726, 2018.

[61] D. Yang, W. Wang, E. Lv, H. Wang, B. Liu, Y. Hou, and J.-h. Chen, "Programmable vo2 metasurface for terahertz wave beam steering," *IScience*, vol. 25, no. 8, 2022.

[62] X. You, C. Fumeaux, and W. Withayachumnankul, "Tutorial on broadband transmissive metasurfaces for wavefront and polarization control of terahertz waves," *Journal of Applied Physics*, vol. 131, no. 6, 2022.

[63] H. Hasani, J. S. Silva, S. Capdevila, M. García-Vigueras, and J. R. Mosig, "Dual-band circularly polarized transmitarray antenna for satellite communications at (20, 30) ghz," *IEEE Transactions on Antennas and Propagation*, vol. 67, no. 8, pp. 5325–5333, 2019.

[64] M. N. Iqbal, M. F. M. Yusoff, M. K. A. Rahim, M. R. Hamid, Z. Johari, and H. U. Rahman, "A high gain and compact transmitarray antenna for ku-band satellite communications," *Electromagnetics*, vol. 41, no. 5, pp. 331–343, 2021.

[65] S. Kausar, A. Kausar, M. U. Hadi, and H. Mehrpouyan, "Multi-beam high gain steerable transmitarray lens for satellite communication and 5g mm-wave systems," *AEU-International Journal of Electronics and Communications*, vol. 173, p. 154888, 2024.

[66] S. B. Yeap, X. Qing, and Z. N. Chen, "77-ghz dual-layer transmit-array for automotive radar applications," *IEEE Transactions on Antennas and Propagation*, vol. 63, no. 6, pp. 2833–2837, 2015.

[67] F. Greco, E. Arnieri, G. Amendola, R. De Marco, and L. Boccia, "A 77 ghz transmit array for in-package automotive radar applications," in *Telecom*, vol. 5, pp. 792–803, MDPI, 2024.

[68] N. Melouki, F. Ahmed, P. PourMohammadi, H. Naseri, and T. A. Denidni, "Wideband transmitarray with independent phase/amplitude control for millimeter-wave vehicular sensing and communication," *AEU-International Journal of Electronics and Communications*, p. 155771, 2025.

[69] J. A. Ganie and K. Saurav, "Two-dimensional switchable beam transmitarray antenna for mm-wave base stations and vehicular networks," *IEEE Access*, vol. 11, pp. 34563–34574, 2023.

[70] F. Vaquero, M. R. Pino, and M. Arrebola, "Evaluation of a transmit-array base station for mm-wave communications in the fresnel region," in *2022 IEEE International Symposium on Antennas and Propagation and USNC-URSI Radio Science Meeting (AP-S/URSI)*, pp. 788–789, 2022.

[71] P. PourMohammadi, H. Naseri, N. Melouki, F. Ahmed, Q. Zheng, A. Iqbal, and T. A. Denidni, "A wideband beam steering transmitarray antenna for ka-band applications," *AEU-International Journal of Electronics and Communications*, vol. 193, p. 155720, 2025.

[72] Z.-H. Fu, X.-S. Yang, and B.-Z. Wang, "Low-cost conformal transmit-reflect-array antenna for unmanned aerial vehicle relay communications," *IEEE Transactions on Antennas and Propagation*, pp. 1–1, 2024.

[73] T. B. Nguyen, T. T. Nguyen, M. L. Nguyen, and T. M. Nguyen, "A c-band 1-bit reconfigurable transmitarray unit-cell for airborne uav applications," in *2024 IEEE International Symposium on Antennas and Propagation and INC/USNC-URSI Radio Science Meeting (AP-S/INC-USNC-URSI)*, pp. 2295–2296, 2024.

[74] P.-Y. Qin, L.-Z. Song, and Y. J. Guo, "Conformal transmitarrays for unmanned aerial vehicles aided 6g networks," *IEEE Communications Magazine*, vol. 60, no. 1, pp. 14–20, 2022.

[75] T. Djerafi, A. Doghri, K. Wu, and Z. Chen, "Substrate integrated waveguide antennas," *Handbook of Antenna Technologies*, pp. 1585–1655, 2015.

[76] P. Kumawat and S. Joshi, "Review of slotted siw antenna at 28 ghz and 38 ghz for mm-wave applications," in *2020 12th International Conference on Computational Intelligence and Communication Networks (CICN)*, pp. 8–13, IEEE, 2020.

[77] M. Bozzi, F. Xu, D. Deslandes, and K. Wu, "Modeling and design considerations for substrate integrated waveguide circuits and components," in *2007 8th International Conference on Telecommunications in Modern Satellite, Cable and Broadcasting Services*, pp. P–VII, IEEE, 2007.

[78] F. Xu and K. Wu, "Guided-wave and leakage characteristics of substrate integrated waveguide," *IEEE Transactions on microwave theory and techniques*, vol. 53, no. 1, pp. 66–73, 2005.

[79] A. Dewantari, J. Kim, I. Scherbatko, and M.-H. Ka, "A sidelobe level reduction method for mm-wave substrate integrated waveguide slot array antenna," *IEEE Antennas and Wireless Propagation Letters*, vol. 18, no. 8, pp. 1557–1561, 2019.

[80] D. Deslandes and K. Wu, "Integrated microstrip and rectangular waveguide in planar form," *IEEE Microwave and Wireless Components Letters*, vol. 11, no. 2, pp. 68–70, 2001.

[81] M. A. Sufian and N. Hussain, "Metasurface-based phone case for the sar reduction of the 5g mobile phones," *IEEE Transactions on Electromagnetic Compatibility*, vol. 66, no. 2, pp. 417–426, 2024.

[82] W. A. Awan, N. Hussain, S. G. Park, and N. Kim, "Intelligent metasurface based antenna with pattern and beam reconfigurability for internet of things applications," *Alexandria Engineering Journal*, vol. 92, pp. 50–62, 2024.

[83] N. Hussain and N. Kim, "Integrated microwave and mm-wave mimo antenna module with 360° pattern diversity for 5g internet of things," *IEEE Internet of Things Journal*, vol. 9, no. 24, pp. 24777–24789, 2022.

[84] S. Islam, T. H. J. Van Linh Pham, and H. Yoo, "Wave manipulation with mmwave wide bandwidth and extensive spatial coverage using 1-bit reconfigurable intelligent surface," *Progress In Electromagnetics Research*, vol. 179, pp. 83–94, 2024.

[85] S. Bellofiore, C. A. Balanis, J. Foutz, and A. S. Spanias, "Smart-antenna systems for mobile communication networks. part 1. overview and antenna design," *IEEE Antennas and Propagation Magazine*, vol. 44, no. 3, pp. 145–154, 2002.

[86] M. Ibnkahla, Q. M. Rahman, A. I. Sulyman, H. A. Al-Asady, J. Yuan, and A. Safwat, "High-speed satellite mobile communications : technologies and challenges," *Proceedings of the IEEE*, vol. 92, no. 2, pp. 312–339, 2004.

[87] W. Hong, Z. H. Jiang, C. Yu, D. Hou, H. Wang, C. Guo, Y. Hu, L. Kuai, Y. Yu, Z. Jiang, *et al.*, "The role of millimeter-wave technologies in 5g/6g wireless communications," *IEEE Journal of Microwaves*, vol. 1, no. 1, pp. 101–122, 2021.

[88] M. Elkashlan, T. Q. Duong, and H.-H. Chen, "Millimeter-wave communications for 5g : fundamentals : Part i [guest editorial]," *IEEE Communications Magazine*, vol. 52, no. 9, pp. 52–54, 2014.

[89] N. Chukhno, O. Chukhno, S. Pizzi, A. Molinaro, A. Iera, and G. Araniti, "Efficient management of multicast traffic in directional mmwave networks," *IEEE Transactions on Broadcasting*, vol. 67, no. 3, pp. 593–605, 2021.

[90] M. Xiao, S. Mumtaz, Y. Huang, L. Dai, Y. Li, M. Matthaiou, G. K. Karagiannidis, E. Björnson, K. Yang, I. Chih-Lin, *et al.*, "Millimeter wave communications for future mobile networks," *IEEE Journal on Selected Areas in Communications*, vol. 35, no. 9, pp. 1909–1935, 2017.

[91] M. Wang, F. Gao, S. Jin, and H. Lin, "An overview of enhanced massive mimo with array signal processing techniques," *IEEE Journal of Selected Topics in Signal Processing*, vol. 13, no. 5, pp. 886–901, 2019.

[92] J. Kim, H.-S. Chung, I. G. Kim, H. Lee, and M. S. Lee, "A study on millimeter-wave beamforming for high-speed train communication," in *2015 International Conference on Information and Communication Technology Convergence (ICTC)*, pp. 1190–1193, IEEE, 2015.

[93] W. Wang, Z. Fang, K. Tang, X. Wang, Z. Shu, Z. Zhao, and Y. Zheng, "Wideband gain enhancement of mimo antenna and its application in fmcw radar sensor integrated with cmos-based transceiver chip for human respiratory monitoring," *IEEE Transactions on Antennas and Propagation*, vol. 71, no. 1, pp. 318–329, 2023.

[94] J. Koppenborg, H. Halbauer, S. Saur, and C. Hoek, "3d beamforming trials with an active antenna array," in *2012 international ITG workshop on smart antennas (WSA)*, pp. 110–114, IEEE, 2012.

[95] N. Melouki, F. Ahmed, P. PourMohammadi, H. Naseri, A. Iqbal, and T. Denidni, "3d-printed conformal metamaterial lens with multiple beam steering functionalities," in *2023 IEEE International Symposium on Antennas and Propagation and USNC-URSI Radio Science Meeting (USNC-URSI)*, pp. 791–792, IEEE, 2023.

[96] H. Naseri, P. Pourmohammadi, P. Fei, N. Melouki, A. Iqbal, and T. Denidni, "Butler matrix-based beamforming with polarization reconfigurability for reducing electromagnetic interference," *AEU-International Journal of Electronics and Communications*, vol. 170, p. 154833, 2023.

[97] M. C. Tan, M. Li, Q. H. Abbasi, and M. A. Imran, "A wideband beamforming antenna array for 802.11 ac and 4.9 ghz in modern transportation market," *IEEE Transactions on Vehicular Technology*, vol. 69, no. 3, pp. 2659–2670, 2019.

[98] W. Roh, J.-Y. Seol, J. Park, B. Lee, J. Lee, Y. Kim, J. Cho, K. Cheun, and F. Aryanfar, "Millimeter-wave beamforming as an enabling technology for 5g cellular communications : Theoretical feasibility and prototype results," *IEEE communications magazine*, vol. 52, no. 2, pp. 106–113, 2014.

[99] P. PourMohammadi, H. Naseri, F. Ahmed, and T. A. Denidni, "A wideband transmit array based on huygens' metasurface for millimeter-wave applications," in *2024 IEEE International Symposium on Antennas and Propagation and INC/USNC-URSI Radio Science Meeting (AP-S/INC-USNC-URSI)*, pp. 1807–1808, IEEE, 2024.

[100] C. Tian, Y.-C. Jiao, G. Zhao, and H. Wang, "A wideband transmitarray using triple-layer elements combined with cross slots and double square rings," *IEEE Antennas and Wireless Propagation Letters*, vol. 16, pp. 1561–1564, 2017.

[101] Q. Luo, S. Gao, M. Sobhy, and X. Yang, "Wideband transmitarray with reduced profile," *IEEE Antennas and Wireless Propagation Letters*, vol. 17, no. 3, pp. 450–453, 2018.

[102] W. An, S. Xu, F. Yang, and M. Li, "A double-layer transmitarray antenna using malta crosses with vias," *IEEE Transactions on Antennas and Propagation*, vol. 64, no. 3, pp. 1120–1125, 2016.

[103] A. H. Abdelrahman, A. Z. Elsherbeni, and F. Yang, "Transmission phase limit of multilayer frequency-selective surfaces for transmitarray designs," *IEEE Transactions on Antennas and Propagation*, vol. 62, no. 2, pp. 690–697, 2014.

[104] K. T. Pham, R. Sauleau, E. Fourn, F. Diaby, A. Clemente, and L. Dussopt, "Dual-band transmitarrays with dual-linear polarization at ka-band," *IEEE Transactions on Antennas and Propagation*, vol. 65, no. 12, pp. 7009–7018, 2017.

[105] A. H. Abdelrahman, A. Z. Elsherbeni, and F. Yang, "Transmission phase limit of multilayer frequency-selective surfaces for transmitarray designs," *IEEE Transactions on Antennas and Propagation*, vol. 62, no. 2, pp. 690–697, 2013.

[106] H. Nematollahi, J.-J. Laurin, J. Page, and J. A. Encinar, "Design of broadband transmitarray unit cells with comparative study of different numbers of layers," *IEEE Transactions on Antennas and Propagation*, vol. 63, no. 4, pp. 1473–1481, 2015.

[107] Z.-W. Miao, Z.-C. Hao, G. Q. Luo, L. Gao, J. Wang, X. Wang, and W. Hong, "140 ghz high-gain ltcc-integrated transmit-array antenna using a wideband siw aperture-coupling phase delay structure," *IEEE Transactions on Antennas and Propagation*, vol. 66, no. 1, pp. 182–190, 2017.

[108] H. Kaouach and A. Kabshi, “Design and characterization of 1-bit passive unit-cells for transmit-arrays and frequency selective surfaces in v-band,” in *2015 IEEE-APS Topical Conference on Antennas and Propagation in Wireless Communications (APWC)*, pp. 27–30, IEEE, 2015.

[109] F. Diaby, A. Clemente, L. Di Palma, L. Dussopt, K. Pham, E. Fourn, and R. Sauleau, “Design of a 2-bit unit-cell for electronically reconfigurable transmitarrays at ka-band,” in *2017 47th European Microwave Conference (EuMC)*, pp. 1321–1324, IEEE, 2017.

[110] S. Liu, H. Sato, and Q. Chen, “A wideband, 1 bit transmitarray antenna design with flat gain response,” *IEEE Transactions on Antennas and Propagation*, vol. 68, no. 10, pp. 7046–7055, 2020.

[111] S. Ghosh and D. Sen, “An inclusive survey on array antenna design for millimeter-wave communications,” *IEEE Access*, vol. 7, pp. 83137–83161, 2019.

[112] F. Ahmed, K. Singh, and K. P. Esselle, “State-of-the-art passive beam-steering antenna technologies : Challenges and capabilities,” *IEEE Access*, vol. 11, pp. 69101–69116, 2023.

[113] F. Vaquero, J. Teixeira, S. A. Matos, M. Arrebola, J. R. Costa, J. M. Felício, C. A. Fernandes, and N. J. G. Fonseca, “Design of low-profile transmitarray antennas with wide mechanical beam steering at millimeter waves,” *IEEE Transactions on Antennas and Propagation*, vol. 71, no. 4, pp. 3713–3718, 2023.

[114] S. H. R. Tuloti, A. Lamecki, and M. Mrozowski, “An optimized ka-band low profile dual-polarized transmitarray antenna with 2d beam switching,” *IEEE Access*, vol. 12, pp. 8924–8931, 2024.

[115] J. R. Reis, M. Vala, and R. F. Caldeirinha, “Review paper on transmitarray antennas,” *IEEE Access*, vol. 7, pp. 94171–94188, 2019.

[116] L.-Z. Song, T. Zhang, J.-X. Lai, Y. Yang, and J. Du, “A 180-ghz to 220-ghz wideband transmitarray with wide-angle beam steering for intersatellite communications,” *IEEE Transactions on Antennas and Propagation*, vol. 72, no. 1, pp. 950–955, 2024.

[117] Y. Ge, C. Lin, and Y. Liu, “Broadband folded transmitarray antenna based on an ultrathin transmission polarizer,” *IEEE Transactions on Antennas and Propagation*, vol. 66, no. 11, pp. 5974–5981, 2018.

[118] G.-B. Wu, S.-W. Qu, and S. Yang, “Low-profile transmitarray antenna with cassegrain reflectarray feed,” *IEEE Transactions on Antennas and Propagation*, vol. 67, no. 5, pp. 3079–3088, 2019.

[119] C. Song, L. Pan, Y. Jiao, and J. Jia, “A high-performance transmitarray antenna with thin metasurface for 5g communication based on pso (particle swarm optimization),” *Sensors*, vol. 20, no. 16, p. 4460, 2020.

[120] Á. F. Vaquero, J. Teixeira, S. A. Matos, M. Arrebola, J. R. Costa, J. M. Felício, C. A. Fernandes, and N. J. Fonseca, “Design of low-profile transmitarray antennas with wide mechanical beam steering at millimeter waves,” *IEEE Transactions on Antennas and Propagation*, vol. 71, no. 4, pp. 3713–3718, 2023.

[121] S. Tiwari, A. K. Singh, and A. Dubey, “Wide-band wide-angle beamsteerable meta-lens antenna for terrestrial/nonterrestrial 5g communication systems,” *IEEE Journal on Miniaturization for Air and Space Systems*, vol. 5, no. 2, pp. 117–124, 2024.

[122] M. Jiang, Z. N. Chen, Y. Zhang, W. Hong, and X. Xuan, “Metamaterial-based thin planar lens antenna for spatial beamforming and multibeam massive mimo,” *IEEE Transactions on Antennas and Propagation*, vol. 65, no. 2, pp. 464–472, 2017.

[123] N. Melouki, F. Ahmed, H. Nasseri, P. Pourmohammadi, A. Iqbal, and T. A. Denidni, "Multi-bit wideband transmitarray aperture with independent phase and amplitude control for high gain with low sidelobe mm-wave applications," in *2024 18th European Conference on Antennas and Propagation (EuCAP)*, pp. 01–04, 2024.

[124] N. Melouki, F. Ahmed, P. PourMohammadi, H. Naseri, M. S. Bizan, A. Iqbal, and T. A. Denidni, "3d-printed conformal meta-lens with multiple beam-shaping functionalities for mm-wave sensing applications," *Sensors*, vol. 24, no. 9, p. 2826, 2024.

[125] H. Yu, J. Su, Z. Li, and F. Yang, "A novel wideband and high-efficiency electronically scanning transmitarray using transmission metasurface polarizer," *IEEE Transactions on Antennas and Propagation*, vol. 70, no. 4, pp. 3088–3093, 2022.

[126] F. Ahmed, T. Hassan, N. Melouki, H. Naseri, P. PourMohammadi, A. Iqbal, and T. A. Denidni, "A multi-bit and frequency-reconfigurable reflecting surface for ris applications," *IEEE Antennas and Wireless Propagation Letters*, 2023.

[127] T. Jiang, Z. Wang, D. Li, J. Pan, B. Zhang, J. Huangfu, Y. Salamin, C. Li, and L. Ran, "Low-dc voltage-controlled steering-antenna radome utilizing tunable active metamaterial," *IEEE Transactions on Microwave Theory and Techniques*, vol. 60, no. 1, pp. 170–178, 2011.

[128] P.-Y. Qin, L.-Z. Song, and Y. J. Guo, "Beam steering conformal transmitarray employing ultra-thin triple-layer slot elements," *IEEE Transactions on Antennas and Propagation*, vol. 67, no. 8, pp. 5390–5398, 2019.

[129] P. Pourmohammadi, V. Volski, and G. A. Vandenbosch, "Medium-sized highly coupled planar arrays with maximum aperture efficiency," *Sensors*, vol. 21, no. 17, p. 5925, 2021.

[130] Z. Ma and G. A. Vandenbosch, "Low-cost wideband microstrip arrays with high aperture efficiency," *IEEE transactions on antennas and propagation*, vol. 60, no. 6, pp. 3028–3034, 2012.

[131] J. Y. Lau and S. V. Hum, "Reconfigurable transmitarray design approaches for beamforming applications," *IEEE Transactions on Antennas and Propagation*, vol. 60, no. 12, pp. 5679–5689, 2012.

[132] J. Yang, S. T. Chen, M. Chen, J. C. Ke, M. Z. Chen, C. Zhang, R. Yang, X. Li, Q. Cheng, and T. J. Cui, "Folded transmitarray antenna with circular polarization based on metasurface," *IEEE Transactions on Antennas and Propagation*, vol. 69, no. 2, pp. 806–814, 2020.

[133] M. Selvanayagam and G. V. Eleftheriades, "Discontinuous electromagnetic fields using orthogonal electric and magnetic currents for wavefront manipulation," *Optics express*, vol. 21, no. 12, pp. 14409–14429, 2013.

[134] C. Zhang, Y. Luo, Y. He, N. Yan, and K. Ma, "Multi-beam quad-polarized transmit-array antenna with arbitrary radiation direction for vehicle communication via generalized phase superposition," *IEEE Transactions on Antennas and Propagation*, 2024.

[135] C. Liu, Y. Wu, F. Yang, S. Xu, and M. Li, "Is it possible to design a 1-bit reconfigurable transmitarray element with a single switch?," *IEEE Antennas and Wireless Propagation Letters*, vol. 22, no. 4, pp. 829–833, 2023.

[136] P. PourMohammadi, H. Naseri, N. Melouki, F. Ahmed, M. S. Bizan, A. Iqbal, and T. A. Denidni, "A fabry–perot antenna using a frequency selective surface layer with wideband and low rcs for mm-wave applications," *AEU-International Journal of Electronics and Communications*, vol. 169, p. 154736, 2023.

[137] R. J. Mailloux, *Phased array antenna handbook*. Artech house, 2017.

[138] B. D. Nguyen and C. Pichot, "Unit-cell loaded with pin diodes for 1-bit linearly polarized reconfigurable transmitarrays," *IEEE Antennas and Wireless Propagation Letters*, vol. 18, no. 1, pp. 98–102, 2019.

[139] P. PourMohammadi, H. Naseri, N. Melouki, and T. A. Denidni, “A 1-bit wideband electronically beam steering transmitarray for 5g communication systems,” in *2024 IEEE International Symposium on Antennas and Propagation and INC/USNC-URSI Radio Science Meeting (AP-S/INC-USNC-URSI)*, pp. 139–140, 2024.

[140] C. Liu, F. Yang, S. Xu, and M. Li, “Reconfigurable metasurface : A systematic categorization and recent advances,” *Electromagnetic Science*, vol. 1, no. 4, pp. 1–23, 2023.

[141] M. Nadi, A. Cheldavi, and S. H. Sedighy, “Beam steering toward multi-beam radiation by time-coding metasurface antennas,” *IEEE Transactions on Antennas and Propagation*, 2024.

[142] L.-Z. Song, P.-Y. Qin, and Y. J. Guo, “A high-efficiency conformal transmitarray antenna employing dual-layer ultrathin huygens element,” *IEEE Transactions on Antennas and Propagation*, vol. 69, no. 2, pp. 848–858, 2021.

[143] R. A. I. Asyari, K.-Y. Lee, R. E. Arif, T.-S. J. Horng, and D. Teichmann, “A novel approach to remote detection in medical radar applications using flexible transmit array lenses,” *IEEE Journal of Electromagnetics, RF and Microwaves in Medicine and Biology*, vol. 8, no. 1, pp. 36–50, 2024.

[144] M. H. Dahri, M. H. Jamaluddin, F. C. Seman, M. I. Abbasi, N. F. Sallehuddin, A. Y. I. Ashyap, and M. R. Kamarudin, “Aspects of efficiency enhancement in reflectarrays with analytical investigation and accurate measurement,” *Electronics*, vol. 9, no. 11, p. 1887, 2020.